Department of Built Environment
Structural Engineering and Design - Innovative Structural Design

Development of an analytical model predicting the horizontal shear capacity of Composite Bamboo Shear Walls

Mees Fabel

Supervisors:
First Committee Member - Prof.Dr.Engr. Akke Suiker
Second Committee Member - Engr. Arjan Habraken
Third Committee Member - Dr.Engr. Nischal Pradhan

1

Eindhoven University of Technology

Abstract

Composite Bamboo Shear Walls (CBSWs) are a promising alternative to conventional shear wall systems in tropical regions where bamboo is abundant. However, the structural behavior and design capacity are not yet well established. This thesis investigates the predictability of horizontal shear capacity of CBSW by comparing outcomes of experimental testing and analytical modeling. Two configurations of $2.4 \times 2.4m$ wall panels were subjected to monotonic and cyclic in-plane loading to characterize global force–displacement behavior and failure mechanisms. In parallel, single-fastener tests were conducted to quantify the nonlinear behavior of these fasteners.

An analytical model was developed to predict the horizontal shear capacity of CBSW by explicitly incorporating nonlinear fastener behavior and wall geometry. The model successfully captures the relative influence of fastener type, quantity, and position, as well as the effect of flat bar bracing, and shows good agreement with experimental results, with deviations generally within 10–20%. The model slightly overestimates elastic stiffness and underestimates peak capacity, primarily due to simplifying assumptions regarding component rigidity.

Analysis of force distribution reveals that corner fasteners dominate shear resistance, while central fasteners contribute minimally, providing clear opportunities for structural optimization. Several improvement strategies were explored using the model, including wall reconfiguration, altered embedment conditions, and enhanced fastener properties. The results demonstrate that targeted design modifications can significantly increase shear capacity and stiffness. Finally, comparison with current design values shows that existing shear capacity provisions are highly conservative, underestimating CBSW capacity by at least a factor of 2.8.

Overall, this research validates an analytical framework for CBSW design, provides insight into governing mechanisms and failure modes, and demonstrates the potential for more efficient, reliable, and sustainable structural applications of bamboo-based shear wall systems.

Contents

Chapter 1

Introduction

1.1 Context and topic

The use of bio-based materials shows great potential to reduce carbon emissions in the construction sector and increase circularity [Dams et al., 2023]. Lightweight Framed Timber (LFT) is the most economical building method using a bio-based material, timber. LFT outperforms conventional construction methods in terms of building costs for low- to mid-rise buildings [Horsting et al., 2024], and would therefore be a good replacement option. Unfortunately, a transition to complete timber construction would increase the risk of depleting available timber resources [Horsting et al., 2024]. Pushing for the implementation of alternative bio-based construction methods can help minimize the risk of dependence on timber.

Alternative methods involve the use of uncommon materials such as flax, hemp, cork, or bamboo [Dams et al., 2023]. Lack of experience, low standardization, and infeasibility prevent large-scale application of such materials. On the other hand, these materials have been used throughout history, and are only uncommon because knowledge concerning their application has been lost. In particular, bamboo has been applied for structural use in vernacular architecture in Colombia for centuries.

The building technique in question is called *bahareque*, typically consisting of a timber or bamboo frame, clad in a matrix of split bamboo or timber strips, and finally plastered in soil, sometimes with straw added for strength [Lopez et al., 2004]. The *bahareque* system has been used in buildings for almost 500 years already [FOREC, 2002]. A modern version of the *bahareque* exists, addressed as Composite Bamboo Shear Walls (CBSW). This version is more standardized and has a shorter construction time, and it is the main subject of this research. The CBSW are implemented to provide stability to buildings, and help them resist typhoons and earthquakes.

CBSW are a novel and therefore not yet properly documented structural system. Currently, Base Bahay uses a conservative horizontal yield capacity value of $2.0kN/m$ [BASE, 2024]. There are no characteristic values for shear capacity, stiffness, ductility, or damage. Characterization of any of these values can be achieved by performing tests on standardized walls. Additionally, a model should be developed to predict the shear capacity of these walls for any possible configuration of components. Not only will this reduce the amount of testing that will be required, it will also create a fast and reliable way to calculate the capacity of any configuration of CBSW. The model should be based on theory, equations, and data from previous research. The model will be validated using the results from experimental testing. The focus of the research presented in this thesis will be on developing a model that can be used to predict and improve the shear capacity of standardized sizes of CBSW.

1.2 State of the art

The state of the art acts as a foundation for this research and is the main motivation for further investigation. The boundaries of current knowledge on CBSW and any matter related to it will be discussed in this section. Following from this section, a clear research gap should follow on which the research objectives and research question will be based.

1.2.1 CBSW

CBSW consist of framing components, cladding, and cladding-to-framing nailed connections as illustrated in figure 1.1. The detailed connections have been illustrated in figure 1.2. The framing consists of bamboo culms (B1-B5) used as vertical studs, which are nailed to top (TP1) and bottom (TP2) timber beams using 2.5x50 mm common wood nails (connection i), each stud connected by four nails spaced evenly around the perimeter of the studs. Additionally, Bamboo studs (B1, B3, B5) are anchored to the top timber beam (TP2) using J-bolts (connection v) and to the foundation through an embedded rebar (connection iv). Connection v, the J-bolt, provides a tensile connection between the stud and the top timber beam, and the embedded rebar of connection iv provides anchoring of the wall panel to the foundation. Both connections iv and v are strengthened with mortar infill. Steel flat bar bracing (FB1, FB2) may be installed in the frame, bolted to the timber beams at the four panel edges (connection ii), and to bamboo studs (B2-B4) using bolt connections (connection iii). The matrix which is either rib lath (planar steel mesh) or *tadtad* (flattened bamboo mats), is attached to framing components

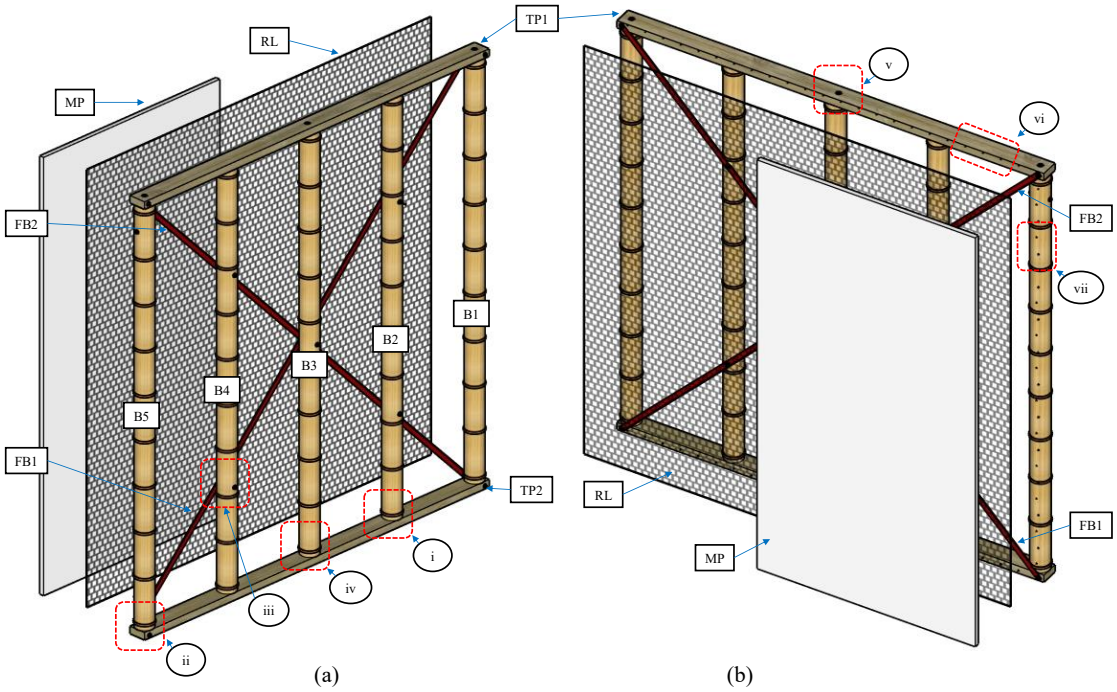

Figure 1.1: **Components of CBSW panel.** (a) the front elevation; and (b) the rear elevation in isometric view.

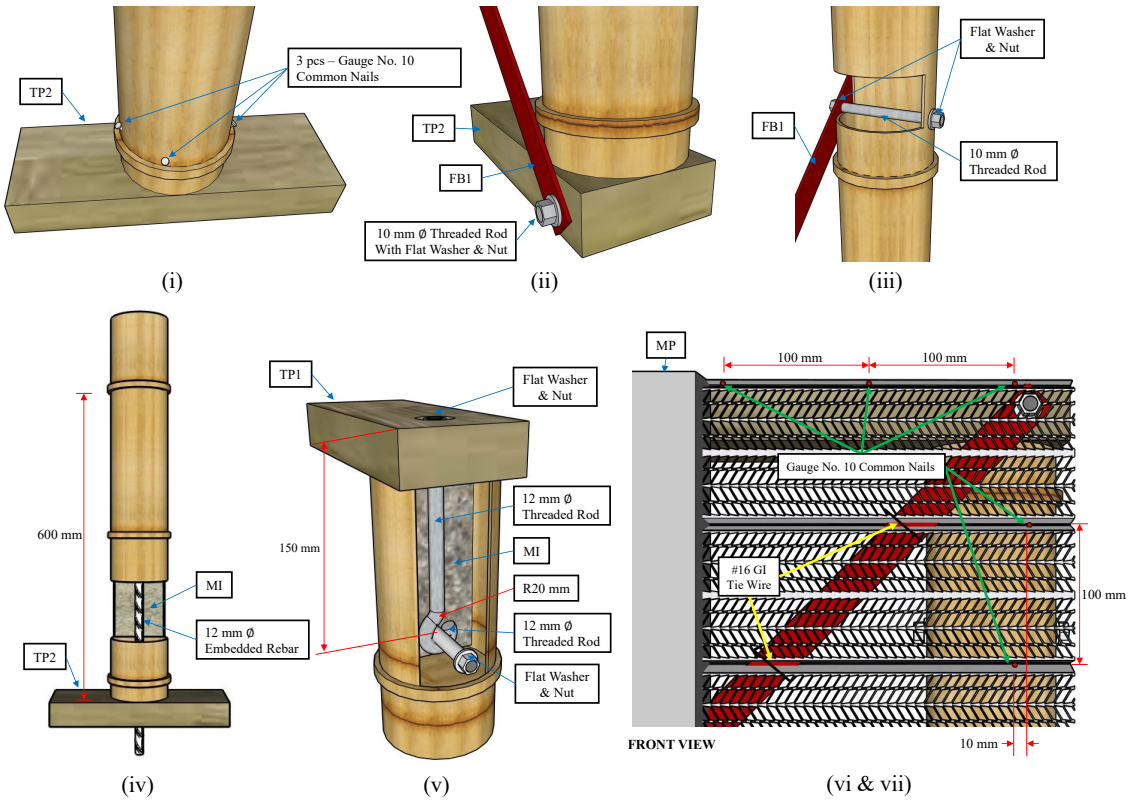

Figure 1.2: **All connections used in CBSW panel.**) Includes: (a) nailed connection between bamboo studs and timber beams; (b) bolt connection between flat steel bar and timber beams; (c) bolt connection between flat steel bar and bamboo studs; (d) embedded rebar connection; (e) J-bolt connection; (f) nailed connection between rib lath and framing components, and tie wires between flat bar and rib lath.

(TP1, TP2) and (B1-B5) with nails (connection vi & vii). The matrix is then covered on one side with mortar plaster (MP), forming the cladding. The mortar plaster has a minimum thickness of 25 mm and is applied in two coats. The second coat is added at least 10 hours after the first to ensure proper curing and bond strength.

The bolts and nails used in the wall panel are collectively addressed as the fasteners. In total, eight fastener types have been identified, out of which five are used in one wall configuration. Fastener types used in combination with rib lath matrix are gathered in table 1.1. Note that fastener types F3-F5 are similar for rib lath and *tadtad* matrices, with the only difference being the type of matrix used. Throughout the research, the fasteners will be addressed by their appropriate number. For clarity about fastener types, readers are redirected to table 1.1 throughout the report.

Many CBSW configurations are possible with the addressed components. In practice, there are four standard combinations which are commonly used, see also table 1.2. These four wall types are used because of their standardized manufacturing process. In housing projects, rib lath is used for the walls that require adequate fire resistance such as home dividing walls. The *tadtad* matrix is used in the other shear walls. Bracing is installed with the sole purpose of stabilizing the frames during transport. Small elements with an aspect ratio of 1:2 are more often not braced.

1.2.2 Materials

The following paragraphs provide a detailed overview of the materials used in this research. Readers are also redirected to figure 1.1 for a visual and dimensional representation of the used materials.

Bambusa blumeana, locally known as *kawayan tinik*, is used as the primary framing material. Bamboo culms are harvested at an age of 3–5 years to ensure adequate maturity and mechanical strength. Culm diameters range from 80–100 mm, with wall thicknesses between 8–20 mm. To enhance durability and resistance to insect and fungal attacks, all culms are chemically treated with a *permethrin* solution. The treated bamboo was sourced from the Kanya Kawayan Treatment Facility in Batangas, Philippines and Kawayan Collective in Tarlac, Philippines. The selection of *Bambusa blumeana* reflects both its local abundance and its established performance in structural applications.

Kiln-dried spruce-pine-fir (SPF) wood is used for the timber beams in the wall frames. The members measure 100 mm in width, 50 mm in thickness, and 2,400 mm in length,

Table 1.1: Overview of CBSW frame-to-cladding fastener types

	Fasteners F1-F5			
	Frame member	**Cladding member**	**Fastener**	**Schematic**
F1.	timber	steel flat bar	bolt	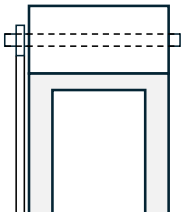
F2.	hollow bamboo	steel flat bar	bolt	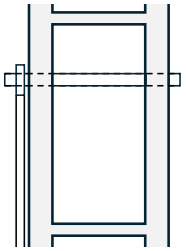
F3.	timber	rib lath	nail	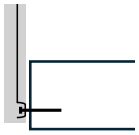
F4.	infilled bamboo	rib lath	nail	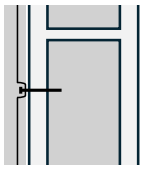
F5.	hollow bamboo	rib lath	nail	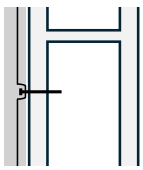

Table 1.2: Overview of CBSW typologies.

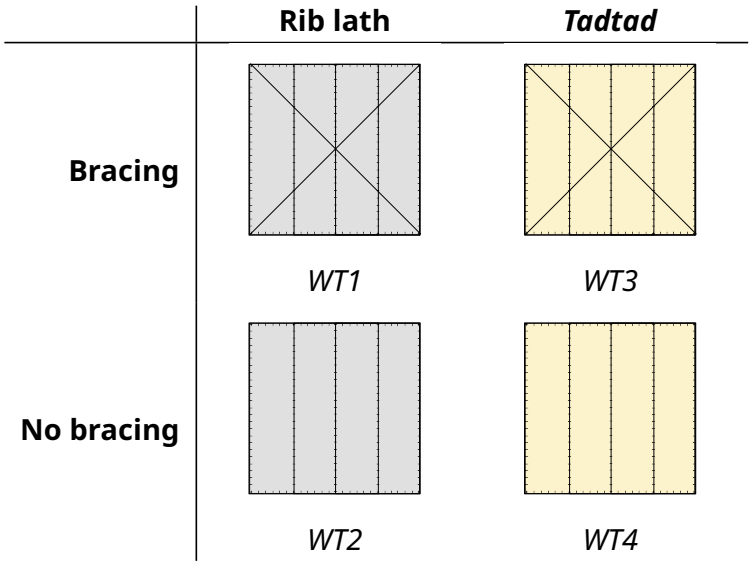

with all sides smoothly finished to ensure uniform connections. SPF was selected due to its availability, standardized mechanical properties, and consistency with timber framing practices documented in literature.

Connections between frame members are achieved using flat steel bars (Grade 43A [Erasmus, 1984], 25 mm wide × 3 mm thick, yield strength 248 MPa), reinforcement bars (12 mm diameter bars, Grade 280W [Erasmus, 1984], yield strength 280 MPa), and threaded rods (10 mm and 12 mm diameter, conforming to ASTM A307 Grade A, yield strength 235 MPa [Erasmus, 1984]). These connection materials were chosen for their proven reliability in structural applications and their compatibility with both bamboo and timber members.

The two wall matrix types considered in this research are rib lath and *tadtad*. Rib lath is an expanded metal lath which is manufactured from hot-dip galvanized sheet steel, has a thickness 0.3–0.5 mm, and a minimum weight of 1400 g/m^2. Standard sheet dimensions are 610 mm × 2,440 mm. Rib lath is selected for its established use as fireproof option in CBSW and its compatibility with cement plaster. The other option for the matrix is *tadtad*, which is produced by splitting and flattening *Bambusa blumeana* culms prior to treatment against fungi and insects. *Tadtad* represents a locally available, sustainable alternative to steel rib lath and is applied in the exterior walls of a CBSW house.

Cement mortar is applied both as infill and as plaster. A volumetric mix ratio of 1:3 (cement:sand) is used. The water–cement ratio equals 0.5 for plaster applications and 0.9

for infill. This mix is selected to balance workability, bonding capacity, and compressive strength within typical construction practices in the Philippines.

Fasteners used in this study consist of 40 mm and 65 mm common wood nails, consistent with conventional practice and literature on LFT shear wall assemblies. The CBSW system can be applied over any width of wall, but this project focuses on shear walls with a width of 2.4 meters. The height of the shear walls is commonly chosen as 2.4 meters as well. Another important notice is that this research focuses on the rib lath matrix, used in WT1 & WT2. The *tadtad* wall types are outside the scope of this research.

As noted in section 1.1, CBSW has not yet been fully characterized within the field of structural engineering. Although the connections in the frame have been analyzed [Bangoy et al., 2024], the interaction between frame and cladding or the behavior of full-size CBSW is not yet documented. In particular, no standardized methods currently exist for calculating its shear capacity. This lack of characterization poses a significant limitation to the widespread adoption of CBSW, as reliable design methods are a prerequisite for the integration of any structural system into engineering practice and building codes. To address this gap, it is essential to develop a systematic approach for evaluating and quantifying the structural behavior of CBSW.

1.2.3 State of the art - timber structures

A logical first step in this process is to examine how established structural systems are currently analyzed and designed. By comparing CBSW to systems with well-documented performance characteristics, such as LFT, it may be possible to identify methodological parallels and adapt existing calculation procedures. Such comparative analysis will not only provide a foundation for formulating a design model specific to CBSW but also highlight the unique mechanical behaviors introduced by the use of this novel system. This section identifies the main similarities and differences between LFT and CBSW resulting in a well-considered comparison.

LFT structures are among the most widely studied and applied structural systems for low- to mid-rise construction [Casagrande et al., 2016]. Their popularity stems from the relative ease of construction, and the well-established body of knowledge regarding their structural performance [Folz and Filiatrault, 2001]. Over the past decades, extensive experimental and analytical research has been carried out to evaluate the behavior of LFT systems under various loading conditions, particularly with respect to their lateral load resistance and energy dissipation capacity during seismic events [Benedetti

et al., 2022].

In LFT construction, load-bearing elements typically consist of closely spaced timber studs and beams, connected with cladding such as plywood or oriented strand board that together provide lateral stiffness and shear capacity. The performance of these systems is governed by the behavior of the cladding-to-frame fasteners, which have been the focus of numerous studies [Wakashima et al., 2003], [Li et al., 2015], [Hadi et al., 2012]. Based on the yielding of cladding-to-frame fasteners, a calculation method has been developed to evaluate the yield force and deformation of LFT shear walls under lateral load [Källsner and Girhammar, 2009]. . Modern design codes, including Eurocode 5 [European Committee for Standardization, 1994], provide comprehensive methods for the design of timber frame elements and assemblies. These guidelines can be used to calculate stiffness, yield strength, and failure mechanisms, and they form the foundation for reliable design practices.

From a methodological perspective, LFT systems provide a valuable point of reference for the characterization of CBSW. Both systems share the concept of a lightweight frame connected to cladding to resist in-plane forces. However, CBSW introduces new uncertainties because of its higher complexity. The framing consists of timber and bamboo, the latter containing mortar infill in certain locations. Optional bracing is applied. Basically, LFT systems are easier to assess because of the relative homogeneity of materials used. Previous research clearly indicates yielding of cladding-to-frame fasteners, while this failure mode has not been mentioned in CBSW research [Bibal, 2024]. Applying the theory used for LFT to CBSW will therefore yield new insights.

From LFT research, it becomes clear that the capacity of a shear wall consisting of frame and cladding is dependent on its weakest component, which is the cladding-to-frame connection. The most variable mechanical property of a fastener is its embedment type. The embedment types in CBSW range from timber beams, hollow bamboo studs, to bamboo studs with mortar infill. The strength and stiffness of the fastener is related to its embedment type. Documentation on the strength and stiffness is missing for any of the fastener types present in CBSW. Although the European Yield Model (EYM) can be used to determine these values, it has not yet been validated whether this method is applicable to bamboo. Evidently, further research is required into the shear strength and stiffness of the fasteners. This research will be covered in chapter 2.

1.2.4 Assumptions

The research is based on a number of assumptions to eliminate ambiguity and to maintain a consistent scope.

- A standard shear wall size of 2.4 meters width by 2.4 meters height is considered in this research.
- Only wall types including rib lath matrix, WT1 and WT2, are included in this research.
- The frames of the shear walls are assumed to be clamped at the bottom and uniformly loaded in-plane horizontally along the top timber beam. Out-of-plane buckling or vertical forces are neglected.
- Only shear capacity and related failure mechanisms are considered, fire performance and long-term creep are excluded.
- The framing members and the cladding are assumed to be rigid, deformations of these elements are neglected.
- The joints between the studs and the top and bottom timber beam of the frame act as hinges.
- The cladding is free to rotate, it is assumed not to be restricted by any external boundaries.
- In case flat bar bracing is applied, it is assumed to be embedded within the cladding.
- Connections and assembly are assumed to be executed with uniform quality, without significant deviations in fastener placement or material preparation.
- Mechanical properties of bamboo, timber, mortar, and steel are assumed to be consistent within the ranges provided, neglecting natural variability outside those ranges.
- Effects of long-term weathering, moisture variation, and degradation are not considered within the scope of this research.

By specifying the above materials and assumptions, the scope of the study is clearly bounded, enabling reproducibility and avoiding ambiguity in the interpretation of results. The validity of the assumptions will be discussed in chapter 6.

1.3 Research question

As stated in section 1.1, this thesis focuses on the development of a shear capacity model for CBSW. The model will be based on theory, equations, data from small-scale experiments, and data from previous research, and will be validated using the results from full-scale experiments that will be performed to characterize the shear walls. The objective of the research will be described in this section through the research question and its sub-questions.

1.3.1 Main question

The research question has multiple sub-questions that will guide the research towards its goal; the objective of the research will be to develop a model that can be used to describe the structural behavior of any configuration of CBSW shear wall. In this investigation, all relevant configurations of the shear wall components, as described in section 1.2, will be considered. The sub-questions related to the research are subdivided into different categories which relate to the phases of the project which will be elaborated in section 1.4. The research question states:

- *How can an analytical model be developed to predict and improve the horizontal shear capacity of a Composite Bamboo Shear Wall?*

1.3.2 Sub-questions

Each subcategory has a set of questions that will lead to a more complete answer of the research question. The subcategories are: literature review, theoretical approach, model development, and validation.

1. **Literature review**
   The first step of the research is to investigate previous work that has been done on CBSW. Since CBSW and LFT behave similarly, research on both subjects will be considered. The following sub-questions relate to this phase of the project:

   - *What existing methods are used to determine the structural behavior of CBSW or LFT shear walls?*
   - *What are the critical design factors in these methods, and how are these critical factors characterized in existing research?*
   - *Which key features require additional experimental research, and how should this research be executed?*

2. **Theoretical approach**
   The outcome of previous research can be used to establish a theoretical approach to the behavior of CBSW. The goal is to set up an equation or a set of equations that can describe the behavior. The following sub-questions apply:

   - *Which existing shear wall theories can be applied to CBSW?*
   - *How can critical shear wall design factors be incorporated into a set of equations?*

3. **Model development**
   The creation of the model is based on the equations and data of the theoretical approach. If data cannot be collected from previous research, additional experiments will be required. The objective, predicting the behavior of a shear wall, can be reached by considering the following sub-questions:

   - *How can the theoretical methodologies be applied in the model?*
   - *How should assumptions and limitations be incorporated in the model?*

4. **Validation and application**
   The model will be validated to assess its functionality. In this phase of the project, validation will be evaluated by comparing with experimental test results. The following sub-questions will act as a guide:

   - *How do the results of the model compare with experimental data?*
   - *How can the accuracy of the model be evaluated?*
   - *What are the potential applications and limitations of the model in practical scenarios?*
   - *Can the model be applied to improve the horizontal shear capacity of CBSW?*

1.4 Methodology

The methodology is described in a flowchart presented in the research proposal. For the flowchart, see appendix A. The following sections describe in further detail what are the objectives of the four subcategories presented in section 1.3.2.

1.4.1 Literature Review

The first phase of the methodology involves an extensive and critical review of existing literature on CBSW and other structural systems that are suitable to describe the behavior of CBSW. This review not only provides an overview of relevant studies but

also evaluates their methodologies, assumptions, and limitations. Research addressing shear wall performance is examined in detail, particularly in terms of experimental testing approaches, and modeling strategies.

Within this phase, significant emphasis is placed on understanding the influence of boundary conditions and wall configurations. Analytical and numerical studies are analyzed to evaluate the assumptions and simplifications that are used in existing models, and their relevance to being used in this research. The review also identifies key factors influencing the behavior of CBSW, such as the stiffness and shear strength of fasteners, and the interaction between cladding and framing elements. By synthesizing these findings, the review establishes the critical gaps in knowledge and the unresolved challenges that need to be addressed in subsequent phases of this research. A summary of the main insights and their implications is presented at the end of Chapter 2, providing a conceptual foundation for the theoretical framework.

1.4.2 Theoretical Approach

Drawing on the findings of the literature review, the second phase develops a theoretical framework to describe the structural behavior of CBSW under lateral loading. This framework evaluates the applicability of existing shear wall theories and extends them to cater specifically to the characteristics of CBSW. The framework contains all the necessary formulas and methods to determine the shear capacity and stiffness of any CBSW.

At the system level, the framework considers how load is distributed over the fasteners, and what reaction forces occur in the frame and the foundation. The result is a set of governing equations that can be used to find shear wall yield force, ultimate force and stiffness. Simplifications and assumptions are explicitly stated, with their implications critically discussed to ensure transparency. This theoretical work, which can be found in full detail in chapter 3, establishes the mathematical foundation for the analytical model that is developed in Chapter 4.

1.4.3 Model Development

The model is developed using python. The theoretical framework is translated into an analytical model that predicts the horizontal shear capacity and load–displacement response of CBSW. The fastener stiffnesses used in the model are based on experimental data. The model is meant to act as a basis for design applications, and assessment of improvements to the CBSW system.

The inputs for the model should follow from chapters 2 & 3. Material properties together with their geometric configurations form the basis of model parameterization. The structure of the model is developed to be modular, allowing for application to any type of CBSW. The full development and refinement process is presented in Chapter 4.

1.4.4 Validation and Application

The experimental data that is used for the model comes from small-scale testing of single fastener connections. Fasteners F4 and F5 (fastener types involving bamboo) from table 1.1 will be assessed, since there is no previous research into these connections. Each fastener type is tested monotonically six times. Results of the fastener tests are discussed in detail in chapter 5. Tests are performed according to ISO standard 6891 [International Organization for Standardization, 1983].

the outcomes of the experiments should be analyzed so that true mean and characteristic values can be used in the model. The single nail tests will result in input values for the model, and the full-scale wall tests act as a reference for assessing the validity of the model. The experimental data from fasteners will be compared to analytical results. The comparison will be analyzed using the R^2 method, as has been done in previous research [Malkowska et al., 2022]. Based on this comparison, the capacity and stiffness of fastener types F4 and F5 will be determined for use in the model. This comparison is executed in chapter 5.
Following up on the single nail tests, chapter 5 contains a full description of all the full-scale tests that have been performed. This includes an explanation and sequence of test procedures. Subsequently, the wall configurations mentioned in section 1.2.1 will be tested, both monotonically and cyclically. Tests will be performed according to ISO standard 21581 [International Organization for Standardization, 2010]. One monotonic and five cyclic tests will be performed for each wall type. A full overview of the testing and all the specifications for testing can be found in chapter 5. The testing will result in force-displacement curves which will be analyzed according to ISO standard 21141 [International Organization for Standardization, 2022] to find the yield force and displacement, maximum force and displacement, and ultimate force and displacement.

Additionally, the final phase consists of validating the analytical model against the previously presented experimental data on CBSW. Model predictions of shear capacity and load–displacement behavior are compared systematically with the observed results. Statistical measures such as mean error, standard deviation, and coefficient of varia-

tion are gathered for each tested wall type to evaluate accuracy. The full validation is found in chapter 5.

Following validation, the practical applications of the model are explored. These include demonstrating how the model can be used to optimize wall configurations for enhanced shear performance, and assessing its potential integration into design guidelines or software tools. Chapter 5 presents the validation results and discusses the broader implications of applying the model in engineering design and practice. To showcase the application possibilities in practice, three optimization possibilities are presented, and their improvements are quantified and evaluated.

1.5 Conclusion and discussion

The evaluation setup is designed to assess the accuracy and applicability of the developed analytical model in predicting the horizontal shear capacity of CBSW. The results presented in chapter 5 are discussed and interpreted in this chapter. All the findings from this section will contribute to answering the research question.

This phase also acknowledges the limitations of the developed model, such as its reliance on available experimental data and the simplifications inherent in the theoretical framework. Recommendations for future research are proposed, including the need for large-scale cyclic testing of fasteners, more detailed modeling of fastener behavior, and investigation into innovative sheathing and fastening systems.

From a broader perspective, this research contributes to bridging the gap between experimental investigations of CBSW and practical design methodologies. By offering a systematic approach for predicting shear wall behavior that greatly reduces the amount of required tests, it brings both science and engineering practice a step closer to recognizing CBSW as a reliable and sustainable structural system.

Chapter 2

Literature Review

In this chapter, all previous research that is relevant to the development of the CBSW model is presented, summarized, and conclusions are gathered. First, an overview of the literature on CBSW is presented, to clearly point out the knowledge gaps that exist in this system. Afterwards, literature on LFT is presented, to provide possible applications for CBSW. Then literature on fasteners is analyzed. This literature is analyzed to get a clear understanding of the stiffness behavior of fasteners, and to gather more information about the yield strength and ultimate strength of some types of fasteners. The protocols and design standards used in this research are also highlighted in their own individual section.

2.1 Composite Bamboo Shear Walls

2.1.1 *Bahareque*

In 2024, a paper has been published which gives an overview of all the types of bamboo shear walls, and their potential for application. The paper, titled *Seismic Performance of Whole Culm Bamboo Structures and Recommendations for Design Using ISO 22156* [Kaminski et al., 2024], investigates how bamboo buildings perform during earthquakes. It combines evidence from past seismic events in Colombia, Ecuador, and El Salvador (which is mentioned also in an earlier paper [Lopez et al., 2004]), with results from experimental testing and an assessment of current design codes. The study challenges some widespread misconceptions about bamboo's behavior and highlights both the strengths and weaknesses of bamboo as a structural material. Its findings have been incorporated into the international bamboo design code ISO 22156 [International Organization for Standardization, 2021].

The good seismic performance of *bahareque* has already been documented in Colombia

Figure 2.1: Photograph showing buildup of bahareque wall, from [FOREC, 2002].

[FOREC, 2002]. This historic structural system has proven to be an effective application in earthquake prone areas. It is also indicated to be the original inspiration for the CBSW structural system. The main difference between *bahareque* and CBSW is that in the traditional building method, instead of attaching a cladding to one side of the frame, the cavities within the frame were filled, primarily with mud, see also figure 2.1

2.1.2 Performance of CBSW

Bamboo buildings receive relatively low ductility values, with response modification factors of 1.5–2. CBSW is the one system consistently shown to achieve higher ductility and is supported by explicit design and detailing rules, which have also been documented by Kaminski [Kaminski et al., 2016]. The paper recommends keeping bamboo buildings as light as possible, particularly in floors and roofs, ensuring durability through both treatment and moisture-protective design, and maintaining good construction practices. It proposes conservative design values for different systems, suggesting a factor of 1.5 for traditional full-culm bamboo and *bahareque* structures, 1.5 for modern bamboo frames with steel fasteners, and up to 2 for CBSW designed according to established guidelines.

In conclusion, the paper finds that bamboo structures can perform very well in earthquakes if designed and maintained appropriately. Their main advantages are lightness, ductile connections, and the ability to dissipate energy at the system level. Among modern systems, CBSW stands out as the most effective solution, combining affordability, safety, and durability. Kaminski worked on a paper focusing on CBSW beforehand [Kaminski et al., 2023], which shares the same conclusions.

The aforementioned research papers discuss the benefits of CBSW, but no information is given about the structural performance. The thesis *Monotonic and Cyclic Response of Cement-Bamboo Frame Technology Walls* [Bibal, 2024] presents an experimental investigation on the structural performance of CBSW when subjected to monotonic and cyclic lateral loadings. The study builds upon the concept of *bahareque*, integrating it with traditional Filipino housing typologies such as the *bahay kubo*. The research aims to establish the in-plane shear capacity and seismic performance of CBSW.

The experimental program consisted of six full-scale wall specimens, which have the same dimensions and materials as presented in section 1.2. Three specimens were subjected to monotonic loading, and another three specimens underwent cyclic loading. Experiments were performed following Method II of ISO 21581 [International Organization for Standardization, 2010], which is used to document the behavior of a shear wall in a combined shear and rocking failure mechanism. The walls were fabricated and tested at the Base Innovation Center in Makati City under controlled laboratory conditions.

Failure modes observed during testing included buckling and splitting of bamboo studs, spalling of cement plaster and rib-lath layers, and the formation of tensile cracks on the plaster surface. Additionally, connection failures at the base of the panels were documented and used to compute the shear capacity of the walls. The results demonstrated that CBSW could achieve lateral resistance capacities exceeding the 3.0–7.0 kN design range for conventional lightweight walls, thus validating their structural viability for seismic applications. The thesis recommends future investigations involving larger sample sizes and the inclusion of ISO 21581 Method I [International Organization for Standardization, 2010] tests to further specify the behavior of the CBSW under lateral loading.

2.2 Lightweight Framed Timber

2.2.1 Folz & Filliatrault

There are two papers which have been unmatched in their importance for the analysis of LFT shear walls. The first article titled *Cyclic Analysis of Wood Shear Walls* [Folz and Filiatrault, 2001] presents a numerical model for predicting the behavior of LFT shear walls subjected to quasi-static cyclic loading, which resembles earthquake loading. Authors Folz & Filliatrault develop a simple but accurate modeling approach which considers framing members as rigid, the cladding as linear elastic, and cladding-to-frame fasteners as nonlinear elements.

The fasteners are considered as nonlinear elements of which the force-displacement relationship can be described by equation 2.1. The terms used in these equations have been altered to match the terms used in other research. The first part of the equation has been based on the work of Foschi [Foschi, 1974], who proposed a nonlinear method to evaluate the force-displacement relationship of a fastener. Folz & Filliatrault expanded on this work by including the decay behavior in the equation after the maximum force has been reached at displacement u_{max}, described by the second function. Finally, the failure of the fastener is considered by $F = 0$ after ultimate displacement u_u has been reached.

$$F = \begin{cases} \left(F_0 + k_p s\right)\left[1 - \exp\left(-k_e s / F_0\right)\right], & \text{if } s < u_{\max} \\ F_{\max} + k_u (s - u_{\max}), & \text{if } u_{\max} \leq s \leq u_u \\ 0, & \text{if } s > u_u \end{cases} \tag{2.1}$$

The first equation in this set defines a value for F based on fastener slip s. The equation makes use of the plastic stiffness k_p and the intersection of k_p with the x-axis F_0, and elastic stiffness k_e. As soon as the fastener slip exceeds the displacement at maximum force u_{max}, the value for F depends on the ultimate stiffness or decay parameter k_u. Not all of these variables can be determined analytically, some rely on experimental evaluation instead. F_0 for example is found from visual analysis of the experimental graphs. This point should be considered when using equation 2.1 in a different application.

According to Folz & Filliatrault, the fasteners determine the capacity of the wall and dictate the cyclic behavior. Therefore, the presented model focuses on accurately documenting the pinching behavior. Pinching is a degrading phenomenon which occurs during cyclic loading of certain materials. Degradation in fastener strength and stiff-

ness are dictated by pinching. The fastener behavior including pinching is incorporated into the shear wall model.

The model is then validated against full-scale monotonic and cyclic shear wall tests. While some differences appear in monotonic loading due to construction variability, the cyclic predictions match experimental results closely in overall stiffness, peak load, hysteresis shape, and cumulative energy dissipation. Folz & Filliatrault note particularly good agreement in the degradation patterns that cyclic loading produces. Instead of relying on full-scale cyclic tests to determine global hysteretic properties, this approach uses connector-level hysteresis to generate an accurate wall-level hysteresis model. When applied to a shake-table experiment, the model reproduces measured wall displacements and response characteristics with strong fidelity.

2.2.2 Källsner & Girhammar

The second paper, *Analysis of fully anchored light-frame timber shear walls - elastic model* [Källsner and Girhammar, 2009], expands on the work done by Folz & Filliatrault. Källsner & Girhammar present an analytical static model for predicting the behavior of fully anchored LFT shear walls. Their model assumes a linear elastic load–slip relationship for the cladding-to-frame fasteners and considers only static loading conditions, thereby simplifying the behavior. Their theory is based on the assumption that all fasteners have the same stiffness and shear capacity, and that the fasteners in the corners will yield first. Formulas are derived both for the yield load and yield displacement of the shear walls.

A shear wall segment is defined as a timber frame with cladding connected by fasteners, and the analysis builds upon several simplifying assumptions. The model assumes that framing members and cladding are rigid, that there is no contact between adjacent cladding sheets or surrounding structures, and that framing joints act as hinges. It also assumes that cladding-to-frame joints have a constant elastic slip modulus, independent of force direction, and that displacements are small relative to wall dimensions. When a horizontal force H is introduced, the top of the frame deforms horizontally, and the cladding will start to rotate about its center of gravity.

See figure 2.2. By treating the fasteners as discrete points, a model of the shear wall is created. The relative displacements of the sheathing and the timber frame are expressed as u_i and v_i. These are the slip of fastener i in the x-direction and y-direction, respectively. Variable u_0 is the initial displacement of the cladding in the x-direction,

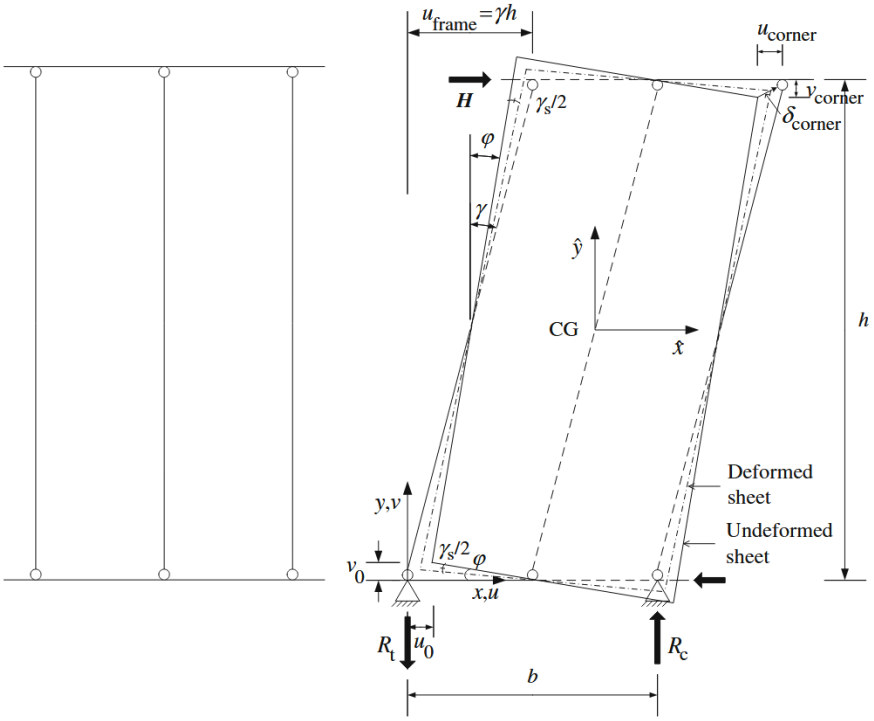

Figure 2.2: Static model of an LFT shear wall, from [Källsner and Girhammar, 2009].

and v_0 in the y-direction. Variables φ and γ are the angle of the deformed cladding and frame, respectively. Lastly, x_i and y_i are the x- and y-position of fastener i. The force acting on fastener i is dependent on fastener stiffness k and fastener slip. As deformations of the shear wall increase, the fasteners located furthest from the center of the cladding will deform the most, and thus yield first. In their paper, Källsner & Girhammar prove that omitting fasteners in the intermediate stud of an LFT shear wall has little effect on load capacity, though such fasteners are still necessary to prevent buckling and detachment of the cladding. Additionally, they prove that deformation of the cladding has no influence on the capacity, since it deforms in the same direction as the fasteners.

An equation is formulated to calculate the shear capacity of an LFT shear wall. This equation is valid for any framed shear wall where the frame-to-cladding connections are governing for the capacity. In this equation, a relation for φ and γ is used, see equations 2.2. For the full derivation of these relations and the capacity equation, readers are redirected to [Källsner and Girhammar, 2009]. The paper also mentions a method to evaluate the forces acting on the framing members. This can be used to verify the assumption of rigid members, and if not the case, the framing members can alternatively

only be considered as supporting in their respective longitudinal direction.

$$\varphi = \frac{Hh}{k} \frac{1}{\sum_{i=1}^{n} \hat{x}_i^2} \tag{2.2a}$$

$$\gamma = \frac{Hh}{k} \left[\frac{1}{\sum_{i=1}^{n} \hat{x}_i^2} + \frac{1}{\sum_{i=1}^{n} \hat{y}_i^2} \right] \tag{2.2b}$$

The squared distances of all the fasteners to the $\hat{x}$- and $\hat{y}$-axes make up the summand terms in equations 2.2. The origin of this coordinate system is located at the center of gravity of the cladding, see figure 2.2. The summand terms represent the second moment of area of the shear wall in individual x- and y-directions. Equation 2.2b shows a relationship between shear wall rotation angle γ and shear wall horizontal capacity H. This is a very useful equation that can be used to determine the capacity at any given rotation of the shear wall. In their research, Källsner & Girhammar also present an equation for the yield horizontal capacity of a shear wall:

$$H = \frac{F_y}{h\sqrt{\left[\frac{x_{corner}}{\sum_{i=1}^{n} x_i^2}\right]^2 + \left[\frac{y_{corner}}{\sum_{i=1}^{n} y_i^2}\right]^2}} \tag{2.3}$$

This equation only focuses on the point where the corner fastener is yielding. Note that in LFT research only one fastener type is considered. The shear capacity equation derived by Källsner & Girhammar is therefore only valid for walls where all fasteners have the same stiffness and yield strength. For the full elaboration, readers are redirected to [Källsner and Girhammar, 2009]. Chapter 3 develops a method to incorporate varying fastener types into a horizontal yield capacity calculation based on equation 2.3.

Both papers derive a method to calculate the capacity of a shear wall based on the fastener behavior, but where Folz & Filliatrault's approach is very global, Källsner & Girhammar's approach focuses purely on the elastic behavior. In other words, Källsner & Girhammar consider a bilinear force-displacement relation and only consider the behavior of the shear wall at the yield point. The bilinear fastener force-displacement curve can be constructed for each fastener using F_y (yield force) and k_e (elastic stiffness). The bilinear relation does not provide any information about capacity decay, or post-yielding behavior of fasteners, but it can be used for the derivation of the yield force of the full shear wall. Meanwhile, the approach of Källsner & Girhammar results in equations that describe the progression of forces in a shear wall, and can be applied also in nonlinear derivations [Hadi et al., 2012][Wakashima et al., 2003]. A nonlinear fastener force-displacement relation will be considered in the analytical CBSW model.

2.3 Fastener research

2.3.1 Fastener modeling

The paper by Folz and Filliatrault presented in section 2.2 provides a method for modeling the force-displacement behavior of a fastener. A three parameter equation describes the behavior of fasteners until the maximum force. Equation 2.1 works well for fasteners with a force-displacement relation that displays a distinct elastic and plastic region.

$$F = F_{max}\left[1 - \exp\left(-\frac{k_e}{F_{max}}s\right)\right] \tag{2.4}$$

An alternative equation is proposed in *Force–displacement relations of bolted timber joints with slotted-in steel plates parallel to the grain* [Liu et al., 2020], for fasteners that do not display distinct elastic and plastic zones in their force-displacement relationship. Equation 2.4 can be used to replace the first part of equation 2.1. It is preferred, as it uses only two input variables, F_{max} and k_e.

Substituting nonlinear force-displacement function 2.4 in equation 2.1 yields:

$$F = \begin{cases} F_{max}\left[1 - \exp\left(-\frac{k_e}{F_{max}}s\right)\right], & \text{if } s < u_{\max} \\ F_{\max} + k_u(s - u_{\max}), & \text{if } u_{\max} \leq s \leq u_u \\ 0, & \text{if } s > u_u \end{cases} \tag{2.5}$$

This equation (2.5) now relies solely on the maximum force F_{max}, corresponding displacement u_{max}, and ultimate stiffness k_u.

2.3.2 European Yield Model

Eurocode 5 [European Committee for Standardization, 1994] prescribes how to calculate fastener properties for the fasteners that are embedded in the timber. This concerns fastener types F1 and F3. The Eurocode is a practical design code, so the focus lies on serviceability and ultimate limit states. Elastic stiffness (addressed as slip modulus in Eurocode 5) values can be determined based on average timber density ρ_m and fastener diameter d. In this research, equation 2.6 will be used to evaluate the elastic stiffness k_e of F1 and F3.

$$k_e = \frac{1}{30}\rho_m^{1.5} d^{0.8} \tag{2.6}$$

The yield strength of fasteners F1 and F3 can be determined using the European Yield Model (EYM). This method, first described by Johansen [Johansen, 1949], determines which element in a timber fastener connection fails first. Only two EYM failure modes are considered in this research, both concerning a timber element connected to a thin steel plate. These modes were selected based on the appearance of CBSW as in section 1.2, where the rib lath is seen as a thin steel plate. The main failure modes are timber embedment failure, and timber embedment failure combined with fastener yielding. Equations 2.7 form the basis for evaluating the EYM failure modes. Equation 2.7a for timber embedment strength (in MPa) is based on fastener diameter d and characteristic timber density ρ_k. When a load is applied under an angle α relative to the grain of the timber, equation 2.7c evaluates the embedment strength in the direction of the load. Factor k_{90}, evaluated in equation 2.7b, is applied to SPF lumber when it is loaded under an angle. In CBSW, SPF lumber is used for the top and bottom timber beams, see also section 1.2.2. The fastener yielding moment, calculated in equation 2.7d, depends on the fastener tensile capacity f_u, and the fastener diameter d.

$$f_{h,0,k} = 0.082(1-0.01d)\rho_k \tag{2.7a}$$

$$k_{90} = 1.35 + 0.15d \tag{2.7b}$$

$$f_{h,\alpha,k} = \frac{f_{h,0,k}}{k_{90}\sin^2\alpha + \cos^2\alpha} \tag{2.7c}$$

$$M_{y,Rk} = 0.3 f_u d^{2.6} \tag{2.7d}$$

The shear capacity $F_{v,Rk}$ of a fastener is the minimum value of the timber embedment failure or timber embedment failure combined with fastener yielding. These two failure modes are described in Eurocode 5. Equation 2.8 represents timber embedment failure and combined failure, respectively. In these equations, $f_{h,0,k}$ can be replaced with $f_{h,\alpha,k}$ in case loading is applied under an angle.

$$F_{v,Rk} = \min \begin{cases} 0.4 f_{h,0,k} t_1 d \\ 1.15\sqrt{2M_{y,Rk} f_{h,0,k} d} \end{cases} \tag{2.8}$$

For fasteners F1-F3, the values of F_{max}, k_p, and k_p can be based on literature. This will reduce the amount of single nail tests that need to be done, but it also reduces the reliability of the results. Chapter 6 contains a discussion on this topic. Sawata et al. [Sawata et al., 2006] defined a relationship between yield and ultimate load for bolted connections in timber, which can be used for F1 and F3. A safe estimate of maximum strength

$F_{max} = 1.10F_y$ is retrieved from this paper for bolted connections, nailed connections have more plastic region, so for F3 the relation equals $F_{max} = 1.6F_y$. Plastic stiffness is defined as $k_p = \frac{1}{50}k_e$ (the behavior of timber fasteners can, in contrast to bamboo fasteners, be seen as bilinear with almost pure plastic behavior after the yield point), and ultimate stiffness or decay parameter $k_u = -\frac{1}{30}k_e$. For fastener type F2, the relations between yield and ultimate parameters are derived in section 2.3.3.

2.3.3 Doweled connections in bamboo

The capacity of doweled connections in *Bambusa blumeana* has been thoroughly examined in the paper titled *Experimental Study on the Dowel-Bearing Strength of Bambusa blumeana Bamboo Used for Sustainable Housing Construction* [Bangoy et al., 2024]. The mean bearing strength F_v of a doweled connection in bamboo, loaded symmetrically, equals $9.48kN$. Bangoy et al. mention nothing about the stiffness of this doweled connection. This paper gives a range for the values that can be expected for the embedment strength and shear resistance of *Bambusa blumeana*. For the derivation of the actual value used for calculation, see section 2.3.4 where an equation for the embedment stress is given.

Meanwhile, the stiffness of doweled connections has been described in abundant detail in *Stiffness characterization of bolted multi-culm bamboo members* [Khodabakhshi et al., 2025]. Khodabakhshi et al. developed a formula for the embedment stiffness of bamboo. This formula utilizes a dimensionless embedment elastic modulus E_{emb} retrieved from previous research [Mouka and Dimitrakopoulos, 2022]. Equation 2.9 evaluates the stiffness of a doweled connection in bamboo. Note that it is only related to the wall thickness, the bolt diameter, and the density of the bamboo used.

$$K_{emb} = 2t\psi_E \rho g d \tag{2.9}$$

In this equation, t is the bamboo wall thickness, ρ is the density of the bamboo culm, g is the gravitational acceleration, and d is the bolt diameter. Parameter ψ_E is evaluated using equation 2.10. Note that in this equation, the unit magnitude differences are compensated by the multiplication term.

$$\psi_E = 4.7 \times 10^{-3}\left[\left(\frac{t}{d}\right)^{0.66} + 0.4\right] \tag{2.10}$$

The stiffness of fastener type F2 will be based on the proposed equation. In their research, Khodabakhshi et al. point out that the E_{emb} value results in a slight overestimation of K_{emb}, and that the most accurate stiffness value follows from incorporat-

ing a lower bound value of E_{emb}. In their reseach, Khodabakhshi et al. point out that because of plastic deformation, the maximum capacity for bolted connections equals $F_{max} = 1.1F_y$ For the plastic stiffness, a safe estimate of $k_p = \frac{1}{40}k_e$ can be used. The ultimate stiffness is defined as $k_u = -\frac{1}{30}k_e$.

2.3.4 Nailed connections in bamboo

Whereas bolted or doweled connections in bamboo have already been a common research subject, smaller sized connectors such as nails largely remain undocumented. The behavior of screws in *Guadua* bamboo has been analyzed [Trujillo and Malkowska, 2018], and the behavior of a single nail was tested in *Moso* bamboo [Malkowska et al., 2022]. Both references point out that for a good understanding of fastener behavior, derivation of an analytical model is a must. The model can be verified using experimental data.

Such comparison is required for fastener types F4 and F5, which both consider nails connected to bamboo. The research by Malkowska et al. proposes a modified version of equation 2.8 which can be used to calculate shear capacity F_v of a fastener in bamboo, see equation 3.2.

$$F_v = \min \begin{cases} 0.7A_{net}f_v \\ 2t\sqrt{\frac{1}{b}G_f E_0 d \sin\alpha\,(b - d\sin\alpha)} \\ 1.4 \times 0.4dtf_h \end{cases} \tag{2.11}$$

The first section is used to calculate plug shear resistance, with shear area A_{net} and shear stress f_v. The second equation evaluates shear capacity based on splitting of the bamboo. In this equation, G_f represents the fracture energy of the bamboo. A conservative value of $360J/m^2$ is proposed for all bamboo species. E_0 is the elastic modulus which is dependent on the bamboo density, and can be calculated using equation 2.12

$$E_0 = 0.0296\rho - 6.56 \tag{2.12}$$

The angle α relates to the friction coefficient. A conservative friction coefficient of 0.4 is assumed for all bamboo species, resulting in $\alpha = 22°$. Variable b is the diameter of the culm. Finally, the third function in equation 3.2 provides a shear capacity based on the bamboo embedment strength. An alternative method is proposed for determining the embedment strength, see equation 2.13

$$f_h = -54.43 - 1.33t - 3.41d^2 + 28.37d + 0.12\rho \tag{2.13}$$

These equations can be used to describe the behavior of fastener type F5. Herein, the equation relating to plug shear is not considered since plug shear can only occur in situations where a fastener is applied close to an exposed edge of a bamboo stud, which is not the case in CBSW. The behavior of fastener type F4, due to its mortar infill, is more difficult to evaluate analytically. Chapter 3 will derive an additional set of equations that will be verified in chapter 5.

It is emphasized in various papers [Malkowska et al., 2022][Liu et al., 2020][Khodabakhshi et al., 2025] to use the mean values for all material properties when comparing analytical results to experimental results. This is already the case for the elastic moduli or stiffness values, but for the calculations of capacities, it means that average input values should be used instead of characteristic values.

2.4 Protocols and design standards

2.4.1 Experimental procedures

For the validation phase experimental testing will be necessary. International standards exist which prescribe reproducible and standardized testing procedures. Single nail shear tests are executed according to ASTM D1761-20 [ASTM International, 2020]. The full-scale CBSW tests covered in this research are performed according to ISO standard 21581:2010 method I [International Organization for Standardization, 2010]. A full description of these test protocols can be found in appendix B. Single fasteners will be exposed to monotonic tests, six tests will be performed per fastener type. The full shear wall will be analyzed through one monotonic and five cyclic tests per wall configuration.

The paper *Bamboo joint capacity determined by ISO 22156 'complete joint testing' provisions* [Harries et al., 2022] proposes a methodology to evaluate and characterize bamboo structures according to ISO 22156 [International Organization for Standardization, 2021]. The joint testing methodology described in the paper is a way to determine how a bamboo joint actually behaves by testing the complete joint itself rather than trying to calculate its strength from its individual components. The resulting curve from testing is used to determine fastener properties. After these raw values are obtained, they can be turned into design values using statistical rules from ISO 12122 [International Organization for Standardization, 2017]. The results may also be normalised to account for differences in bamboo geometry, such as diameter or wall thickness. Doing this can reduce the scatter in the data and helps ensure that the results reflect the behaviour of the joint rather than random differences in specimen size.

Table 2.1: *Bambusa Blumeana* mean & characteristic values, from [Cacanando et al., 2025].

Property	Mean	Characteristic	Unit
Culm diameter D	97.32	81.68	mm
Wall thickness t	8.12	6.11	mm
Density ρ	721.61	553.43	kg/m^3

Another important takeaway from this paper is a standard value for the ultimate force F_u, which is the point where the fastener fails. This point, if not determined from experiments, is given as $F_u = 0.8F_{max}$. In chapter 3, this point is incorporated into equation 2.5.

2.4.2 Bamboo design values

As mentioned in section 2.1, structural design standards exist for bamboo. ISO 22156:2021 [International Organization for Standardization, 2021] gives an overview of how to determine design values for all mechanical properties of bamboo used for structural applications. As mentioned in section 1.2.2, bamboo species *Bambusa Blumeana* is applied in the CBSW in this research. Extensive research into the properties of this species has been executed [Cacanando et al., 2025]. The mean and characteristic (fifth percentile with 75% confidence) values resulting from the work of Cacanando et al. are used in this research, see table 2.1.

2.5 Synthesis

This section combines the findings and lessons from literature. Summarizing the literature will result in a retraceable and concise overview of insights on which the next chapters will be based.

Bahareque is a traditional antecedent to CBSW, the main improvement lies in the use of cladding rather than mud infill. CBSW is a more ductile, higher capacity bamboo system when designed according to the guidelines. Previous tests have yielded results that indicate the potential capacity of CBSW, but because of observed failure modes in these experiments, these tests failed to accurately describe the behavior of CBSW. Additional testing is required.

Fasteners dictate the behavior of LFT shear walls, Folz & Filliatrault suggest modelling

the fastener force–displacement and assembling a wall-level model based on the individual behavior. The model predicts cyclic response well, including pinching and degradation. Their nonlinear piecewise model is a practical template. Meanwhile Källsner & Girhammar provide an analytical elastic model for fully anchored LFT walls assuming identical fastener properties. They derive closed-form relations for rotation and capacity. Their model highlights that corner fasteners yield first and intermediate fasteners have limited effect on peak capacity. Using the equations for φ and γ, the horizontal yield capacity can be determined, although the presence of multiple fastener types requires some extra attention. When considering the stiffness of the fasteners, a nonlinear force-displacement relationship will be assessed in the CBSW model.

Modeling of the nonlinear force-displacement is linked to an equation containing four main variables, k_e, F_{max}, u_{max}, and k_u. This equation is fitting for fasteners showing no distinct pre- and post-yielding behavior, as is the case in CBSW. To create an accurate CBSW model, the bearing capacity and elastic stiffness of each fastener should be obtained. For fastener types F1 and F3, the EYM can be used. For bamboo fastener F2, the work of Malkowska et al. is considered for F_v, and the work of Khodabakhshi et al. is considered for K_{emb}. Fasteners F4 and F5 also incorporate bamboo, but there is insufficient research to retrieve reliable data from for the model. Testing of fastener types F4 and F5 is required. Through comparison with an analytical method, the most suitable bearing capacity and stiffness should be derived. See section 3.1 and table 3.1 for an overview of the available information on fastener types.

Experiments will be executed according to ASTM D1761-20 and ISO 21581:2010 standards for single fastener and full-scale tests, respectively. Both single fastener and full-scale wall tests are executed to validate analytical methods. Statistical treatment through ISO 12122 determines characteristic values.

Chapter 3

Theoretical approach

This chapter develops an approach for calculating the shear capacity of a CBSW panel using the findings from chapter 2 and theoretical knowledge. The remaining fastener equations, those applying to fastener type F4 are determined. Afterwards, a stepwise method is developed which can be used to determine the shear capacity at any given deformation of a CBSW panel.

3.1 Fastener forces

3.1.1 Fastener displacements

For the overview of fastener types, readers are redirected to table 1.1. From literature, a value for F_y, F_{max}, F_u, k_e, k_p, and k_u has been evaluated for fastener types F1-F3. The displacements can now be determined based on these inputs through equations 3.1:

$$u_y = \frac{F_y}{k_e} \tag{3.1a}$$

$$u_{max} = u_y + \frac{F_{max} - F_y}{k_p} \tag{3.1b}$$

$$u_u = u_{max} + \frac{F_u - F_{max}}{k_u} \tag{3.1c}$$

3.1.2 Derivation using EYM

Fastener types F4 and F5 will be evaluated based on experimental test results. However, deriving equations for the capacity of these fasteners will aid in (a) forming a full understanding of the behavior causing failure of these fasteners and (b) presenting possible improvements. As discussed in chapter 2, fastener types F1, F2, F3, and F5 have exist-

Table 3.1: Overview of CBSW fastener types and available equations for properties.

	k_e	F_y	F_{max}	u_{max}	F_u	k_u
F1	$\frac{1}{30}\rho_m^{1.5}d^{0.8}$	$1.15\sqrt{2M_{y,Rk}f_{h,0,k}d}$	$1.1F_y$	$\frac{F_y}{k_e}+\frac{F_{max}-F_y}{k_e/50}$	$0.8F_{max}$	$-\frac{1}{30}k_e$
F2	$t\psi_E\rho g d$	$1.4\times 0.4dtf_h$	$1.1F_y$	$\frac{F_y}{k_e}+\frac{F_{max}-F_y}{k_e/40}$	$0.8F_{max}$	$-\frac{1}{30}k_e$
F3	$\frac{1}{30}\rho_m^{1.5}d^{0.8}$	$1.15\sqrt{2M_{y,Rk}f_{h,0,k}d}$	$1.6F_y$	$\frac{F_y}{k_e}+\frac{F_{max}-F_y}{k_e/50}$	$0.8F_{max}$	$-\frac{1}{30}k_e$
F4 F5	*From experiments*					

ing methods for capacity and stiffness calculations. Fastener type F4 consists of a nail inserted in a bamboo culm with mortar infill. The mortar infill acts as an extra restraint for the nail. Pure embedment failure of the bamboo as observed in fastener type F5 is no longer a realistic failure method. Instead, a combined failure mechanism should be considered, such as the EYM from Eurocode 5. In the case of fastener F4, embedment failure of the bamboo and yielding of the nail is considered simultaneously in figure 3.1(a). Alternatively, represented in figure 3.1(b), the bamboo wall is sufficiently thick, and yielding of the nail will occur in the culm wall. A third failure mode that can be considered is splitting, according to the second part of equation 3.2. Appendix C contains the full derivation of the failure mode equations. Accordingly, failure of fastener type F4 is determined by:

$$F_{v,F4} = \min \begin{cases} \frac{M_y}{t_1} + \frac{t_1}{2} d f_h \\ 1.15\sqrt{2M_y d f_h} \\ 2t\sqrt{\frac{1}{b} G_f E_0 d \sin\alpha (b - d\sin\alpha)} \end{cases} \tag{3.2}$$

The values of M_y, f_h, and E_0 can be evaluated using methods described in section 2.3. Chapter 5 will see the validation and application of this equation. With the theory of fasteners complete, all information on fastener calculation is gathered in table 3.1. The validation of failure modes of fasteners is not included in this table, but instead will be discussed in chapter 5.

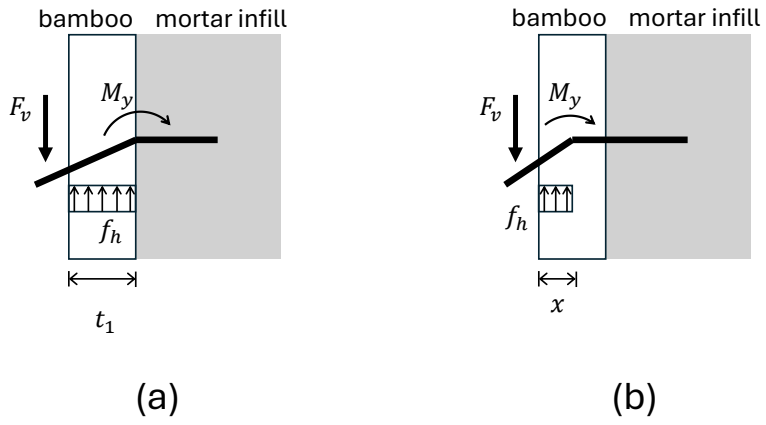

Figure 3.1: Free body diagrams of fastener type F4 comprising (a) bamboo culm with thin wall and (b) bamboo culm with thick wall.

3.2 Static model

Relying on the literature from chapter 2, the best approach for determining shear wall yield capacity is by considering a static model of said shear wall. See figure 4.1. Consider a shear wall with a frame consisting of timber beams, bamboo studs, and optional flat bar bracing. The connections between the studs and the timber beams are assumed to be hinges, and the flat bar bracing is considered to be incorporated in the cladding. The cladding is a matrix of either rib lath or *tadtad* which is plastered in a layer of cement mortar, and it is connected to the frame via fasteners. The shear wall has a height h and width b. The number and spacing of studs depends on the configuration of the shear wall. Frame-to-cladding fasteners are distributed over the frame by a spacing s. Consider the exemplary case in figure 4.1 where five studs are used and the aspect ratio $h : b$ equals $1 : 1$. The frame is considered to be fully clamped along its base, and forces or displacements out of plane are not considered. Next, a horizontal force H is introduced at the top left corner. Force H causes the frame to deform over a distance u_{SW} horizontally, resulting in a rotation angle γ. External forces in tension R_t and compression R_c occur at the left and right corners at the base of the shear wall, respectively. The cladding connects to the frame through the fasteners which are symmetrically distributed around the centroid of the cladding. As the frame deforms it causes a rotation of the cladding around its centroid, with rotation angle φ.

Consider now a coordinate system (x, y) with its origin at the centroid of the cladding.

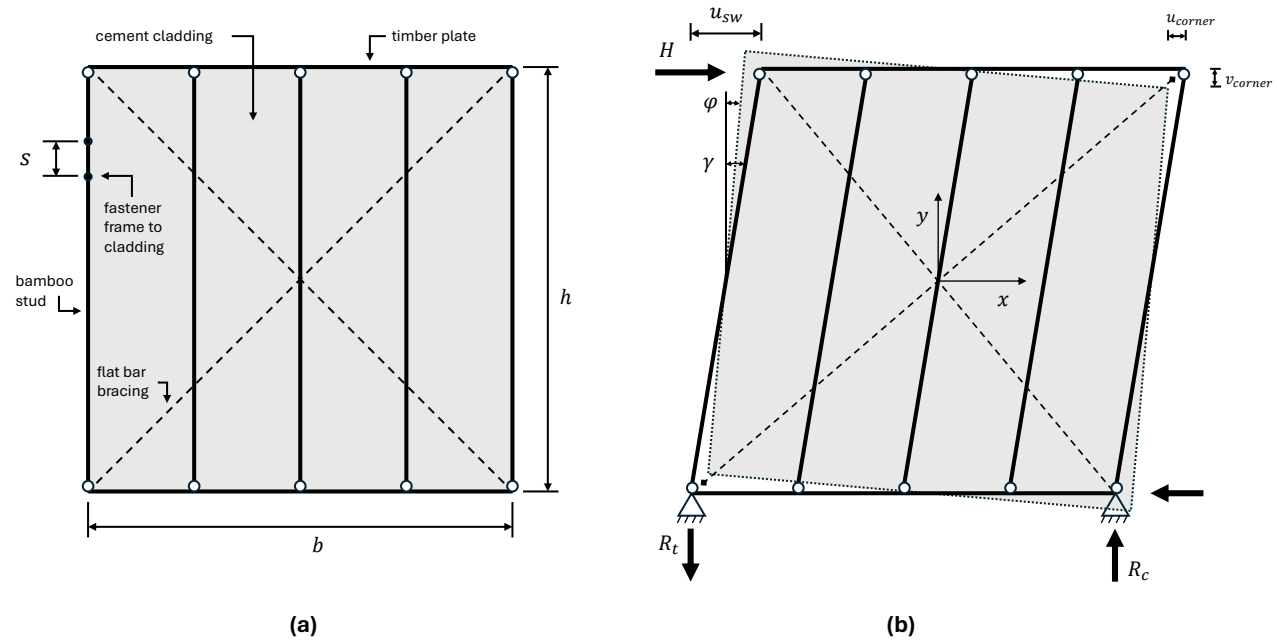

Figure 3.2: (a) schematic of CBSW panel. (b) static model of CBSW panel.

Each individual fastener has a unique position in this coordinate system on the frame, and a corresponding position on the cladding. As force H increases, the distance between the frame and cladding positions of the fasteners increases. This difference in displacement, which is equal to the fastener slip, can be evaluated discretely, since the angles φ and γ can be calculated.

The equation that Källsner and Girhammar proposed to determine the yield capacity only applies to fasteners with the same stiffness properties. This theory can be extended to the case of CBSW, where a total of five fastener types are considered. The idea is that if the yielding of the outermost fastener is considered, and the capacity of the fasteners does not increase after yielding, then the yield capacity can be calculated per fastener type. Consider also the alternative modeling approach, using equation 2.5. The capacity of each fastener extends beyond the yield point. If then instead the maximum capacity of the outermost fastener is considered, a more realistic approach of the yielding of fasteners is considered. To achieve this approach, the shear capacity F_v in equation 2.3 should be replaced with the maximum capacity F_{max}, and evaluated per fastener type. The yield capacity of the shear wall is then defined as the sum of the individual fastener type yield capacities. The yield capacity of a CBSW panel is is evaluated

as per equation 3.3, based on equation 2.3.

$$F_y = \sum_{i=1}^{n} \frac{F_{max,Fi}}{h\sqrt{\left[\frac{x_{Fi}}{\sum x_{Fi}^2}\right]^2 + \left[\frac{y_{Fi}}{\sum y_{Fi}^2}\right]^2}} \tag{3.3}$$

Note that since the stiffness is considered equal for all fasteners within the same fastener type group, it has no influence on the eventual yield capacity.

3.3 Nonlinear model

Contrary to the situation where a constant stiffness is assumed for all fasteners, the nonlinear model assumes all fasteners to have variable stiffness. Consider equation 2.5 which defines a value for the capacity of a fastener for a given slip s. The stiffness of this system can be defined as $k = \frac{\partial F}{\partial s}$. This results in the following equation:

$$k = \begin{cases} k_e \exp\left(-\frac{k_e}{F_{max}} s\right), & \text{if } s < u_{\max} \\ k_u, & \text{if } u_{\max} \leq s \leq u_u \\ k_u, & \text{if } s > u_u \end{cases} \tag{3.4}$$

In this equation, the decay parameter or ultimate stiffness is preserved to accurately model the decay of the shear wall. If the stiffness would instead be reduced to zero, the model would flatten out after a certain displacement, and thus give limited to no information about the post-peak behavior of the shear wall.

Appendix D contains the full derivation of the relation between φ and γ, with equations 3.5 as a result. Note the slight difference compared to the equations derived by Källsner & Girhammar, presented in section 2.2. Where for LFT, it could be assumed that all fasteners are similar and thus share the same stiffness, this assumption cannot hold for CBSW, as proven in section 2.3. Therefore, the stiffness is included in the summand terms.

$$\varphi = Hh \frac{1}{\sum_{i=1}^{n} k_i x_i^2} \tag{3.5a}$$

$$\gamma = Hh \left[\frac{1}{\sum_{i=1}^{n} k_i x_i^2} + \frac{1}{\sum_{i=1}^{n} k_i y_i^2} \right] \tag{3.5b}$$

The relation between these angles, addressed as $\frac{\gamma}{\varphi}$, equals

$$\frac{\gamma}{\varphi} = 1 + \frac{\sum_{i=1}^{n} k_i x_i^2}{\sum_{i=1}^{n} k_i y_i^2} \tag{3.6}$$

This relation is important for determining angle φ. Angle γ is related to the displacement u_{SW}, and can thus be evaluated relatively easily. One point for discussion is how accurately the ratio between the two angles should be determined. As the stiffness of fasteners is expected to decrease for increasing deformations, the relations between $\sum_{i=1}^{n} k_i x_i^2$ and $\sum_{i=1}^{n} k_i x_i^2$ (hereafter addressed as $\sum k_i x_i^2$ and $\sum k_i y_i^2$) might change. As a result, angle φ will display a different rotation pattern than angle γ. For the sake of simplification, the ratio $\frac{\gamma}{\varphi}$ is considered at zero displacement, when all fasteners retain their full elastic stiffness. Appendix D contains a full derivation of $\sum k_i x_i^2$ and $\sum k_i y_i^2$, depending on which fastener types are considered.

Angle γ, as mentioned, relies on shear wall displacement $u_S W$. This has a big advantage; if an incremental displacement δu_{SW} (hereafter addressed as δu) is considered, equation 3.5b can be used to evaluate the difference in horizontal capacity δH. The derivation starts at the equation for $\delta\gamma$:

$$\delta\gamma = \frac{\delta u}{h} \tag{3.7}$$

Substituting this in equation 3.5b yields

$$\frac{\delta u}{h} = \delta H h \left[\frac{1}{\sum k_i x_i^2} + \frac{1}{\sum k_i y_i^2} \right] \tag{3.8}$$

Rewriting this equation will lead to a relation for the shear wall stiffness, K.

$$\frac{\delta H}{\delta u} = \frac{1}{h^2} \left[\frac{1}{\frac{1}{\sum k_i x_i^2} + \frac{1}{\sum k_i y_i^2}} \right] \rightarrow K = \frac{1}{h^2} \left[\frac{\sum k_i x_i^2 \sum k_i y_i^2}{\sum k_i x_i^2 + \sum k_i y_i^2} \right] \tag{3.9}$$

For any given δu, the horizontal capacity H can be evaluated by measuring the area under the curve of K. In other words, the horizontal capacity is equal to the integral of K with respect to u. Consider an infinitesimally small value for the displacement, du, the equation for the capacity of the shear wall then becomes:

$$H = \int K du \tag{3.10}$$

There is unfortunately no direct way to expand the integral presented in equation 3.10, since it relies on the stiffness of each fastener. The summand terms have a different value for any increment of du. This underlines the necessity of a model space, so that iterations can be performed without requiring labor-intensive hand calculations. Using the equations of this chapter and chapter 2, the horizontal capacity of a CBSW panel can be predicted. Chapter 4 elaborates the translation from theoretical equations and assumptions to a parametrized workflow, resulting in an adaptable and configurable model used for prediction of any arbitrary configuration of CBSW panel.

Chapter 4

Model development

This chapter elaborates on the logic steps taken to reproduce the theory from chapter 3 and 2 for implementation of real data. So far, only theory has been discussed. The goal of this chapter is to develop a model that can handle unique input data, to result in an accurate prediction.

4.1 Geometry

The first step in the modeling process is determining what input parameters are required. First parameters to be considered are the geometrical properties of the wall, hence the title of this section. Based on input values for height h, width b, fastener spacing s, and number of studs n, the locations of all fasteners can be determined, see figure 4.1. The timber beams each facilitate $b/s+1$ fasteners. On each of the bamboo studs, $h/s-1$ fasteners can be found. The spacing between studs can be derived as $b/n-1$. What type of fastener can be found where depends on another input parameter; which wall type (from table 1.1) is used.

Consider a CBSW of standard dimensions including bracing (WT1). In this case, the fasteners located at the intersection of frame member and flat bar are assigned as bolts. Fasteners F1 are located in the four corners of the frame. Fasteners F2 are located along the intermediate and middle stud. The timber beams contain fastener type F3. Fastener types F4 and F5 can be found on the bamboo studs. The mortar infill is applied to the edge and center studs, and can be found in the top and bottom nodes of these studs. Fasteners F4 are considered to be present at the first and last four fastener positions on the edge and center studs, this is based on the description of CBSW configuration from section 1.2.1. The remaining fasteners all belong to F5. Appendix D contains a quantification of fasteners for an exemplary WT1 shear wall.

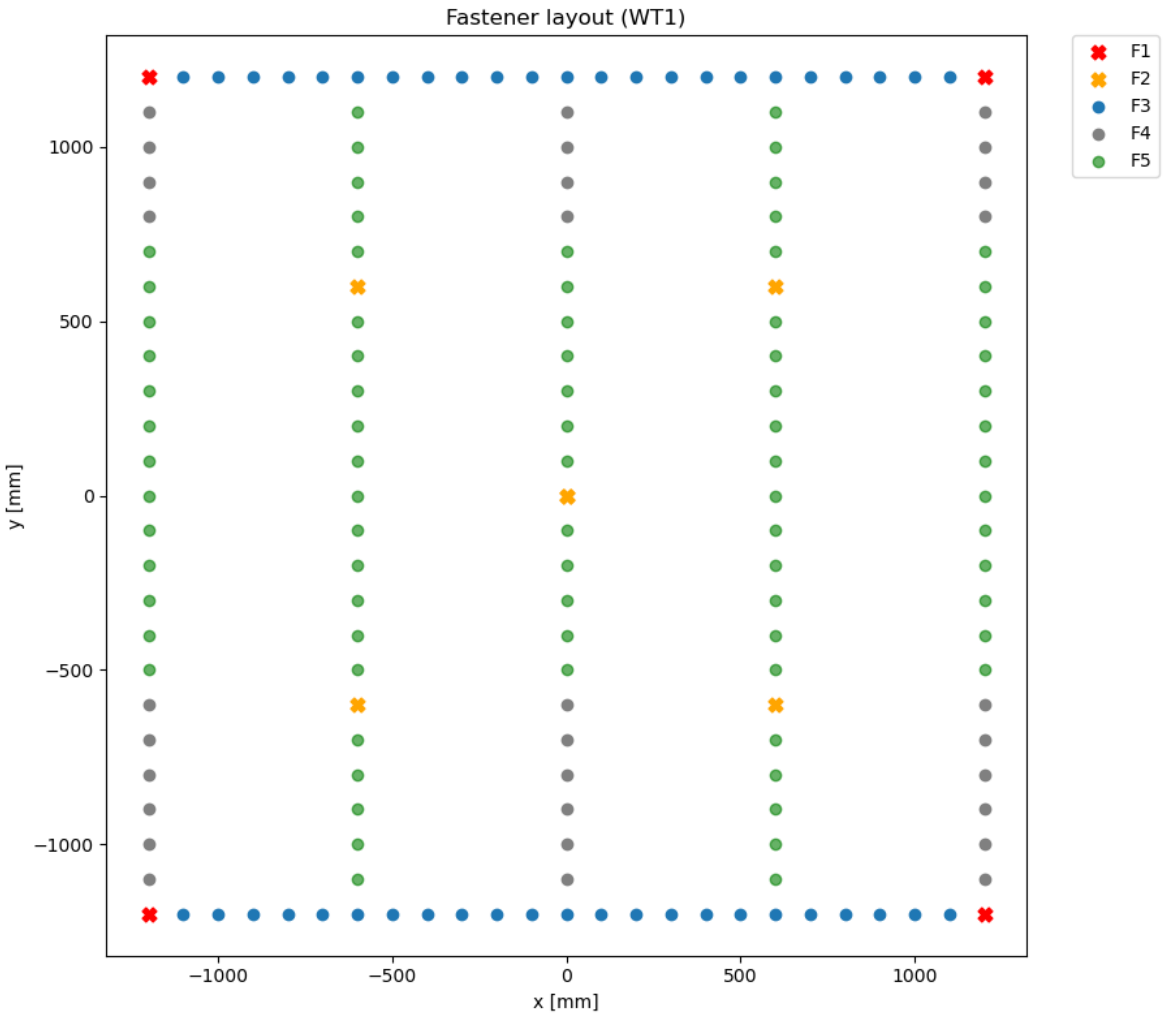

Figure 4.1: Exemplary modeled layout of fasteners in WT1.

4.2 Fastener properties

Now that the position of fasteners has been determined, the corresponding properties can be assigned. As mentioned in chapter 2, each fastener type has unique properties. The inputs for the fasteners relate to the equations that have been proposed for each individual fastener type. The outputs are the the fastener properties, and they are similar for each fastener type. The outputs are the elastic and ultimate stiffness (k_e, k_u), maximum force (F_{max}), and the displacements at the maximum force and ultimate force (u_{max}, u_u). Fastener types F1, F2, and F3 have unique calculation steps that lead to the output values. The outputs of fastener types F4 & F5 are evaluated through experiments.

Figure 4.2 contains an overview of all the calculation steps taken in the preparation for the actual calculation of CBSW capacity. The geometry and properties of the fasteners are evaluated separately. Due to this separate calculation approach, it becomes easier to apply changes to either one of these workflows. This is beneficial for the implementation of shear wall improvements, see section 4.4.

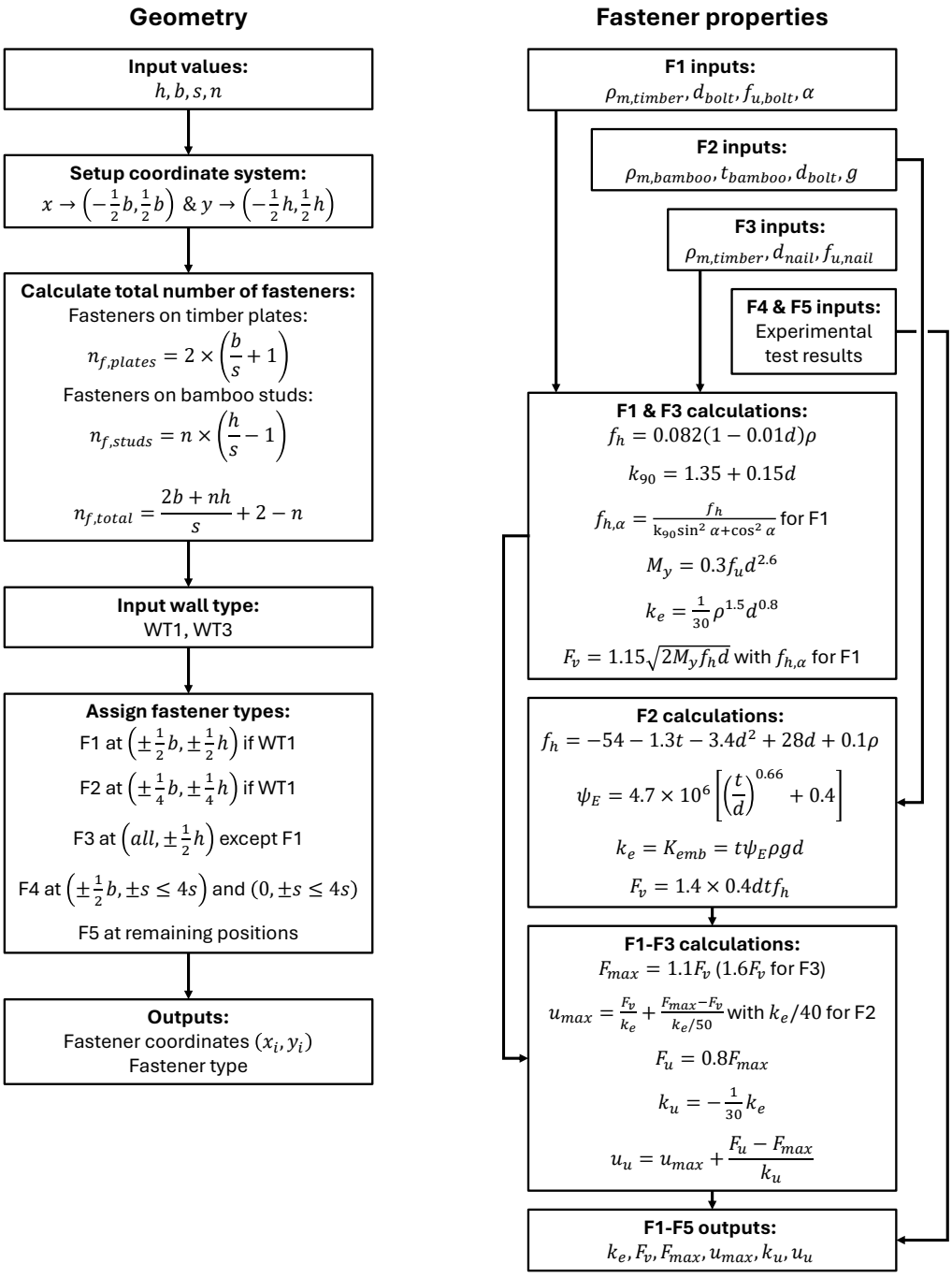

Figure 4.2: Schematic of calculation steps for geometry and fastener properties inputs.

4.3 Calculation space

When all the required inputs for the model are calculated, they can be collected and a workflow for the actual model can be set up. Based on the fastener geometry and properties alone, two preliminary calculations are made. The first is the calculation of the horizontal yield force F_y, as described in section 3.2. This calculation does not depend on the stiffness of the fasteners, only on the shear capacity $F_{v,i}$. The other preliminary calculation is the ratio (hereafter addressed as ξ) between angle φ and γ. As mentioned in section 3.3, ratio ξ is determined at $u = 0$ to simplify the calculations. Exploratory calculations point out that a constant value of ξ yields almost exactly the same results as varying ξ.

After the initial calculations an iterative loop is introduced in the calculation workflow. Since a nonlinear stiffness is assumed for the fasteners, each new slip value will result in a new stiffness value. The calculation of the shear wall is segmented into increments of δu to incorporate this variable stiffness of each fastener. The resolution of the model is dependent on step size δu. The displacement of the shear wall is defined as the displacement of the previous step plus the incremental displacement: $u_j = u_{j-1} + \delta u$. The loop is repeated until $u_j = u_{last}$, which will be based on experimental results.

For each iteration, the calculations as mentioned in section 3.3 are repeated. The outcomes of each iteration are collected to form a list for displacement u, horizontal capacity H, and shear wall stiffness K. Additionally, the yield point of the shear wall and the maximum point are evaluated.

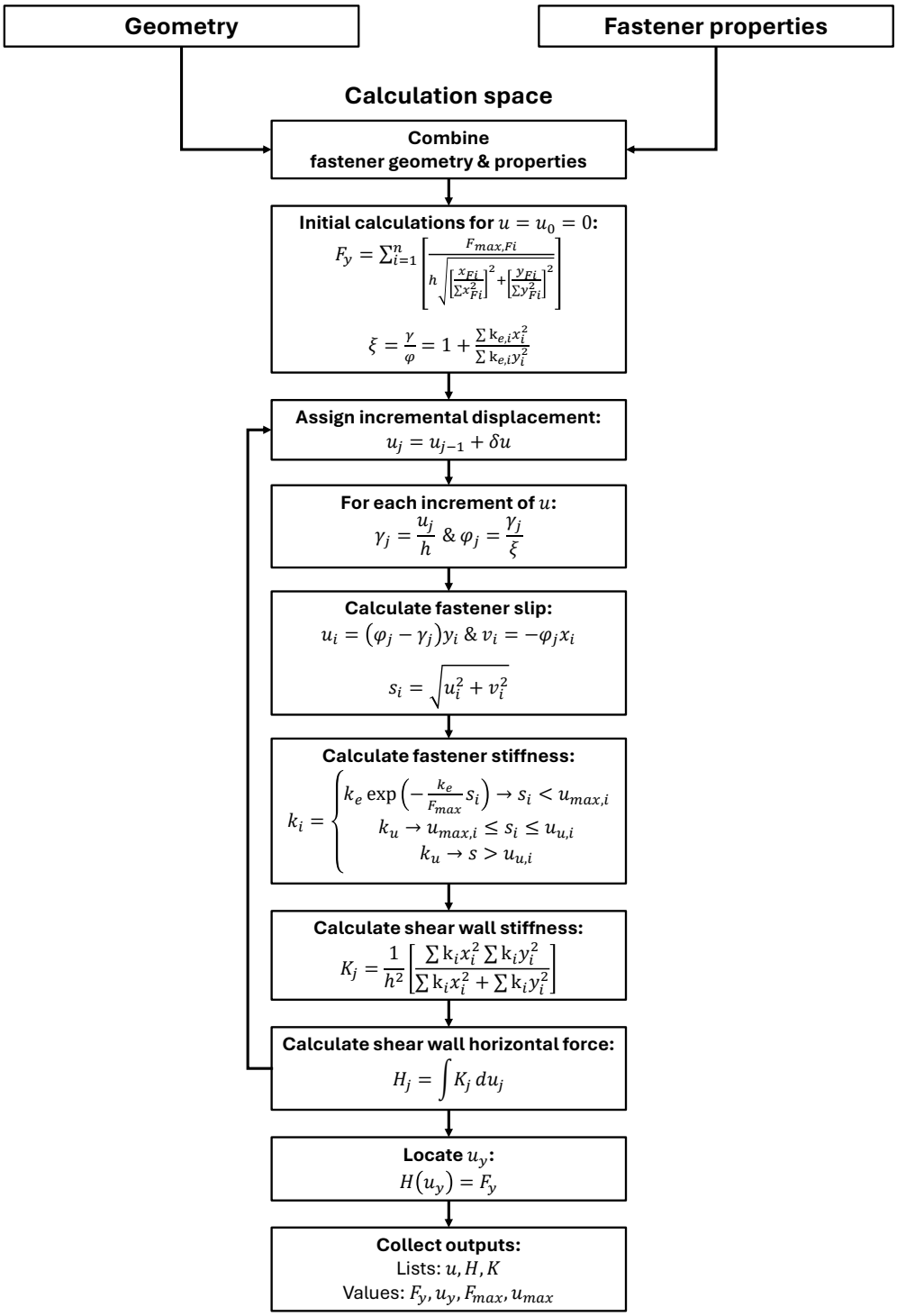

Figure 4.3: Schematic of calculation steps of CBSW model.

4.4 Comparison with experimental results or improvements

The result of the calculation is a list of the displacements, and the horizontal capacity and stiffness corresponding to each displacement value. These can be displayed in a force-displacement or stiffness-displacement diagram for quick visual comparison with the experimental results. Alternatively, the main points of interest (yield point, maximum point, ultimate point) are also collected so that they can be compared in a table.

The segmented approach of the model makes it easy to adapt certain sections and afterwards run the model as usual. This is especially beneficial for the comparison of the initial model with improved adaptations of the CBSW panel. Improvements only affect the geometry or the fastener properties, so the calculation space can remain unchanged. The same iterations can be calculated for proposed improvements, and the same output variables can be collected.

This concludes the description of the proposed analytical CBSW model. All the necessary steps and constraints have been discussed. As a result, a clear and reproducible workflow has been presented. In the following chapter, real experimental data will be collected and applied in the model to validate the analytical CBSW model.

Chapter 5

Validation and application

The goal of this chapter is twofold: first, experimental tests will be described and evaluated, to which the model will be validated. Second, possible improvements of the model will be applied and compared to the original model, so that advice can be presented on possible improvements of the CBSW system. This table contains all the results and an evaluation of those results. The outcomes of testing will be summarized in chapter 6, as well as points up for discussion.

5.1 Experimental testing

The experimental testing consists of two separate parts. First, the single nail tests that have been performed will be presented. This section also contains a statistical analysis of the results, on which the fastener properties necessary for the analytical model will be based.

5.1.1 Fastener test setup

As mentioned in section 2.5, the single nail tests are based on ASTM D1761-20. This concerns monotonic nail testing, where the setup is loaded once until failure. See figure 5.1 for the applied test setup. Since a realistic representation of actual loading conditions is preferred, a complete section of the shear wall has been considered in the test setup. A section of bamboo stud with a length of $500mm$ is attached to a timber beam according to the bamboo stud to timber beam connection description presented in section 1.2. The stud and plate are constrained by a clamping plate, which connects to the testing frame through four bolts. A small, rectangular patch of rib lath is nailed to the bamboo stud using a single $1'1/2$ inch nail. The dimensions of this patch are assumed to have no significant effect on fastener shear capacity, so a patch size of $200 \times 400mm$ is chosen

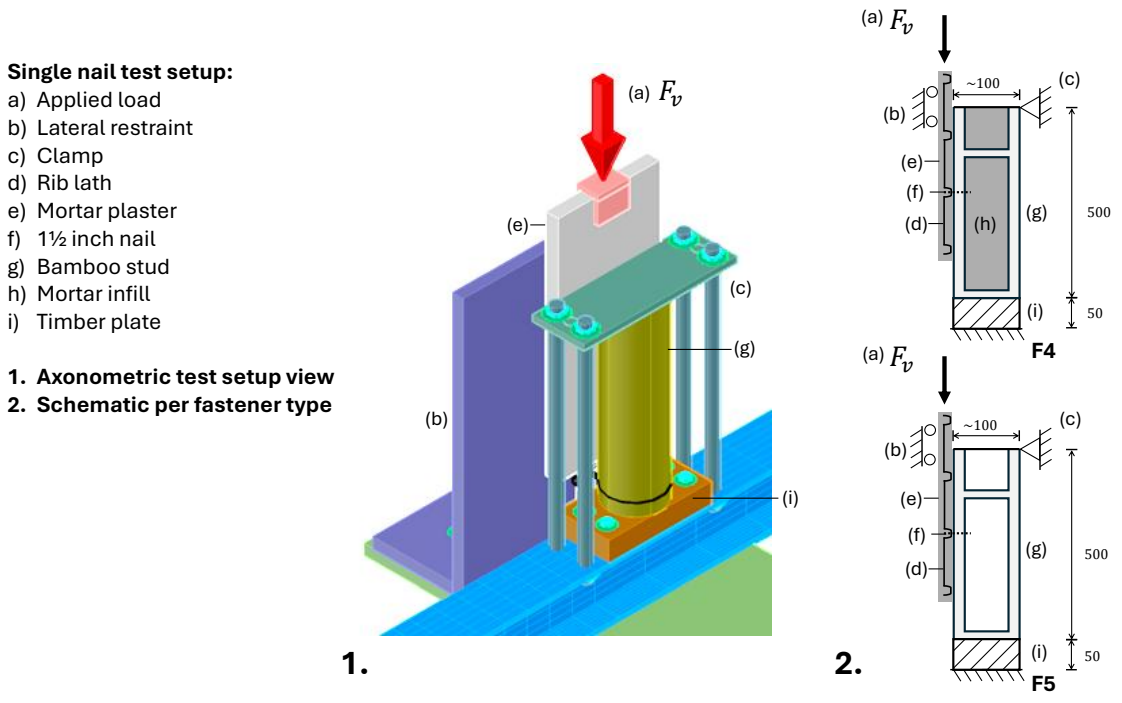

Figure 5.1: Test setup used for fastener type F4 and F5.

for convenience. The rib lath is plastered with a $25mm$ layer of cement mortar, as specified in section 1.2. Together, the rib lath and mortar plaster form the cladding. A rolling lateral restraint is placed against the cladding to prevent prying of the nail or buckling of the cladding. In case fastener type F4 is tested, mortar infill is applied to the bamboo stud after insertion of the nail. This resembles the actual fabrication process.

A vertical load is applied on the cladding. Due to the lateral restraint of the cladding, and clamping of the frame, displacement of the nail is forced. Tests are performed using a Universal Testing Machine (UTM). The UTM records the applied load in Newtons. A Linear Variable Differential Transformer (LVDT) measures the displacement of the cladding. Data from UTM and LVDT is gathered on an Almemo testing device. Six specimens are tested per fastener type, resulting in a total of twelve tests. Outputs of the test are a force-displacement diagram, using the force measured by the UTM and a displacement measured by the LVDT. The test results have been gathered in table 5.1.

In order to use the data from these tests in a CBSW model, the values from table 5.1 should be validated. Validation of these values is done through statistical analysis. The nonlinear curve that will be used in the model is compared to the mean curve of the test data. It can be constructed using the data from the results table. The yield forces

Table 5.1: Overview of retrieved test values of fasteners F4 & F5.

Test ID	F_y [N]	F_{max} [N]	u_{max} [mm]	k_e [N/mm]	k_u [N/mm]	u_u [mm]	t [mm]
F4-S1	663.1	1102.4	4.7	782.0	−22.7	15.2	7.30
F4-S2	418.9	869.6	20.1	157.6	−46.3	24.9	6.83
F4-S3	532.5	550.1	2.7	259.9	−56.5	6.4	6.93
F4-S4	437.1	737.3	5.0	706.7	−145.0	11.7	7.33
F4-S5	778.2	890.2	4.0	533.9	−314.2	5.1	8.20
F4-S6	952.0	1749.2	9.8	639.0	−159.6	17.7	10.23
F4 (mean)	**559.9**	**839.7**	**4.2**	**479.5**	**-42.6**	**13.5**	**7.80**
F5-S1	324.8	669.7	8.3	138.8	−45.6	23.3	6.60
F5-S2	321.7	624.3	6.2	216.0	−44.1	23.3	6.50
F5-S3	385.8	442.5	2.1	374.0	−33.6	21.4	7.30
F5-S4	653.9	833.9	5.3	335.2	−92.3	18.5	12.00
F5-S5	471.9	696.9	5.8	313.9	−34.2	21.1	8.80
F5-S6	331.8	747.3	12.8	132.1	−31.4	23.3	7.20
F5 (mean)	**387.5**	**674.2**	**12.9**	**221.7**	**-37.4**	**21.8**	**8.07**

presented in the table are compared to the fastener shear capacity equations obtained in chapter 3. This comparison is then also statistically analyzed. Statistical analysis will be performed through means of root mean square error (RMSE), mean absolute error (MAE), and coefficient of determination $\left(R^2\right)$.

5.1.2 Results and statistics F4

The results of the experiments of fastener type F4 can be summarized in the following points:

- All F4 specimens exhibited similar failure patterns, indicating consistent overall behavior up to failure. Nail yielding and bamboo embedment failure were observed in each specimen.
- An unexpected failure mode was consistently observed in F4 specimens: rib lath rupture. This failure mode is unpredictable, as it occurred anywhere between a displacement of 5 and 25 mm. Testing F4 with an alternative setup (a vertical row of three nails instead of one) did not improve the predictability of failure.
- More precise or refined testing is recommended for fastener type F4, as discussed further in Chapter 6.

See figure 5.2 for the force-displacement diagrams resulting from the experiments. Testing has resulted in a clarifying overview of fastener behavior in bamboo studs, and

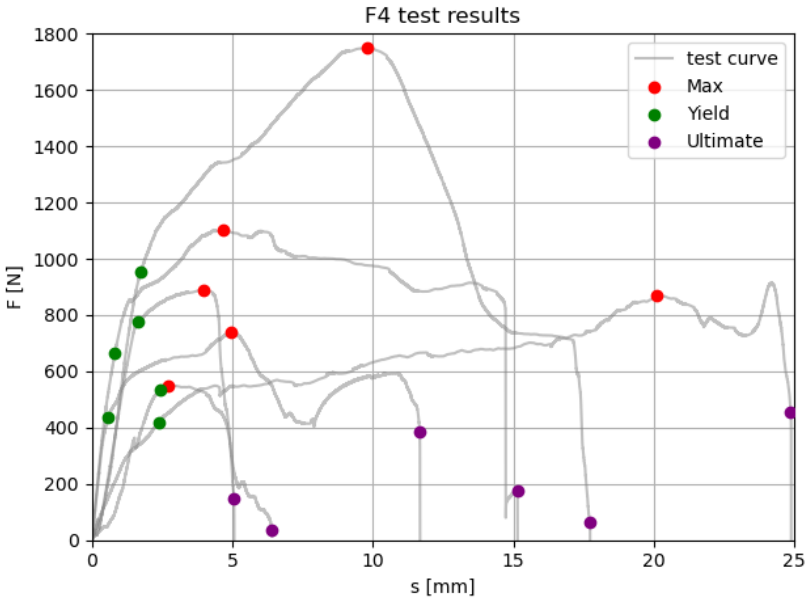

Figure 5.2: F4 experimental results, force-displacement diagram.

it has proven that fastener type F4 and F5 have very distinct behavior. The specimens of fastener type F4 all showed similar failure patterns, see figure 5.3. Nail yielding and bamboo embedment failure has been recorded in all F4 specimens. For all of these experiments, a somewhat unexpected failure mode was documented. After a yielding plateau has been reached, these fasteners fail because of rib lath rupture, indicated by an instant drop in capacity. This drop is very sudden and the displacement at which this drop occurs ranges from as little as $5mm$ until $25mm$. The rupture is an unpredictable failure mode. Fastener type F4 was also tested using a different test setup where instead of one nail, a row of three nails was applied vertically, but it did not yield better results in terms of predictability of failure.

The average values of fastener type are used in equation 2.5. The outcome has been modeled and plotted against the average curve resulting from all F4 fastener tests. Comparing the two graphs can be done by measuring the difference between them, resulting in a residuals graph. The full analysis of the comparison can be found in appendix E. The analysis results in an R^2-value of 0.871, indicating relatively good correlation between the model and the average curve of F4. However, the analysis also indicates that there is a lot of variance, especially after a displacement of approximately $15mm$. This can be seen from the standard deviation, which increases spontaneously at this displacement. This indicates that more concise testing might be necessary for fastener type F4, this is discussed in further detail in chapter 6.

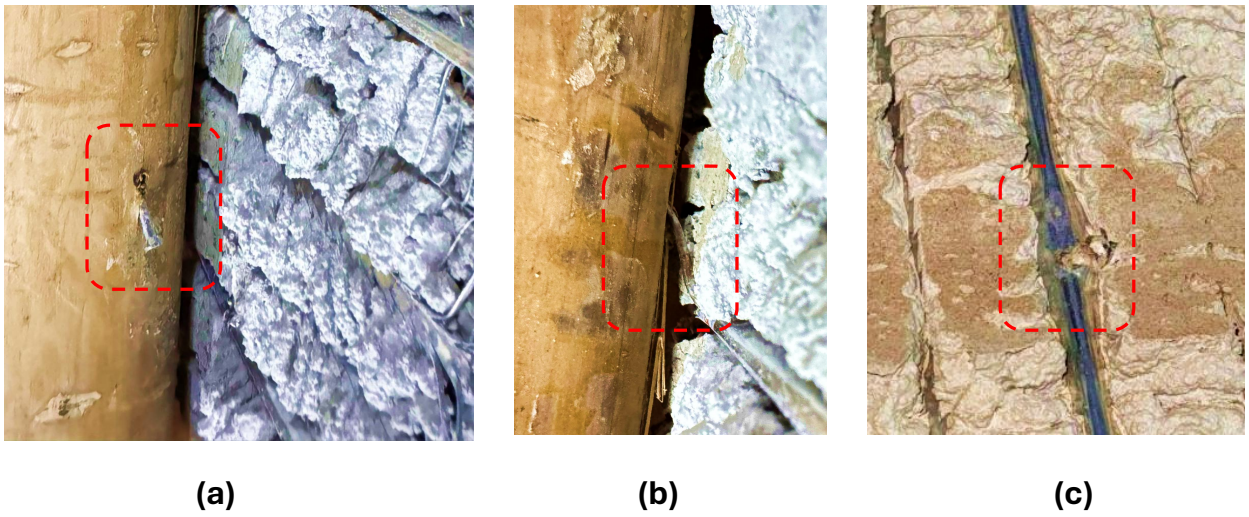

Figure 5.3: Recorded failure modes of fastener type F4: (a) bamboo embedment failure, (b) nail yielding, (c) rupture of rib lath.

Finally, the fastener capacity will be compared with capacity predictions based on section 3.1. To perform these calculations, some input values are needed. They are collected in table 5.2. The minimal value of F_v is chosen, and compared to F_y from F4 experiments. The individual experiments are compared to the outcome of the equations using the bamboo wall thickness from table 5.1.

See figure 5.4. All three functions in the proposed shear capacity equation yield at least one minimal value. This indicates that for fastener type F4, where mortar infill has been added, the bamboo behaves less predictable. Splitting caused failure three times, and the other three times combined yielding caused failure. Only in one case was the bamboo wall thickness sufficient to cause a plastic hinge to form within the bamboo itself. The R^2-value equals 0.76, which is low compared to the fitness of the nonlinear prediction curve. This relatively low number is caused by the uncertainty of the failure modes for fastener type F4. Nonetheless, the proposed equation manages to give a safe prediction in four out of six cases. This indicates that the equation, while being slightly conservative, is safe to apply. Any improvements to fastener type F4 can therefore be assessed using the proposed equation.

Table 5.2: Overview of performed calculations per fastener type and corresponding input parameter values, based on findings from chapter 2.

	Equations	Input parameters
F4.	$F_v = \min \begin{cases} \frac{M_y}{t_1} + \frac{1}{2} t_1 d f_h \\ 1.15\sqrt{2 M_y d f_h} \\ 2t\sqrt{\frac{1}{b} G_f E_0 d \sin\alpha (b - d\sin\alpha)} \end{cases}$	$\rho_{m,bamboo} = 721 kg/m^3$ $\alpha_{bamboo} = 22°$ $G_{f,bamboo} = 360 J/m^2$
F5.	$F_v = \min \begin{cases} 0.7 A_{net} f_v \\ 2t\sqrt{\frac{1}{b} G_f E_0 d \sin\alpha (b - d\sin\alpha)} \\ 1.4 \times 0.4 d t f_h \end{cases}$	$d_{nail} = 2.44mm$ $f_{u,nail} = 435 N/mm^2$

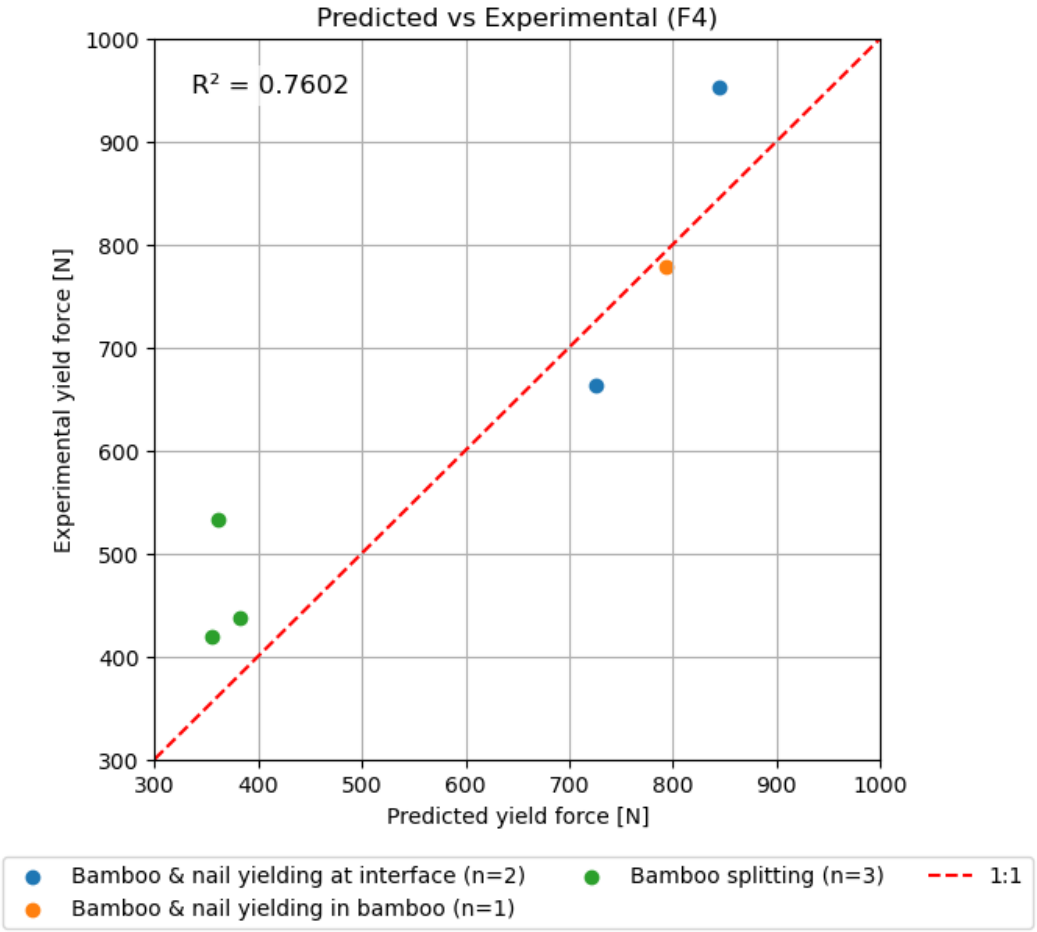

Figure 5.4: Experimental results versus shear capacity predictions of fastener type F4.

5.1.3 Results and statistics F5

The results of the experiments of fastener type 5 can be summarized in the following points:

- Fastener type F5 exhibited more consistent behavior compared to F4. Due to the absence of mortar infill, nails in F5 are less restricted, thus only bamboo embedment failure is governing.
- A secondary failure mode was observed in some tests, bamboo splitting, occurring only as a post-peak failure mode. Splitting was also caused by the method used for specimen preparation.

Fastener type F5 showed more consistent behavior with only two documented failure modes. The nails are less restricted in F5 since no mortar infill has been applied in these specimens, and they are therefore less likely to yield. As a result, only embedment failure of the bamboo caused yielding. In some of the tests another failure mode was recorded, albeit only a post-peak failure mode; splitting of the bamboo. Similar to the rib lath rupture, this failure mode was somewhat unexpected. Nonetheless, the occurrence of splitting can be explained by further investigation of the test setup. Bamboo splitting can happen if a bamboo culm is cut at a position too far from the nodes, which was the case for some of the test specimens. The nodes contain fibers that run in the direction perpendicular to the longitudinal direction of the bamboo, which reduce the risk of splitting. In the area between nodes, all fibers are oriented longitudinally, so resistance against splitting forces is lower. See figure 5.6 for an example of specimen splitting.

Statistical analysis proves that fastener type F5 behavior is predictable. With an R^2-value of 0.937, the prediction model almost perfectly overlays the mean data curve from the experiments. The statistic analysis, which can be seen in full detail in appendix E, provides evidence of the bamboo splitting. This is visible in the test results graph, which indicates fluctuations at the end of the curves. These fluctuations are caused by splittng, since the nail continuously loses and regains connection with the bamboo.

Calculation of the fastener shear capacity is also much more straightforward, see figure 5.7. All fasteners failed due to yielding of the embedment. The comparison yields an R^2-value of 0.958, indicating that the formula for embedment yielding closely predicts the real behavior. Three out of six predictions were an overestimation of the actual shear capacity, and the other three were a slight underestimation. Similar to fastener type F4, this tells us that the equations give a good representation of the real situation, and therefore the equations can be used to improve fastener F5.

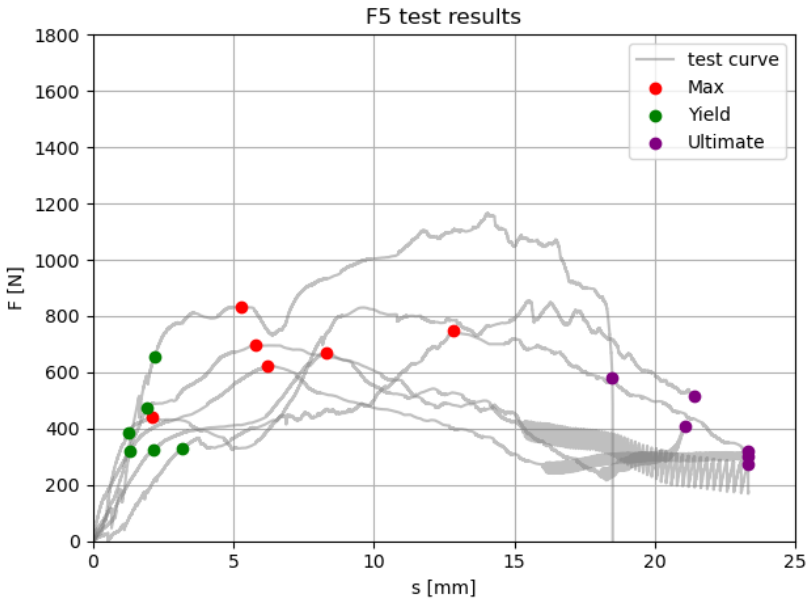

Figure 5.5: F5 experimental results, force-displacement diagram.

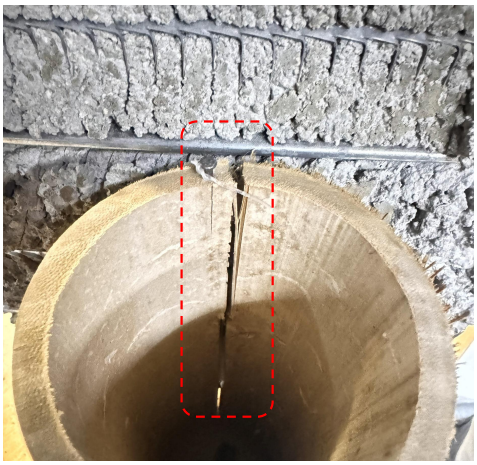

Figure 5.6: Splitting failure of F5 test specimen.

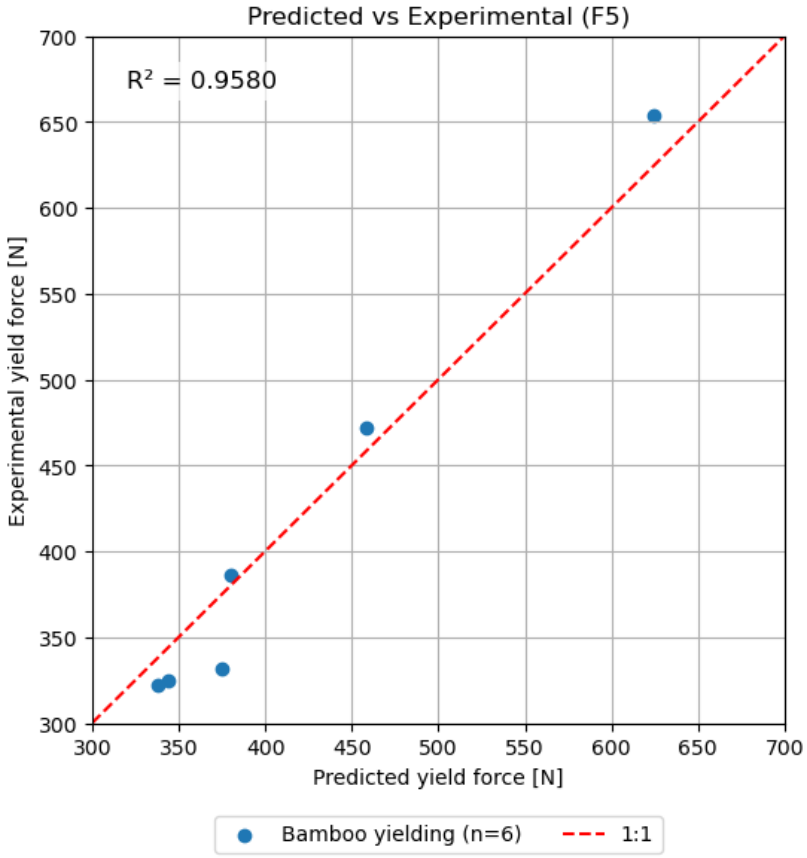

Figure 5.7: Experimental results versus shear capacity predictions of fastener type F5.

5.1.4 CBSW test setup

Figure 5.8 illustrates the experimental setup used to evaluate the shear performance of the wall panels. The wall panels are mounted within a reaction frame, which serves as the primary support structure for both the hydraulic actuator and the wall panel. A base beam is provided to establish a level foundation for the specimens. It is designed with sufficient stiffness so that its deformation during testing could be considered negligible. The bottom of the wall panel is securely anchored to the base beam using embedded rebars (iii), ensuring resistance against sliding and uplift. At the top of the specimen, a loading beam is fastened with high-tensile bolts to facilitate uniform transfer of lateral forces. The hydraulic actuator is mounted to the loading beam and applied the prescribed lateral loading protocol.

Lateral restraints are installed at the top of the wall panel to prevent out-of-plane displacements. Additionally, a pair of tie-down rods (or hold-down connectors) is provided to resist uplift and overturning while still allowing the wall to develop in-plane shear failure. Instrumentation is installed to record both lateral and vertical responses during testing. LVDTs and draw-wire sensors are positioned at four points (1 to 4), as shown in figure 5.8. Point (1) measures the lateral drift, point (2) and (3) capture the overturning displacements from the hydraulic actuator's pushing and pulling actions, and point (4) records central displacement of the panel.

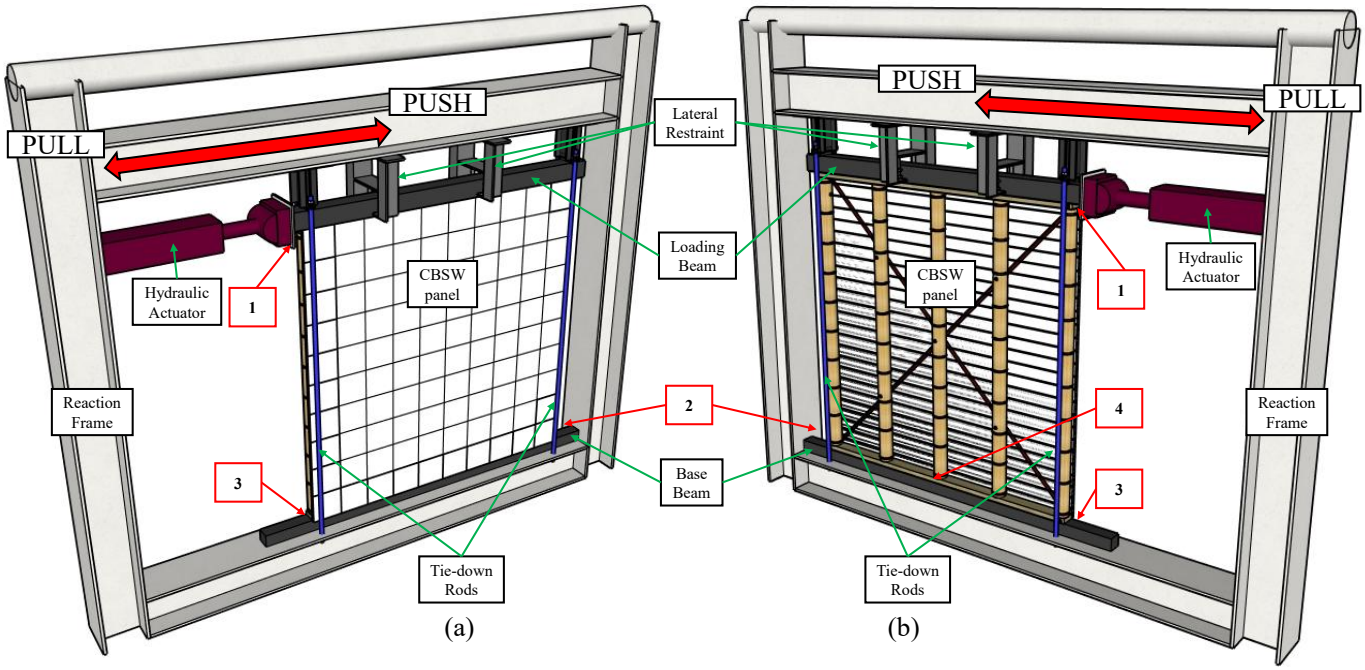

Figure 5.8: Components of the test setup (a) seen from the front, and (b) seen from the back.

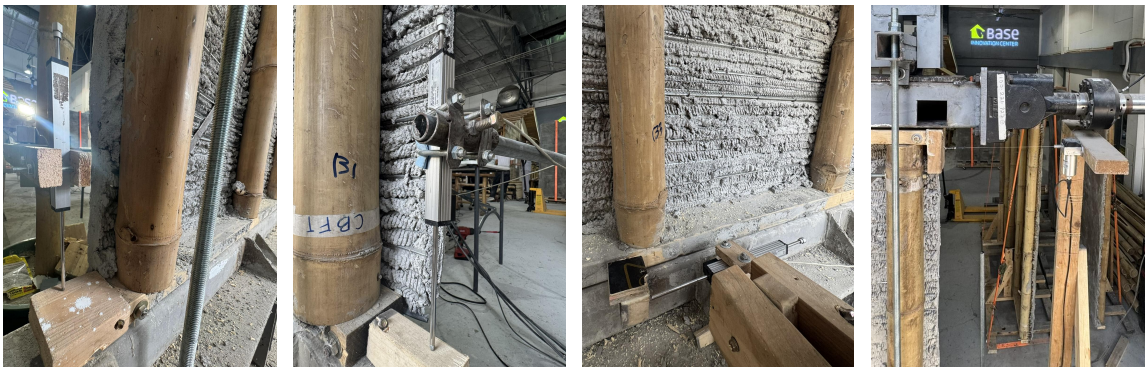

Figure 5.9: Overview of measurement sensors indicated in figure 5.8. (1) draw wire sensor, (2) right overturning LVDT, (3) left overturning LVDT, (4) middle displacement LVDT.

5.1.5 CBSW test results

The results of the full-scale shear wall tests can be summarized in the following bullet points:

- Under monotonic loading, WT1 showed about 25% higher lateral strength and stiffness than WT2 due to flat bar bracing. WT1 exhibited strain hardening beyond yield. WT2 showed lower capacity and a flatter post-peak response, indicating reduced stiffness.
- Under cyclic loading, Both wall types showed asymmetric hysteresis and reduced reloading resistance due to residual deformation and nail yielding. WT2 experienced greater stiffness degradation and pinching, reflecting weaker constraints without bracing. WT2 averages are more affected by damage accumulation due to its limited post-peak resistance.
- The yield force was determined using the Equivalent Energy Elastic–Plastic (EEEP) method, providing a standardized, conservative estimate of yielding behavior.

The lateral behavior of wall panels WT1 and WT2 was evaluated through monotonic and cyclic load–displacement tests. See figure 5.10. Under monotonic loading, WT1 exhibited higher lateral strength and initial stiffness than WT2. The difference in capacity is approximately 25 percent, and is caused by the flat bar bracing presence in WT1,

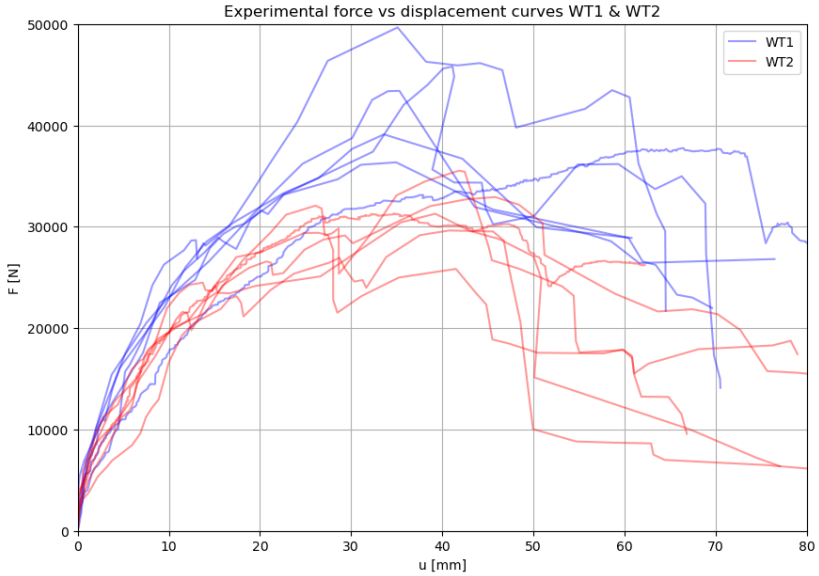

Figure 5.10: Force-displacement diagram displaying monotonic test results and cyclic envelopes of WT1 and WT2.

as opposed to its absence in WT2. WT1 also showed strain-hardening behavior, sustaining increasing load beyond yield before reaching peak resistance. In contrast, WT2 displayed a reduced lateral capacity and a flatter post-peak response, indicating lower stiffness and diminished ability to maintain resistance after peak load.

The cyclic responses revealed asymmetric hysteresis in both wall types, with reduced resistance during reloading phases due to residual deformation and nail yielding from earlier cycles. WT2 showed more severe stiffness degradation and pronounced pinching, reflecting its weaker structural constraints due to the absence of bracing. A full overview of the interpretation of test results can be found in appendix F. Section 5.2 presents a table with the average results of the experiments, for comparison with the analytical model. One important note here is that the results of the cyclic tests have been considered separately in positive and negative loading directions, resulting in a total of eleven samples per experiment. Since WT2 specimens show limited ability to maintain resistance after the peak load is reached, the average result of WT2 is influenced more heavily by damage accumulation.

The yield force is found using the Equivalent Energy Elastic–Plastic (EEEP) method. In this procedure, the EEEP curve is constructed by equating the area under the actual envelope curve up to the ultimate displacement u_u with the area enclosed by two straight lines: one representing the EEEP stiffness K_e and the other representing the idealized post-yield plastic response. The intersection of these two lines defines the equivalent yield displacement u_y, providing an energy-based estimate of the yield point. This

method offers a more standardized and conservative representation of yielding behavior, especially for materials and systems exhibiting gradual transition from elastic to plastic states.

5.2 Model validation

The validation of the model can be summarized in the following bullet points:

- By using nonlinear equations for the fasteners, it is revealed that bilinear elastic assumptions neglect significant plastic behavior, particularly for nail-based fasteners (F3-F5), while bolt-based fasteners (F1 & F2) show much higher stiffness and capacity.
- Fasteners connected to bamboo exhibit lower displacement tolerance, likely due to bamboo splitting, whereas timber fasteners display extended plastic behavior.
- Model predictions give yield forces of $30.19kN$ (WT1) and $20.23kN$ (WT2), correctly capturing the capacity difference caused by bracing.
- Although F2 fasteners are stiff and strong, their contribution to overall wall capacity is small due to location and limited quantity. Meanwhile, F5 fasteners dominate yield capacity in both wall types because of their presence along the perimeter of the wall.
- The analytical model overestimates initial stiffness, particularly for WT1 due to overestimated bolt stiffness. Additionally, unforeseen fastener slip could have occurred in the experiments, resulting in a lower stiffness.
- Experimental force–displacement curves show a distinct peak and steeper post-peak decay, especially for WT2, which the model fails to fully reproduce because nail pull-out due to the absence of bracing is not considered.
- Overall, the model shows reasonable agreement with experiments (10–20% error) and successfully explains load distribution and governing fastener behavior, while highlighting limitations in stiffness estimation and post-peak response modeling.

The validation of the model concerns the two wall types that have been tested: WT1 and WT2. Based on chapter 4, that means that the geometrical inputs for the model can be collected. Simultaneously, the fastener properties of F1-F3 could already be derived. Table 5.3 contains an overview of all the inputs for the two preliminary workflows of the model. Results from the single fastener tests from section 5.1 form the last step in finding all the necessary values for the analytical model. Table 5.4 shows all the final

Table 5.3: Overview of input values used for fasteners F1-F5 in analytical CBSW model.

Geometry	Fastener properties
	$\rho_{timber} = 420$ kg/m^3
	$\rho_{bamboo} = 721$ kg/m^3
	$t_{bamboo} = 8.12$ mm
	$d_{bolt} = 10$ mm
	$d_{nail} = 2.44$ mm
	$f_{u,bolt} = 414$ N/mm^2
$h = 2400$ mm	$f_{u,nail} = 435$ N/mm^2
$b = 2400$ mm	$\alpha = 45°$
$s = 100$ mm	$g = 9.81$ m/s^2
$n = 5$	

Table 5.4: Overview of outputs from fastener properties calculations.

Fastener type	F_y [N]	k_e [N/mm]	F_{max} [N]	u_{max} [mm]	k_u [N/mm]	u_u [mm]
F1	5695	1810	6264	18.9	−60.3	39.7
F2	3056	3435	3362	5.34	−114.0	11.2
F3	475	586	760	25.1	−19.5	32.9
F4	560	479	840	4.25	−42.6	13.5
F5	387	222	674	12.9	−37.4	21.8

fastener properties values for use in the CBSW model.

The nonlinear fastener equations can be plotted for all fastener types. This results in the graph presented in figure 5.11. As can be seen from the differences between bilinear and nonlinear curves, a lot of plastic behavior is not considered in the elastic region. The influence of each fastener type becomes apparent from the figure. Fasteners F1 and F2, those considering a bolt, have a significantly higher stiffness and capacity compared to fasteners F3-F5. Another remarkable insight is that the fasteners connecting to the bamboo seem to have less displacement tolerance. This is likely caused by the splitting behavior of the bamboo. The timber fasteners are assumed to have a much flatter yielding behavior, especially the nails (F3) have a long plastic region. With a geometry overview such as figure 4.1 and the results from table 5.4, the calculation of a CBSW panel can be executed. Note that the wall type, which is specified in the geometry workflow, can easily be switched.

Next, the calculation procedure presented in chapter 4 can be executed. Initial calculations provide a yield force, which equals $30.19kN$ for WT1, and $20.23kN$ for WT2. See figure 5.12 for an overview of the influence on horizontal yield capacity per fastener

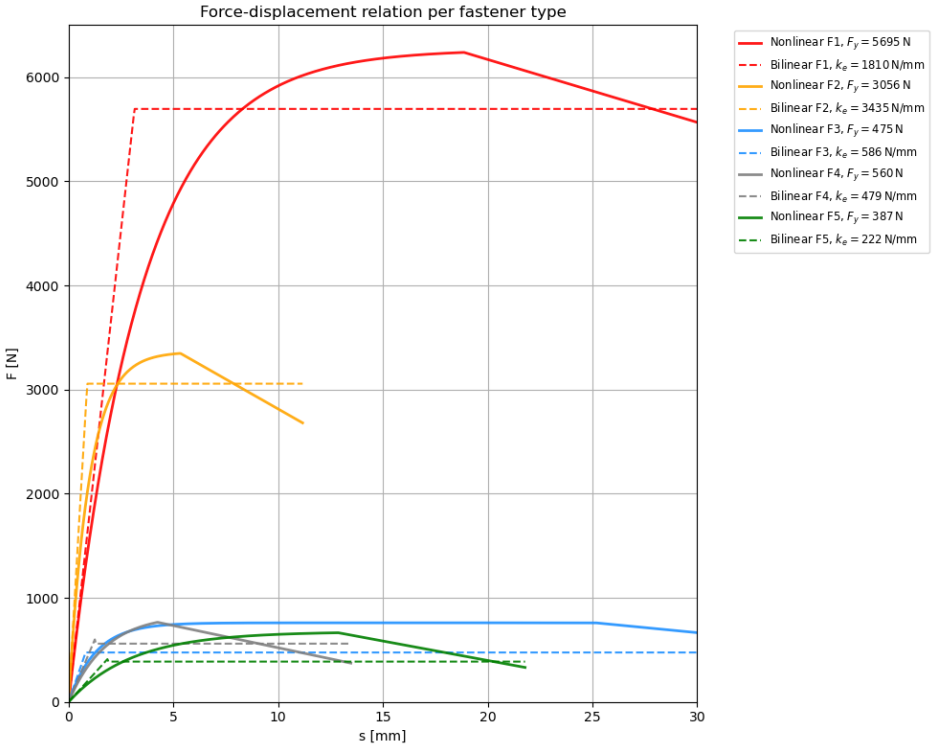

Figure 5.11: Nonlinear (solid) and bilinear (dashed) fastener force-displacement diagrams, with the stiffness and yield force values included per fastener type.

type. The pie charts indicate the importance of fastener position for contribution to shear wall capacity. Fastener F2, while having the highest stiffness and second highest shear capacity out of the fastener types, only contributes 7.9% to the yielding capacity. Additionally, fastener quantity also plays an important role in fastener contribution. In both analyzed wall types, fastener type F5 has a significant contribution to the yield capacity of the shear wall. The number of F5 fasteners in WT1 is 80, and 85 F5 fasteners can be found in WT2.

The ratio between cladding and frame rotation $\xi = \frac{\gamma}{\varphi}$ can be calculated using the elastic stiffness of the fasteners. For WT1, $\xi = 1.738$; for WT2, $\xi = 1.687$. This value is used to evaluate angle φ based on a given angle of γ. Angle gamma depends on the wall displacement, which is evaluated at increments of δu. The model, which runs using Python, has enough computation capacity to facilitate the use of a very small value for δu. However, since the model is a prediction tool with the sole purpose to recreate an average response, using a very small δu value is unnecessary. In the cyclic tests, the maximum displacement was $80mm$ to each side, so the total displacement measured equals $160mm$. For simplicity, a δu-value of $0.001 \times 160 = 0.16mm$ has been selected. Therefore, the loop introduced in the calculation workflow in chapter 4 will be iterated

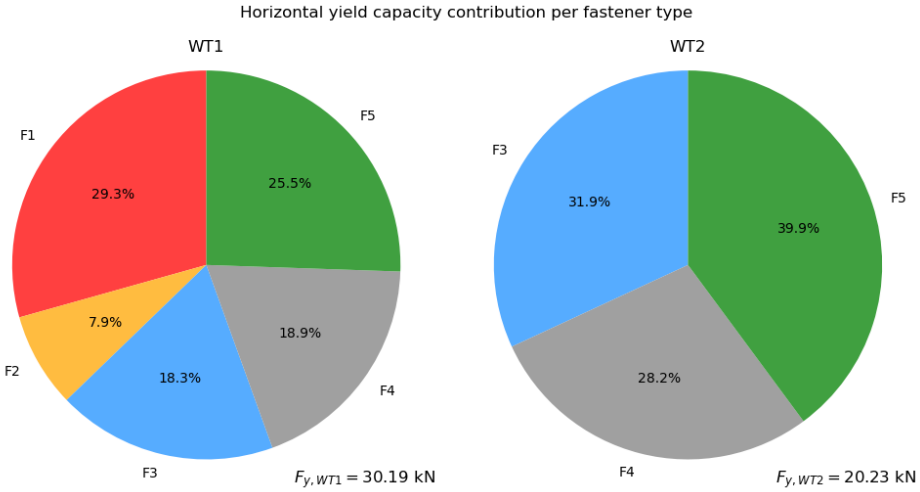

Figure 5.12: Pie charts displaying horizontal yield capacity influence per fastener in percentages.

for every step of δu for a total of 1000 times in case load is considered in both positive and negative direction. If only positive loading is considered, only 500 steps are considered.

Resulting from the model is a force-displacement diagram for both wall types. See figure 5.13 for a comparison of the mean curve resulting from the experiments and the modeled curve. A number of key insights can be drawn from inspection of the figure. The model accurately simulates the influence of the bracing, with a clear difference in capacity for WT1 and WT2 and accurate proportions when compared to experimental data. A second key insight is that the model overestimates the initial stiffness of the system. Especially WT1 overestimates the stiffness of the shear wall in the elastic region. In WT2, this is seemingly less, which indicates that the overestimation is likely caused by the bolt stiffness values that have been used in the models. Simultaneously, it is possible that unforeseen fastener slip could have occurred in the experiments, resulting in a lower stiffness.

Another key insight is that the predicted F_{max} is lower than the experimental mean value of F_{max}, and that the peak which is clearly recognizable from the experimental data has been flattened out in the model. A final insight is that for WT2, the experimental capacity decay slope is steeper than the slope generated by the model. As mentioned in section 5.1.5, one of the benefits of the presence of flat bar bracing is an improved coherence of the wall in post-peak behavior. The cause is likely that the flat bar prevents nail pull-out, due to restraining movement of the cladding perpendicular to the frame. The decreased coherence is not incorporated in the model, as it was an unexpected outcome of the experiments.

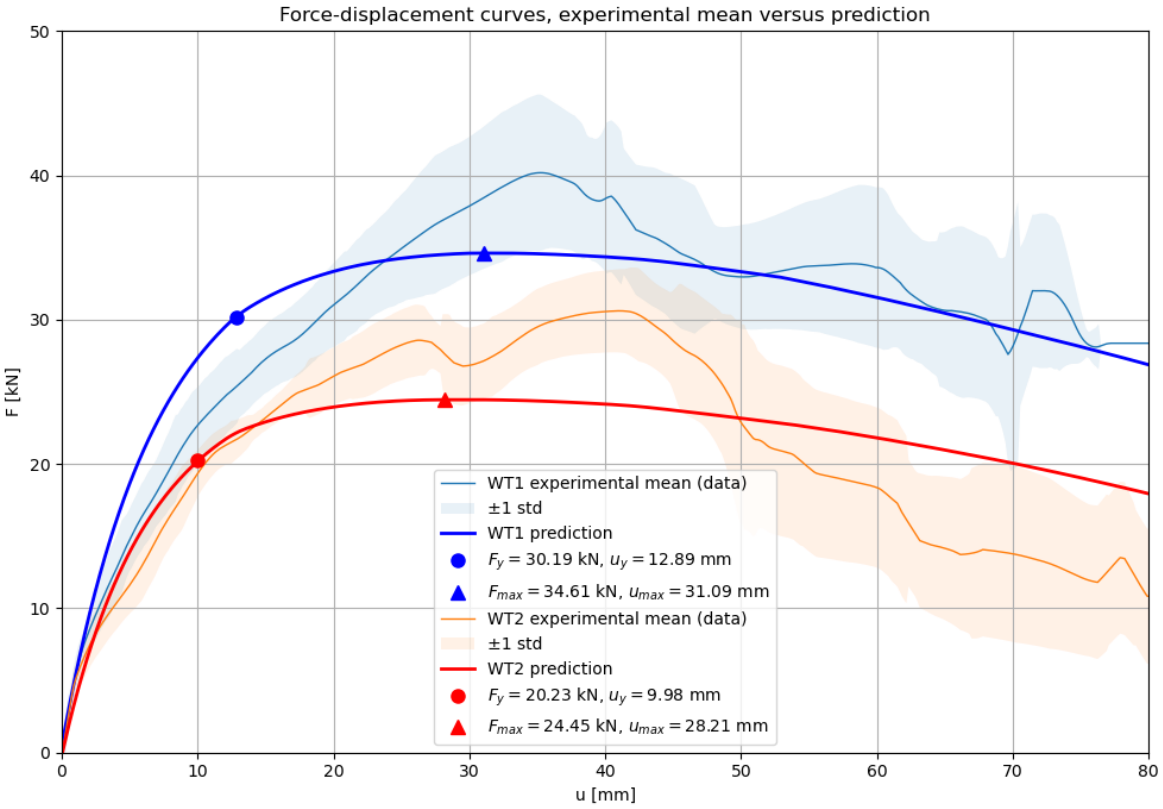

Figure 5.13: Force-displacement relation of experimental results and analytical models of WT1 and WT2.

Table 5.5: Average values of CBSW shear wall panel test results compared to analytical model outcomes, per wall type.

	F_y[kN]	u_y[mm]	K_e[kN/mm]	F_{max}[kN]	u_{max}[mm]
Test average WT1	33.53	15.02	2.43	39.74	37.92
Model result WT1	30.19	12.89	2.94	34.61	31.09
Error [%]	*-10.0*	*-14.2*	*21.0*	*-12.9*	*-18.0*
Test average WT2	24.84	11.78	2.28	28.98	33.87
Model result WT2	20.23	9.98	2.45	24.45	28.21
Error [%]	*-18.6*	*-15.3*	*7.5*	*-15.6*	*-16.7*

Table 5.5 shows a comparison between experiments and the model for the key outputs of the shear wall. The key insights from inspection of the force-displacement relations are reflected in the comparison of values in the table. The model slightly underestimates the forces and displacements, and slightly overestimates the elastic stiffness of the shear wall (all errors lie between $10-20\%$).

Further investigation of the model yields a schematic overview of fastener vectors. These vectors can be assessed at any deformation of the shear wall. This makes it possible to animate the progression of resistance per fastener. Unfortunately, only a snapshot of this animation can be included here, see figure 5.14. This figure indicates clearly that the largest forces occur in the corners of the wall panel, while the fasteners in the shear wall center have almost no contribution to the transfer of forces. This raises some possibilities for improvements of the shear wall. The upcoming section will address these improvements.

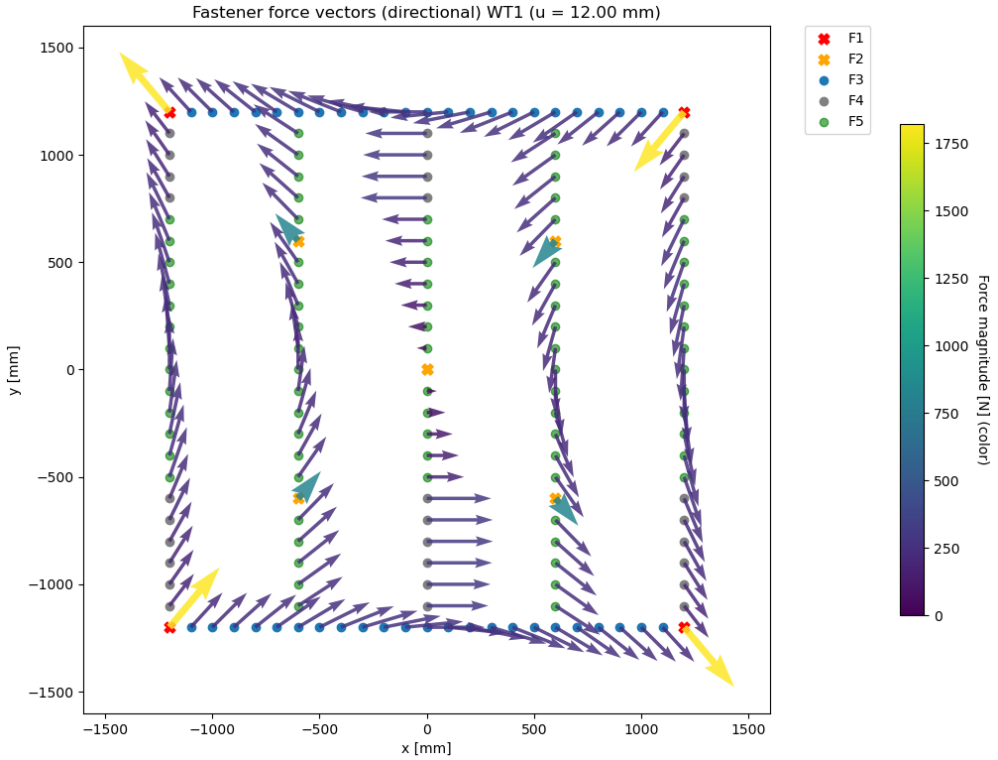

Figure 5.14: Schematic overview of WT1 fasteners, indicating direction and magnitude of fastener force vectors caused by a force in positive x-direction applied at the top left. Situation at the yield deformation ($u = 12mm$) is displayed.

5.3 CBSW improvements

In this research, the goal of shear wall improvements is to reach a higher horizontal shear capacity. This can be achieved by increasing the stiffness of the system, increasing the capacity of individual fasteners, or reducing the rate of damage accumulation. The model can be used to implement possible improvements to CBSW, without having to rely on experimental testing. This is especially useful in the assessment of the improvement ideation process. The geometry and fastener properties can be altered as a means to change the stiffness or capacity of the total system. Three improvement options are presented in this section, and applied in the model thereafter so that the potential can be assessed. The three improvement options all concern a different component of the CBSW system. The following sections present an improvement option for the shear wall configuration, embedment type, and fastener properties, respectively. Afterwards, the options will be implemented in the model and the results will be discussed.

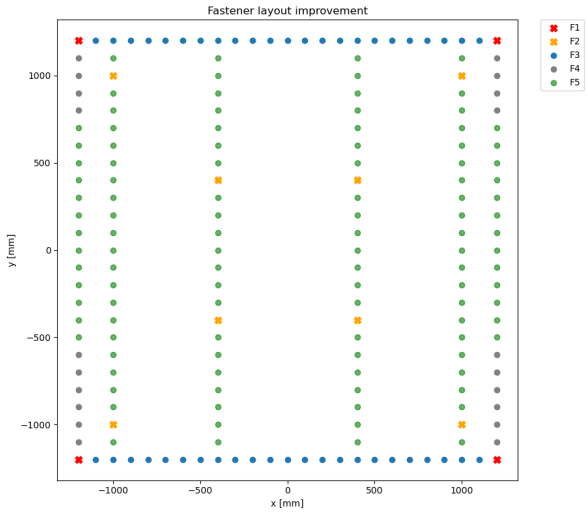

Figure 5.15: Schematic overview of fasteners of an improved CBSW configuration.

5.3.1 Option 1: Wall configuration

Investigation of figure 5.14 concludes that the fasteners at the center of the shear wall do not contribute to the transfer of forces. At the same time, the corners of the shear wall seem to be heavily affected. A straightforward option for improvement would therefore be to rearrange the studs so that they are positioned closer to the edges of the shear wall. Ideally, it would also help to include a second row of timber beams, but due to the geometry of the rib lath, this is not possible. The rib lath has to be fastened to these additional timber beams, but the fastener spacing s is fixed to the distance between rib lath gutters in the vertical direction. As a result, a third layer of timber beams should be added in order to fasten the rib lath which is unpractical. Another constraint exists for the alteration of wall configuration, because the stud spacing should be kept at a value close to $600mm$. If this spacing is not maintained, the cladding has too little support due to which it can buckle.

See figure 5.15. Based on the requirements and constraints presented in the previous paragraph, this configuration has been developed. It has a total of 6 studs, and the stud spacing is kept at a maximum of $600mm$. Two studs have been moved to the edge of the frame, where the deformations are large and thus the influence of fasteners is more significant. The center stud has been removed, as it had the least influence on shear wall capacity. Sufficient spacing is applied between the edge studs and the two adjacent studs to account for variations in bamboo culm diameter. This improvement is expected to increase the overall capacity, since it adds 23 extra fasteners to the shear wall. Additionally, the fasteners that are added are assumed to be fully engaged, which means a higher shear capacity can be reached.

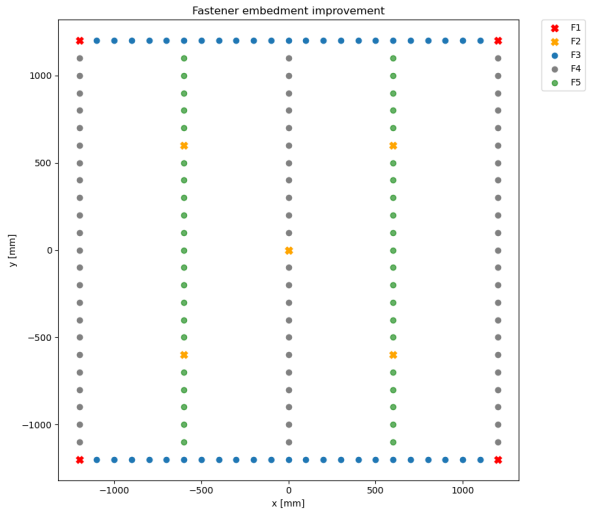

Figure 5.16: Schematic overview of fasteners of a WT1 configuration where the studs with embedded rebar and j-bolt have been completely filled in with mortar.

5.3.2 Option 2: Embedment type

Changing the configuration of the shear wall is a big adjustment, and in some cases not feasible. Other improvement options require less effort, but can still yield an increased capacity. One of these options is increasing the number of fasteners that are embedded in mortar infill, F4, by completely filling the edge and center studs. The F4 fasteners will replace the F5 fasteners that would otherwise be present on the mentioned studs. These studs require infilled nodes at the top and bottom as per section 1.2, so by making a small adjustment, the remaining nodes of these studs can be infilled.

This improvement is expected to increase the stiffness of the shear wall, since fastener type F4 has a higher elastic stiffness than fastener type F5. It is not certain whether this improvement will also increase the shear capacity of the system, since the capacity of fastener type F4 also decays faster than that of F5. When all the F4 fasteners are located along the perimeter, which receives the highest deformations of the system, the capacity is expected to decrease sooner.

5.3.3 Option 3: Fastener properties

Fasteners F3-F5 use common wood nails. Although availability is widespread, these nails are relatively weak, and also smooth. This smoothness causes the nails to lose traction with the embedment material once deformations occur. Especially when the nail yields, it is remarkably easy to pull-out a smooth nail. Using screws is not an alternative for bamboo as the bamboo is very likely to split, as mentioned in chapter 2. Luckily, there are also nail alternatives for smooth nails. Instead of a smooth nail, a

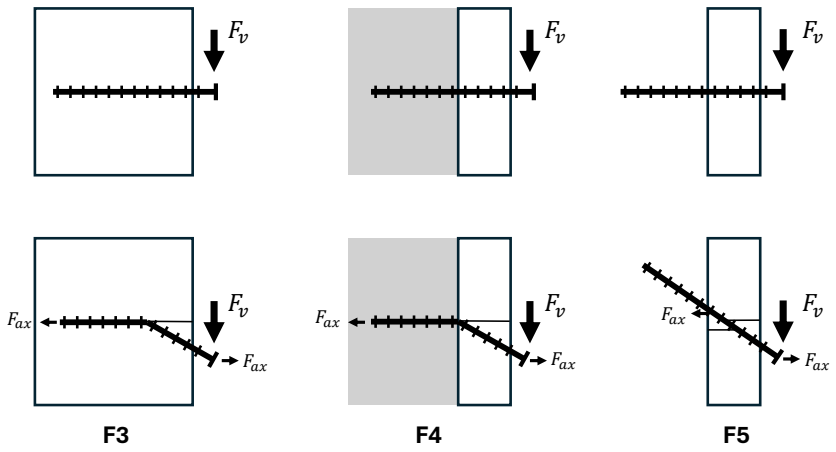

Figure 5.17: Improvement proposal for nail fasteners: ring shank nails, as displayed in undeformed and deformed condition for F3-F5.

ring shank nail can be used. This nail has a rugged surface, caused by the repetition of perimeter rings over the length of the nail. See figure 5.17.

The benefits of using ring shank nails lies in the axial contribution. In contrast to smooth nails, these nails will develop axial stresses, which increase the capacity of the fastener. The ring shank nails are available with the same diameter as the common wood nails. The axial stress equals $f_{ax} = 17.33N/mm$ for low-density embedment materials such as the timber, and $f_{ax} = 22.87N/mm$ for higher density materials such as the bamboo or mortar [Rammer and Zelinka, 2015]. Eurocode 5 proposes that the shear capacity of a fastener is increased by $0.25F_{ax}$, and that for ring shank nails, only 50% of the axial force should be considered [European Committee for Standardization, 1994].

The considered length of the nail equals $25mm$. Then: $F_{ax,F3} = 433N$, $F_{ax,F4} = 572N$, and $F_{ax,F5} = 186N$. Note that the axial force in fastener F5 is significantly lower. This is caused by the fact that the rope effect only acts on the bamboo culm wall, which is on average only $8.12mm$ in thickness. When compared with the shear capacity for common wood nails, the increase in capacity due to the rope effect is approximately $1.1F_v$. This increase can be applied in the fastener properties workflow to achieve results.

5.3.4 Improvement results

All the options have been applied to the model separately, and ultimately all options have been applied simultaneously. Figure 5.18 displays the force-displacement curves for all options. Option 1, as expected, increases the capacity of the shear wall signif-

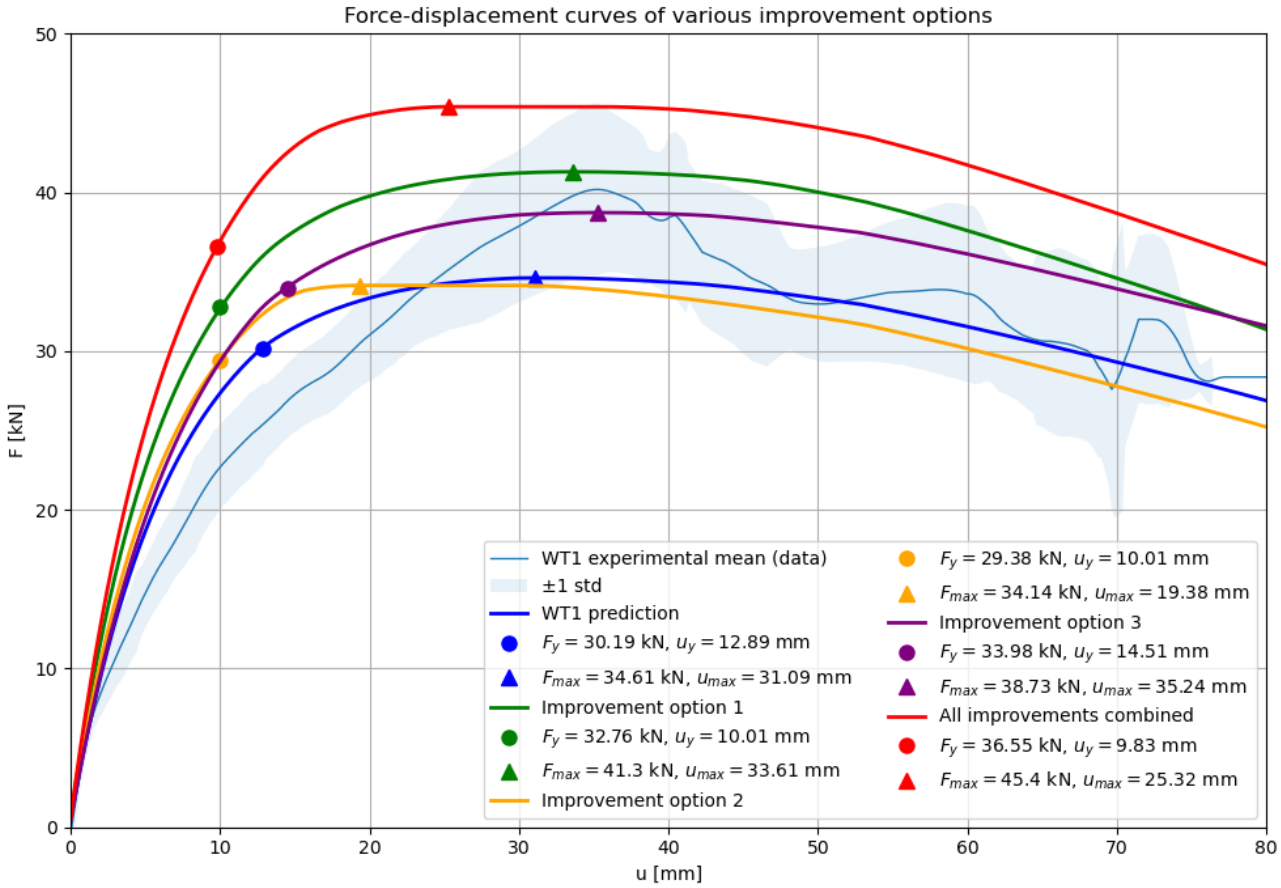

Figure 5.18: Force-displacement relations between WT1 and several improvement options.

icantly. Simply by having more fasteners in the areas with the highest deformations results in higher capacity. Option 2 seems to have a very limited effect, the maximum force slightly decreased. As expected, the elastic stiffness of the proposed improved shear wall did increase. Option 3 yields similar results as option 1. It seems that by incorporating more friction in the fasteners, their capacity increases, and consequently the capacity of the entire shear wall. This demonstration raises new testing opportunities, to see the impact of using ring shank nails in cyclic loading. It is possible that the connection between nail and frame will become more resilient with this improved nail type. As a final demonstration, all of the proposed improvements have been gathered into one model, to showcase the difference in behavior when a CBSW panel has been specifically configured to have maximal horizontal load capacity. The result is clear: this combined improvements shear wall has higher elastic stiffness, higher yield force, higher maximum force, and a more distinguished plastic region than any of the other proposed improvements. This concludes the assessment of the improvements.

Table 5.6: Comparison of shear wall horizontal capacities per meter.

Wall type	**Capacity** $[kN/m]$	**Capacity/**γ $[kN/m]$	**Comparison**
Design (H_{Rd})	3.0	2.0	H_{Rd}
Characteristic WT1	13.85	9.23	$4.6H_{Rd}$
Characteristic WT2	8.71	5.81	$2.9H_{Rd}$
Model WT1	12.58	8.39	$4.2H_{Rd}$
Model WT2	8.43	5.62	$2.81H_{Rd}$
Model improved	15.23	10.15	$5.1H_{Rd}$

A comparison of the horizontal shear capacity per meter will give a good impression of the conservativeness of current design values, as mentioned in section 1.1. This design shear value is divided by a partial factor, $\gamma = 1.5$. The shear value from the model predictions can be derived by dividing by the length of the wall, $2.4m$. See table 5.6 for a comparison against this design value. It is undoubtedly clear that the design value is low compared to the experimental and predicted values, which are at least a factor 2.8 times higher. If instead these more accurate values are adopted, structural design using Composite Bamboo Shear Walls could be more efficient and precise.

Chapter 6

Conclusion and discussion

This chapter summarizes the findings from research, and is simultaneously used to answer the research question and its subquestions. Various shortcomings or unexpected values are discussed and recommendations for future research are given.

6.1 Conclusion

The results retrieved in chapter 5 are synthesized here:

- The equations for evaluating the yield force of fastener types F4 and F5 show a good fit with the experimental values. With an R^2-value of 0.871 and 0.958 respectively, the equations not only give a good prediction of the yield force, but also the failure mode. One unexpected failure mode occurred in fastener F4, where after yielding the rib lath would rupture.

- The analytical model shows good agreement with experimental results for both WT1 and WT2, with force, displacement, and stiffness predictions generally within 10–20% error, validating its use for arbitrary shear wall configurations.

- Analysis of fastener force distribution reveals that corner fasteners govern shear resistance, while fasteners near the wall center contribute minimally, highlighting clear opportunities for structural optimization.

- Among individual improvement strategies, reconfiguring the wall layout (Option 1) and enhancing fastener properties with ring shank nails (Option 3) yield the most significant increases in shear capacity, whereas increasing mortar embedment (Option 2) mainly improves stiffness with limited capacity gains.

- Combining all proposed improvements in the model results in a substantially enhanced CBSW panel, characterized by higher stiffness, higher yield and peak forces, and a more pronounced plastic response, demonstrating the model's effectiveness as a design and optimization tool.
- Comparison of horizontal shear capacity per meter shows that the current design value is highly conservative, underestimating experimental and model-based capacities by at least a factor of 2.8, indicating significant potential for more efficient and accurate design of Composite Bamboo Shear Walls.

The results indicate that the analytical model is capable of capturing the overall behavior of CBSW shear walls with reasonable accuracy. While certain simplifications and assumptions introduce some limitations in precision, the model provides a useful predictive tool for assessing structural performance across different wall configurations and dimensions. Thus, the primary research question (*How to develop an analytical model to predict and improve the horizontal shear capacity of a Composite Bamboo Shear Wall?*) has been successfully addressed.

6.2 Discussion

6.2.1 Model assumptions

The assumptions (see section 1.2.4) adopted in this research are appropriate for bounding the scope and enabling the development and validation of an analytical model focused on the in-plane shear capacity of Composite Bamboo Shear Walls. The use of a standard wall size, idealized boundary conditions, and restriction to WT1 and WT2 configurations reflects common experimental practice and supports reproducibility and internal consistency.

Several assumptions simplify real structural behavior, most notably the neglect of component-level deformations, out-of-plane effects, and long-term influences such as creep, moisture, and degradation. These simplifications are likely contributors to the model's overestimation of elastic stiffness and its inability to fully capture post-peak behavior observed in experiments. Similarly, assuming uniform material properties and construction quality is reasonable for laboratory conditions but does not fully reflect the natural variability of bamboo-based systems.

Overall, the assumptions are valid for a first-order analytical investigation and allow meaningful comparison between experiments and theory. However, they limit direct

applicability to real structures and highlight clear directions for future research aimed at improving model fidelity and design relevance.

6.2.2 Fastener properties

See section 2.3.2. Basing stiffness and capacity values for fasteners F1–F3 on literature is a pragmatic and efficient choice, as it significantly reduces the need for extensive single-fastener testing, which accelerates model development. For well-studied fasteners and materials, published values generally provide a reasonable first-order approximation.

However, this approach reduces reliability, as literature values may not fully reflect the specific materials, geometries, boundary conditions, and interaction effects present in CBSW. Differences in bamboo species, moisture content, embedment conditions, and manufacturing tolerances can lead to deviations from reported behavior. As a result, uncertainties in fastener properties may propagate through the analytical model and contribute to discrepancies between predicted and experimental wall responses.

Overall, the use of literature-based fastener properties is acceptable for exploratory modeling and comparative studies, but targeted experimental validation is recommended if higher predictive accuracy or design-level reliability is required.

6.2.3 F4 experimental results

The experimental results for fastener type F4 (see section 5.1) showed high variability and limited predictability, mainly due to the sudden and brittle rib lath rupture that occurred after the yielding plateau. This failure mode caused abrupt loss of capacity at displacements ranging from approximately 5 to 25 mm, making it difficult to define a reliable post-yield response.

To improve the quality and consistency of F4 test results, several measures can be considered. First, specimen preparation should be further standardized, particularly the quality and geometry of the rib lath and its connection to the bamboo and mortar infill. Small variations in rib lath thickness, alignment, or local defects likely contribute to premature rupture and scatter in results.

Second, the test setup could be refined to better isolate fastener behavior. The current configuration allows rib lath rupture to govern failure, obscuring the intended investigation of nail yielding and embedment behavior. Modifying the setup to strengthen or decouple the rib lath—while keeping boundary conditions representative—could help

ensure that failure is governed by the fastener rather than by secondary components.

Third, increasing the number of test repetitions and grouping specimens by rib lath properties would improve statistical robustness and help distinguish systematic behavior from random variability. Finally, exploring alternative fastener or cladding details could reduce the likelihood of rupture and lead to a more ductile and predictable response. Overall, improving material control, test isolation, and statistical depth would enhance the reliability of F4 fastener characterization.

6.3 Recommendations

Four main recommendations can be given for future research in this topic, they are described in-depth in this section:

- **Effect of cladding–foundation connectivity**
  Future research should investigate the structural implications of connecting the cladding directly to the foundation. Experimental and analytical studies could assess how this connection alters load paths, boundary conditions, and force distribution among fasteners, particularly at low displacements. Given the observed importance of corner fasteners and bracing in post-peak behavior, cladding–foundation connectivity may significantly enhance stiffness, delay damage accumulation, and improve post-peak coherence, effects that are currently not captured in the model.

- **Out-of-plane capacity and stability of CBSW systems**
  The present research focuses on in-plane shear behavior, while the out-of-plane capacity of Composite Bamboo Shear Walls remains unexplored. Future studies should evaluate bending resistance, stability under wind or seismic out-of-plane loading, and interaction effects between in-plane shear and out-of-plane deformation. This is essential for safe structural application and may reveal additional design constraints related to cladding thickness, fastener spacing, and stud configuration.

- **Advanced modeling including component-level deformations**
  The current analytical model assumes rigid wall components and concentrates deformation in the fasteners. Future model development should incorporate deformation of individual CBSW components, such as bamboo studs, timber framing, mortar infill, and cladding panels. Including these effects would improve predictions of initial stiffness, post-peak behavior, and damage accumulation, and could help explain discrepancies observed between experimental results and model predictions, particularly in the elastic and post-peak regions.

- **Optimization of cladding thickness for structural performance**
  Further research should explore the optimization of cladding thickness by balancing structural performance with environmental impact. Parametric studies using the validated analytical model could assess how reduced or variable cladding thickness affects stiffness, shear capacity, and ductility, while life-cycle assessments quantify potential emission savings. This approach could support performance-based, low-carbon design strategies for CBSW systems without compromising safety or reliability.

Additionally, future research including modeling should incorporate experimental testing for each fastener type used in the CBSW. Doing this will significantly increase the reliability of the results.

Appendix A

Research proposal

To address the research question and its sub-questions, a systematic methodology is adopted that integrates literature analysis, theoretical formulation, model development, and validation. This multi-step approach, see also figure A.1, ensures a logical progression from fundamental understanding toward practical application. Each phase not only builds upon the previous one but also includes feedback loops, allowing insights gained in later stages to inform refinements of earlier assumptions. By combining both qualitative (literature-based) and quantitative (analytical and experimental) methods, the approach aims to deliver a robust and comprehensive understanding of CBSW behavior.

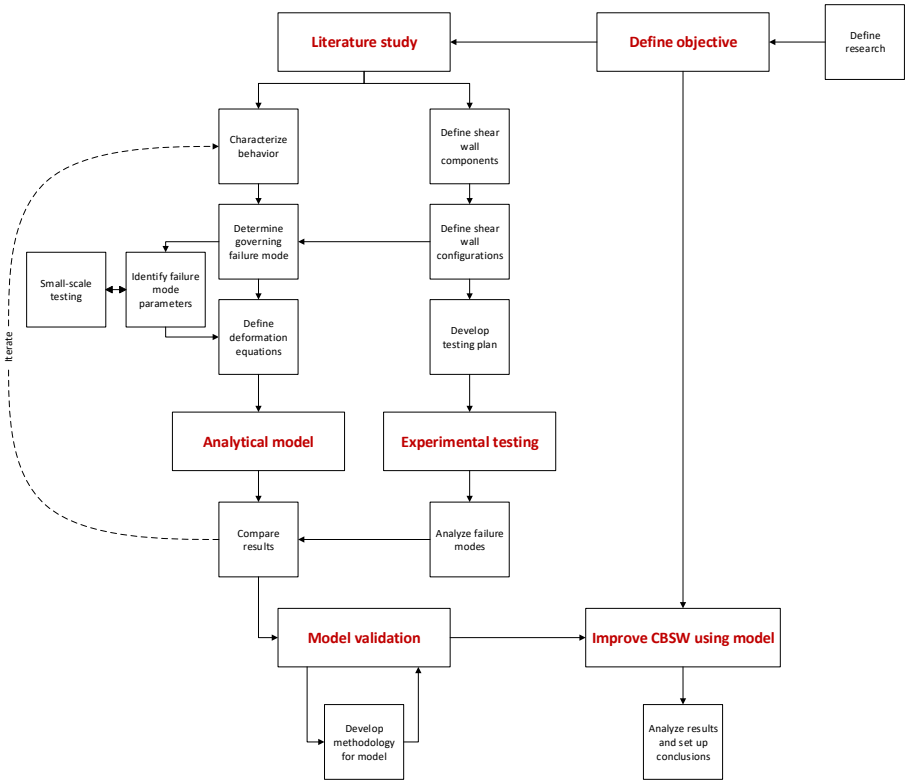

Figure A.1: Flowchart indicating all the steps taken in the research to answer the research question.

Appendix B

Testing protocols

B.1 ASTM D1761-20

International standards exist which prescribe reproducible and standardized testing procedures. Single nail shear tests are executed according to ASTM D1761-20 [ASTM International, 2020]. This test method provides an understandable procedure for evaluating the withdrawal and lateral resistance of fasteners installed in wood and wood-based materials. To achieve a proper analysis of the fastener behavior, test specimens are loaded until complete failure (until no more resistance is measured).

B.2 ISO 21581:2010

The full-scale CBSW tests covered in this research are performed according to ISO standard 21581:2010 [International Organization for Standardization, 2010]. This standard distinguishes between two methods (I & II) for shear wall testing. Method I focuses solely on documenting the shear capacity of the specimen, while in method II overturning of the wall panel is also considered. The distinction is made because overturning, along with other mechanisms related to method II, causes additional displacements that are not caused by shear action of the wall panel. In testing method I, additional boundary conditions should be applied to the wall panel. That way, the focus of testing will be to determine the shear capacity, and all deformations occurring during testing are related to shear action. Method I will be applied in this research so that the shear behavior can be described most accurately. Displacements or capacity losses caused by other failure modes can be calculated relatively effortlessly. ISO 21581 contains a protocol for both monotonic testing as per figure B.1(a), and cyclic testing as per figure B.1(b). Monotonic testing consists of three phases. It is load-controlled, so before performing the experiment a reference load value is selected: $F_{ref} = F_{max}$. In case no previous tests have been done, F_{ref} can be derived from literature. In phase 1, the specimen is loaded until $0.1F_{ref}$ to make sure the test setup is functioning properly. In phase 2 of the loading protocol, the specimen is loaded until $0.4F_{ref}$. This load is sustained for 300 seconds, afterwards the specimen is unloaded again. Phase 2 has the goal to prevent initial slip, so that a more accurate elastic stiffness can be documented. Finally, in phase 3, the specimen is loaded until failure.

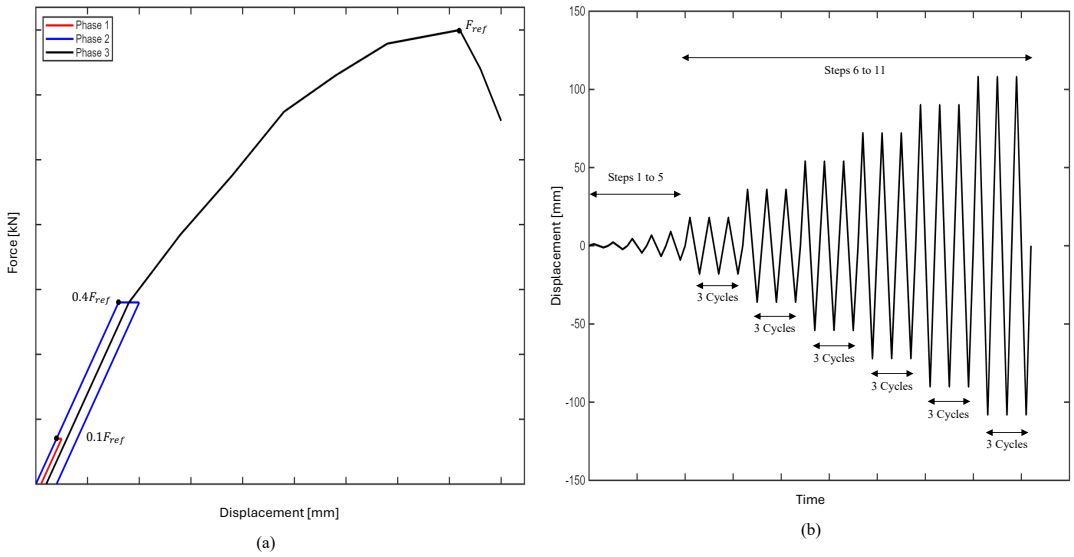

Figure B.1: (a) Monotonic and (b) cyclic loading protocol according to [International Organization for Standardization, 2010].

The cyclic tests are displacement-controlled, which means that a prescribed displacement is applied to the specimen, and the corresponding force is documented. A reference displacement at which the shear wall reaches failure is obtained from the monotonic test. The specimen will be exposed to increasing displacements in a total of eleven steps. The displacement increases incrementally per step, with the ultimate displacement at step 11. In step 1-5, the prescribed displacement is applied once in both positive and negative direction. From step 6 onwards, the same displacement cycle is repeated three times. Performing and documenting the cyclic tests will yield a hysteretic response diagram for that specimen.

Appendix C

Fastener type F4 calculations

See figure C.1. Consider a fastener inserted in a bamboo culm with mortar infill. A shear force F_v is introduced, which causes the fastener to displace. The displacement of the fastener activates the embedment strength of the bamboo and mortar. The mortar, which is confined, is assumed to behave much stiffer than the bamboo. As a result, the bamboo embedment will start yielding, and a plastic hinge forms in the nail at the interface between the bamboo and the mortar. The plastic hinge in the nail can only form if a plastic moment M_y has been reached. The yielding of the bamboo embedment happens at an embedment stress equal to f_h. The thickness of the bamboo culm wall equals t_1. Consider now equilibrium of shear forces and moment around the plastic hinge:

$$\sum V = 0 \rightarrow F_v - f_h t_1 d = 0 \tag{C.1a}$$

$$\sum M = 0 \rightarrow M_y + f_h t_1 d \frac{t_1}{2} - F_v t_1 = 0 \tag{C.1b}$$

As the location of the plastic hinge has been defined as the interface between the bamboo and the mortar, the moment equilibrium can be used to derive an equation for the shear capacity F_v:

$$F_v = \frac{M_y}{t_1} + f_h d \frac{t_1}{2} \tag{C.2}$$

If instead the bamboo culm wall is too thick, and the yielding of the nail happens inside the bamboo, the equilibrium conditions can be combined to reach:

$$F_v = \sqrt{2 M_y d f_h} \tag{C.3}$$

Which is identical to the equation from EC5, which will thus instead be used.

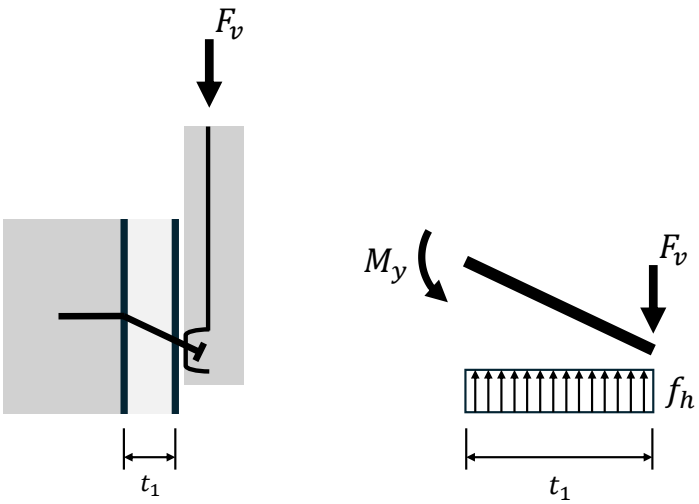

Figure C.1: Mechanical schematic (a) of fastener F4 and Free Body Diagram (b) indicating forces acting on fastener.

Appendix D

Static model calculations

See figure D.1. Let u_i and v_i be the displacements in x- and y-direction of fastener i. Based on the rotation of the cladding φ and the rotation of the frame γ, the displacements are given by

$$u_i = (\varphi - \gamma)\, y_i \tag{D.1a}$$

$$v_i = -\varphi x_i \tag{D.1b}$$

The fasteners behave as translational springs. Let the strain energy of the total system equal

$$U_{str} = \frac{1}{2}\sum_{i=1}^{n} k_i \left(u_i^2 + v_i^2\right) \tag{D.2}$$

The potential energy due to the horizontal load H is given by

$$U_{pot} = -H\gamma h \tag{D.3}$$

The energy function of the system can then be written as

$$U = \frac{1}{2}\sum_{i=1}^{n} k_i \left[\left[(\varphi - \gamma)\, y_i\right]^2 + (-\varphi x_i)^2\right] - H\gamma h \tag{D.4}$$

Relations between unknown quantities can be found by finding the minimum of the potential energy equation with respect to these quantities. Equation D.4 is subjected to partial differentiations $\frac{\partial U}{\partial \varphi} = 0$ and $\frac{\partial U}{\partial \gamma} = 0$. These yield the following relations:

$$(\varphi - \gamma)\sum_{i=1}^{n} k_i y_i^2 + \varphi \sum_{i=1}^{n} k_i x_i^2 = 0 \tag{D.5a}$$

$$(\varphi - \gamma)\sum_{i=1}^{n} k_i y_i^2 - Hh = 0 \tag{D.5b}$$

With these relations, a function can be derived for both φ and γ:

$$\varphi = Hh \frac{1}{\sum_{i=1}^{n} k_i x_i^2} \tag{D.6a}$$

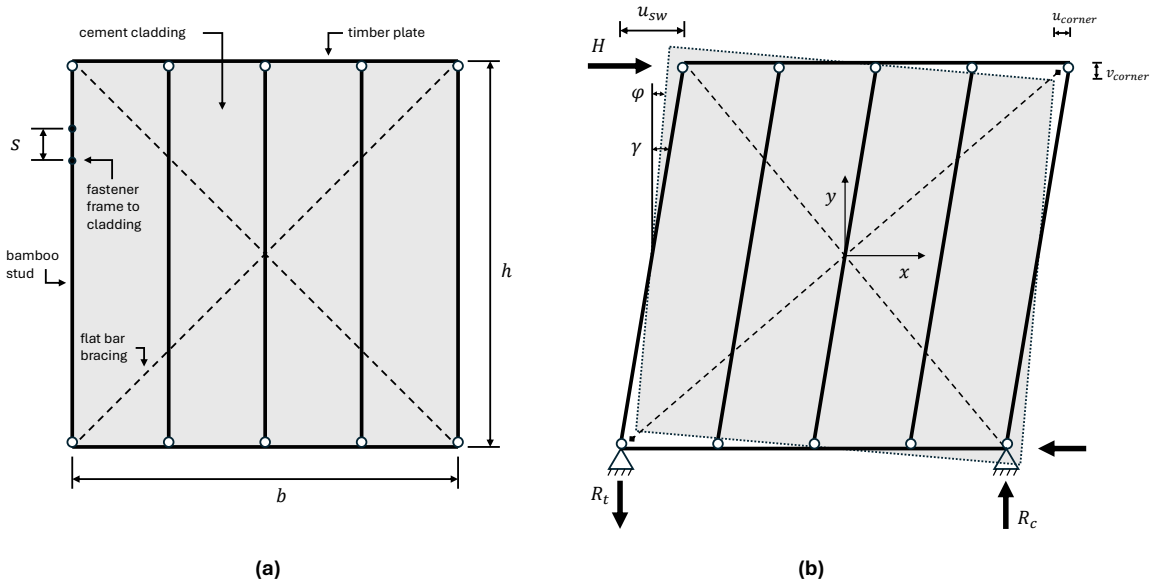

Figure D.1: (a) schematic of CBSW panel. (b) static model of CBSW panel.

$$\gamma = Hh\left[\frac{1}{\sum_{i=1}^{n} k_i x_i^2} + \frac{1}{\sum_{i=1}^{n} k_i y_i^2}\right] \tag{D.6b}$$

A relation between φ and γ can be derived from equations D.6:

$$\frac{\gamma}{\varphi} = 1 + \frac{\sum_{i=1}^{n} k_i x_i^2}{\sum_{i=1}^{n} k_i y_i^2} \tag{D.7}$$

This relation can be used to identify the difference in rotation angle between φ and γ. The remainder of this appendix is dedicated to determining the summand terms in equation D.7 by hand. This requires a concise designation of fastener types and positions. The summand terms and yield capacity are derived per fastener type. Consider figure D.2 for an impression of the distances of each fastener to the origin, as well as an indication of fastener spacing s.

- F1:

$$\sum x_{F1}^2 = 4\left(\frac{b}{2}\right)^2 = b^2 \tag{D.8a}$$

$$\sum y_{F1}^2 = 4\left(\frac{h}{2}\right)^2 = h^2 \tag{D.8b}$$

$$H_{F1} = \frac{F_{v,F1}}{h\sqrt{\left[\frac{b/2}{\sum x_{F1}^2}\right]^2 + \left[\frac{h/2}{\sum y_{F1}^2}\right]^2}} \tag{D.9}$$

- F2:

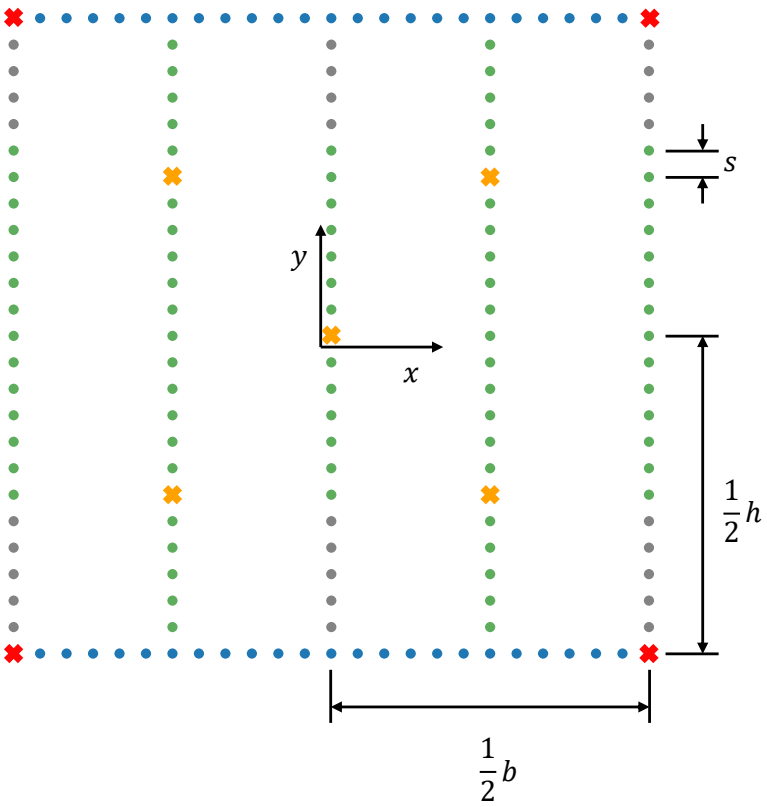

Figure D.2: Schematic fastener overview, indicating the distance of fasteners to the origin.

$$\sum x_{F2}^2 = 4\left(\frac{b}{4}\right)^2 = \frac{1}{4}b^2 \tag{D.10a}$$

$$\sum y_{F2}^2 = 4\left(\frac{h}{4}\right)^2 = \frac{1}{4}h^2 \tag{D.10b}$$

$$H_{F2} = \frac{F_{v,F2}}{h\sqrt{\left[\frac{b/4}{\sum x_{F2}^2}\right]^2 + \left[\frac{h/4}{\sum y_{F2}^2}\right]^2}} \tag{D.11}$$

- F3:

$$\sum x_{F3}^2 = 2\sum_{i=1}^{b/s-1}\left[\left(2\frac{s}{b}i-1\right)\frac{b}{2}\right]^2 = \frac{b^3}{6s} - \frac{b^2}{2} + \frac{bs}{3} \tag{D.12a}$$

$$\sum y_{F3}^2 = 2\left[\left(\frac{b}{s}-1\right)\left(\frac{h}{2}\right)^2\right] = h^2\frac{b-s}{2s} \tag{D.12b}$$

$$H_{F3} = \frac{F_{v,F3}}{h\sqrt{\left[\frac{b/2-s}{\sum x_{F3}^2}\right]^2 + \left[\frac{h/2}{\sum y_{F3}^2}\right]^2}} \tag{D.13}$$

- F4:

$$\sum x_{F4}^2 = 2\left[\left(\frac{h}{s}-16\right)\left(\frac{b}{2}\right)^2\right] = b^2\frac{h-16s}{2s} \tag{D.14a}$$

$$\begin{aligned}\sum y_{F4}^2 &= 3\left[\sum_{i=1}^{h/s-1}\left[\left(2\frac{s}{h}i-1\right)\frac{h}{2}\right]^2 - \sum_{i=0}^{h/s-8}\left[\left(2\frac{s}{h-8}i-1\right)\frac{h-8}{2}\right]^2\right] \\ &= \frac{1}{2}\left(9h^2-18hs+42s^2\right)\end{aligned} \tag{D.14b}$$

$$H_{F4} = \frac{F_{v,F4}}{h\sqrt{\left[\frac{b/2}{\sum x_{F4}^2}\right]^2 + \left[\frac{h/2-s}{\sum y_{F4}^2}\right]^2}} \tag{D.15}$$

- F5:

$$\sum x_{F5}^2 = 2\left(\frac{h}{s}-9\right)\left(\frac{b}{2}\right)^2 + 2\left(\frac{h}{s}-1\right)\left(\frac{b}{4}\right)^2 - 4\left(\frac{b}{4}\right)^2 = b^2\frac{5h-39s}{8s} \tag{D.16a}$$

$$\begin{aligned}\sum y_{F5}^2 &= 3\sum_{i=0}^{h/s-8}\left[\left(2\frac{s}{h-8}i-1\right)\frac{h-8}{2}\right]^2 + 2\sum_{i=1}^{h/s-1}\left[\left(2\frac{s}{h}i-1\right)\frac{h}{2}\right]^2 - 4\left(\frac{h}{4}\right)^2 \\ &= \frac{5h^3-81h^2s+577hs^2-1512s^3}{12s}\end{aligned} \tag{D.16b}$$

$$H_{F5} = \frac{F_{v,F5}}{h\sqrt{\left[\frac{b/2}{\sum x_{F5}^2}\right]^2 + \left[\frac{h/2-5s}{\sum y_{F5}^2}\right]^2}} \tag{D.17}$$

Then, the total summand terms as presented in equations D.6 and D.7 are determined as:

$$\sum_{i=1}^{n} k_i x_i^2 = k_{F1}\sum x_{F1}^2 + k_{F2}\sum x_{F2}^2 + k_{F3}\sum x_{F3}^2 + k_{F4}\sum x_{F4}^2 + k_{F5}\sum x_{F5}^2 \tag{D.18a}$$

$$\sum_{i=1}^{n} k_i y_i^2 = k_{F1}\sum y_{F1}^2 + k_{F2}\sum y_{F2}^2 + k_{F3}\sum y_{F3}^2 + k_{F4}\sum y_{F4}^2 + k_{F5}\sum y_{F5}^2 \tag{D.18b}$$

These equations only hold for $u_{SW} = 0$, since otherwise the stiffness varies for each fastener even if they are the same fastener type. Additionally, the yield force F_y of the total shear wall is determined as follows:

$$F_y = H_{F1} + H_{F2} + H_{F3} + H_{F4} + H_{F5} \tag{D.19}$$

Appendix E

Single nail statistics

E.1 Fastener type F4 statistics

The statistical evaluation of fastener F4 indicates a moderate discrepancy between the model predictions and the measured response. The RMSE equals 91.11, while the MAE is 76.50. This indicates that some error values are present, this is reflected in the coefficient of determination: $R^2 = 0.871$. Nonetheless, the model explains a substantial proportion of the variance.

To relate the error to the scale of the data, two normalized RMSE measures were computed. The NRMSE based on the full range of the dataset is 0.103699, and the NRMSE normalized by the mean is 0.222908. Both indicators suggest that the model deviates from the observed response by approximately 10–22 percent of the characteristic data scale. Additionally, a Q–Q plot was generated to assess whether the residuals follow a normal distribution. The plot shows clear divergence in both tails, with the empirical quantiles falling outside the theoretical quantile line at the lower and upper extremes. This behaviour indicates that the residual distribution exhibits heavier tails than a normal distribution. In practical terms, the model produces more large-magnitude errors than would be expected under the assumption of normally distributed residuals.

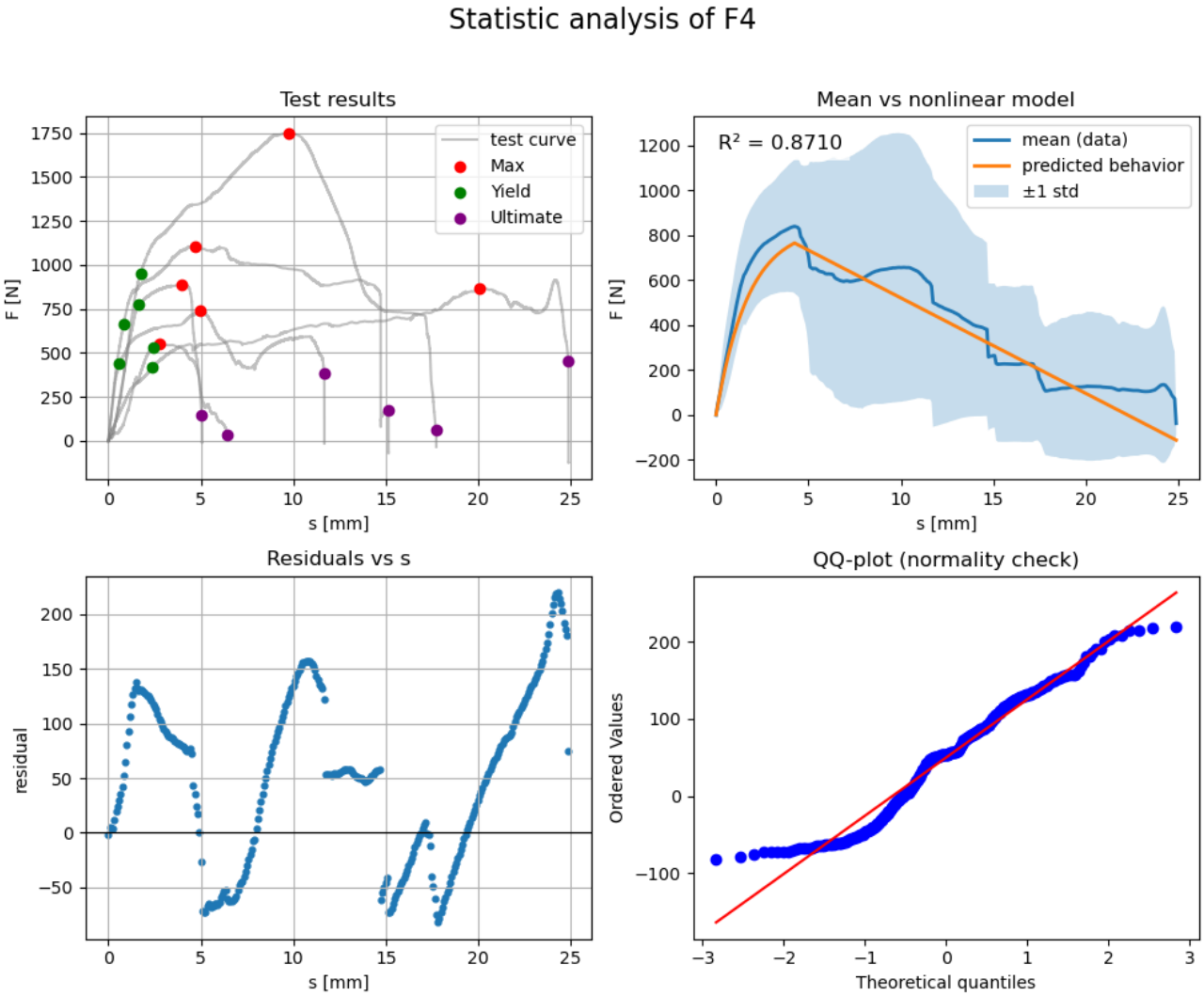

Figure E.1: Statistical analysis of F4. Top left: analysis of tests through ISO 12122. Top right: comparison between data mean and nonlinear prediction. Bottom left: Residuals of mean vs prediction curve. Bottom right: Q-Q plot of test results.

E.2 Fastener type F5 statistics

The overall fit metrics indicate that the model provides a strong representation of the measured response. The RMSE is 40.40, and the mean absolute error MAE is 31.79. The coefficient of determination is high $R^2 = 0.937$, confirming that the model explains the majority of the variance in the test data. Normalised error measures show consistent performance: the NRMSE based on the data range is 0.0598, and the NRMSE relative to the mean response is 0.0806.

The Q–Q plot once again shows divergence in the tails, however significantly less than in F4. The standard deviation is also much lower for F5 tests, with a coefficient of variance which never exceeds 1.0. Overall, the statistical indicators show that the predefined model provides an accurate and robust approximation of the experimental response for F5, although the strong residual autocorrelation suggests that additional structure in the experimental process are not captured by the current formulation.

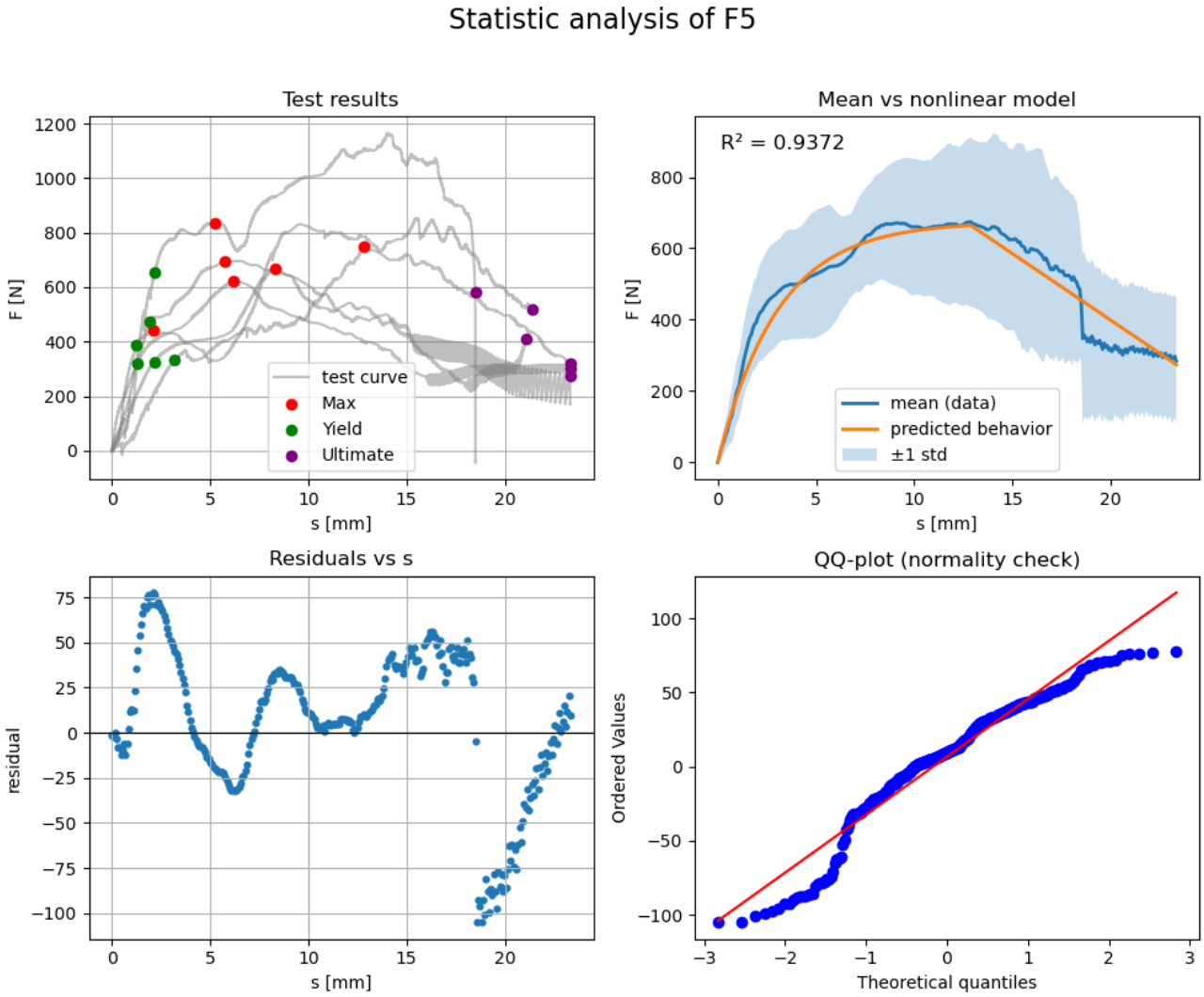

Figure E.2: Statistical analysis of F5. Top left: analysis of tests through ISO 12122. Top right: comparison between data mean and nonlinear prediction. Bottom left: Residuals of mean vs prediction curve. Bottom right: Q-Q plot of test results.

Appendix F

CBSW test results

The overall lateral response of the wall panels was assessed through the load-displacement curves obtained from monotonic and cyclic tests. Figure F.1a and F.2a present the load-displacement relationships of WT1 and WT2 under monotonic loading, respectively. The corresponding envelope curves were derived in accordance with ISO 21581:2010 (E) to represent the strength-deformation behavior. The results indicate that the absence of flat bar cross-bracings in WT2 led to a noticeable reduction in lateral strength and initial stiffness compared to WT1.

Under monotonic loading, WT1 exhibited strain hardening behavior, as evidenced by the continued increase in load beyond the yield point before reaching its peak strength. This indicates that the presence of flat bar cross-bracings enhanced the wall's capacity to sustain additional load after yielding. In contrast, WT2 displayed a flatter post-peak response, signifying a gradual reduction in stiffness and strength with increasing displacement. The post-peak flattening suggests lower rigidity and a diminished ability to sustain lateral resistance once the maximum load was attained. Figure F.1b - F.1f and F.2b - F.2f show the hysteretic load-displacement responses of WT1 and WT2 under cyclic loading. The envelope curves derived from these results reveal an evident asymmetry between the positive loading and reloading phases. The lateral resistance during reloading was generally lower than during the initial positive loading, indicating residual deformation and nail yielding that occurred during the first loading cycles. This asymmetric hysteretic behavior can be attributed to the progressive yielding and partial withdrawal of the nail connectors, which reduced the effective stiffness during subsequent cycles. Compared with WT1, WT2 exhibited greater stiffness degradation and pinching in the hysteresis loops, further confirming the influence of the absence of flat bar cross-bracings on its cyclic performance.

To better understand the observed damage modes, the load path of the wall panels during loading is illustrated conceptually as follows. Under monotonic loading, the lateral force is applied to the loading beam and transferred uniformly to the top timber beam, which distributes the load to the vertical bamboo studs. The bamboo studs, in turn, transfer the force to the mortar cladding through the nail connections. As the wall deforms laterally, the cladding rotates in the direction of the applied force, resisted primarily by the nails in shear. The load is then transmitted from the cladding to the

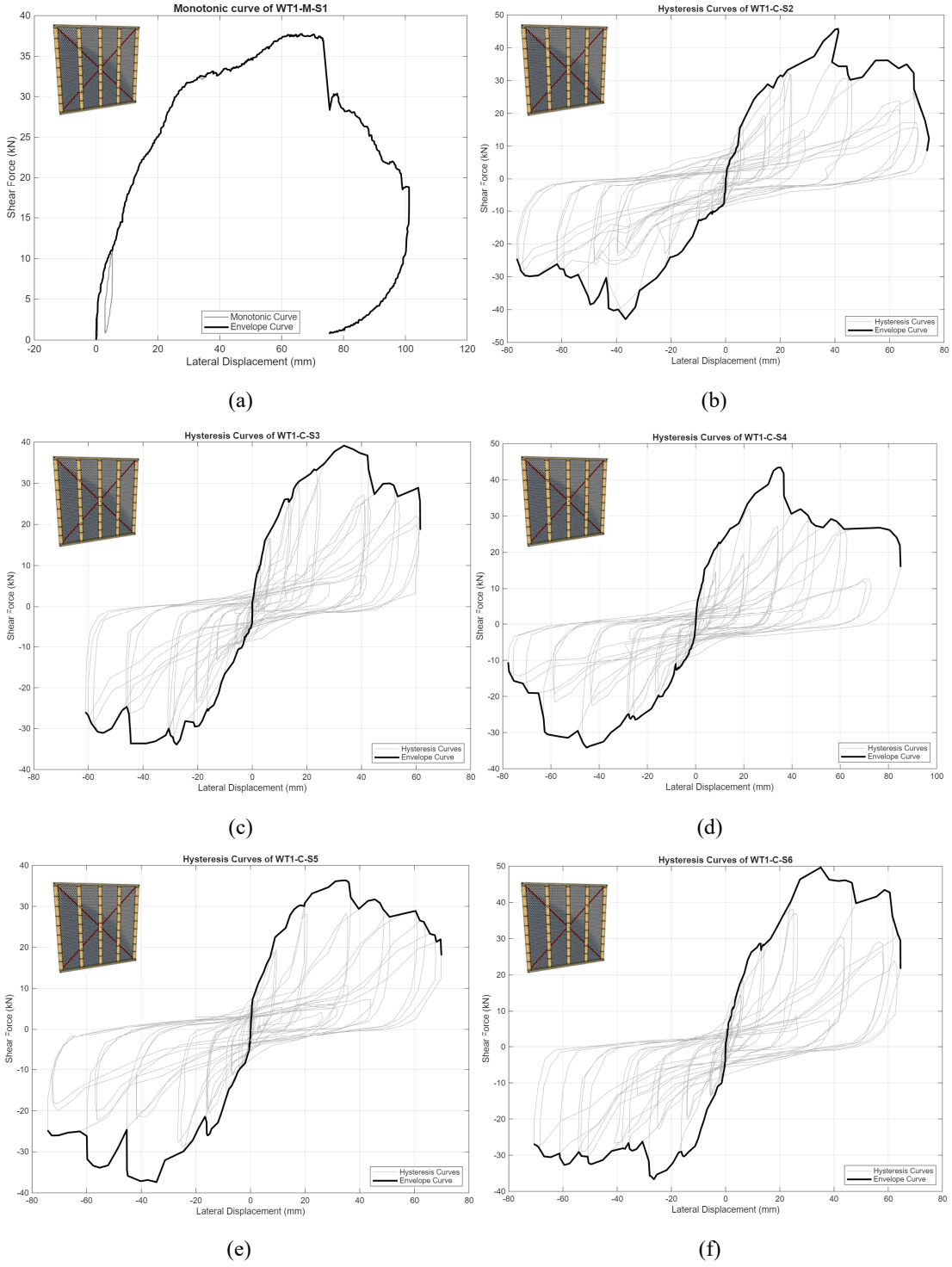

Figure F.1: Load–displacement relationships under monotonic and cyclic loading, including corresponding envelope curves for specimens: (a) WT1-M-S1; (b) WT1-C-S2; (c) WT1-C-S3; (d) WT1-C-S4; (e) WT1-C-S5; (f) WT1-C-S6.

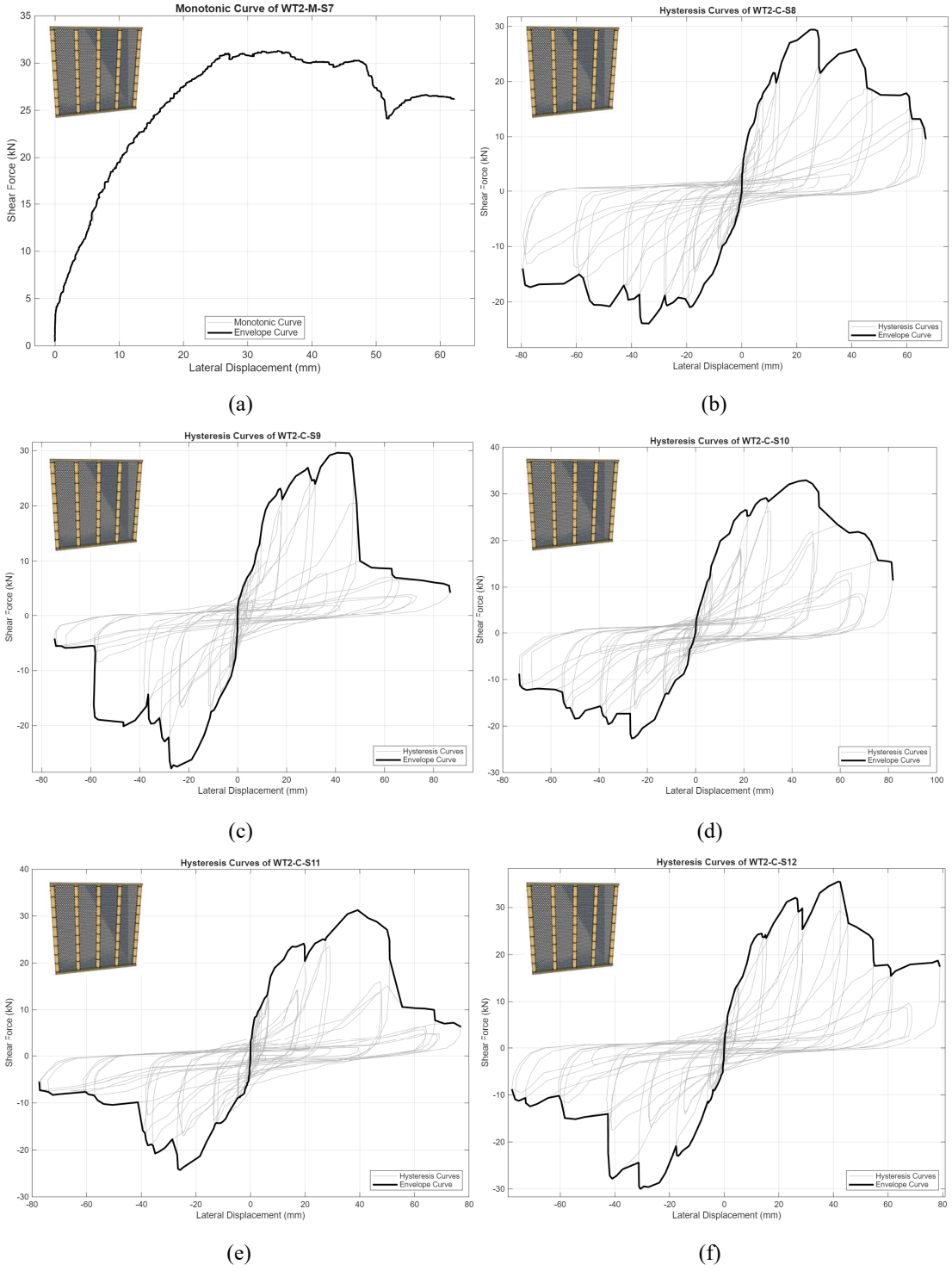

Figure F.2: Load–displacement relationships under monotonic and cyclic loading, including corresponding envelope curves for specimens: (a) WT2-M-S7; (b) WT2-C-S8; (c) WT2-C-S9; (d) WT2-C-S10; (e) WT2-C-S11; (f) WT2-C-S12.

bottom timber beam and finally to the foundation through the embedded rebar anchors. Understanding this load path is essential to explain how and where the different damage modes originated and developed during testing.

Figures F.3 and F.4 present the typical failure mechanisms observed in WT1 and WT2, respectively. For WT1 under monotonic loading, initial damage was characterized by simulataneous buckling of the flat bar cross-bracings and yielding of the connecting bolts at the compression side. Nail yielding occured at the interface between the cladding and the frame, manifested by the rotation of the mortar cladding in the direction of loading. The combined effects of flat bar buckling, bolt yielding, and cladding rotation caused crushing of the mortar at the upper and lower compression corners, followed by surface cracking and chipping. Continued loading led to progressive nail withdrawal, resultng in partial detachment of the cladding from the frame. This nail withdrawal commonly occured along the perimeter, particularly at the corners. Nails embedded in bamboo studs filled with mortar infill exhibited significant yielding due to the restricted movement provided by the infill, whereas nails driven into unfilled bamboo remained relatively straight, indicating minimal plastic deformation. Bamboo splitting was also observed along intermediate studs, typically at maximum load levels.

In the cyclic test of WT1, the overall damage progression was similar to that observed in monotonic loading, with additional deterioration due to repeated reversals of force. Flat bar buckling and bolt yielding were observed on both compression sides, occurring nearly simultaneously. The cladding exhibited a rocking motion corresponding to nail yielding, which was evident through cyclic rotation of the mortar surface. Mortar cracking and chipping were widespread along corner regions and at the timber beam interfaces. The combined yielding of bolts and buckling of flat bar pushed the cladding outward, further promoting nail withdrawal. In one specimen (WT1-C-S5), the nut of the bottom bolt detached due to excessive tension. Similar to the monotonic case, nail withdrawal occurred along the wall perimeter, especially at the corners. Although bamboo splitting was observed in some specimens, it was not a predominant failure mode and appeared only at or near the maximum load in the monotonic test.

For WT2 under monotonic loading, the absence of flat bar cross-bracing and bolt connections shifted the primary failure mechanisms to the nail connections. The damage initiated with nail yielding, particularly along the corner regions, allowing the mortar cladding to rotate relative to the frame. Continued rotation eventually caused nail withdrawal, leading to the detachment of the mortar cladding from the frame. Mortar cracking and chipping were also observed at the corners, similar to WT1 but generally less severe due to the absence of cross-bracing-induced stresses. In the cyclic tests of WT2, the damage patterns was comparable to the monotonic results but worsened by load reversals. Nail yielding and withdrawal were frequent along the entire wall perimeter, especially near the corners, as the mortar cladding exhibited rocking behavior under cyclic loading. Repeated cycles of loading and unloading caused the nails to progressively loosen, detach, and reinsert during reloading, which ultimately led to permanent cladding separation. Unlike WT1, bamboo splitting was not prominent in WT2; the monotonic specimen exhibited splitting, and only one (WT2-C-S11) of the five cyclic specimens showed localized splitting near the maximum load.

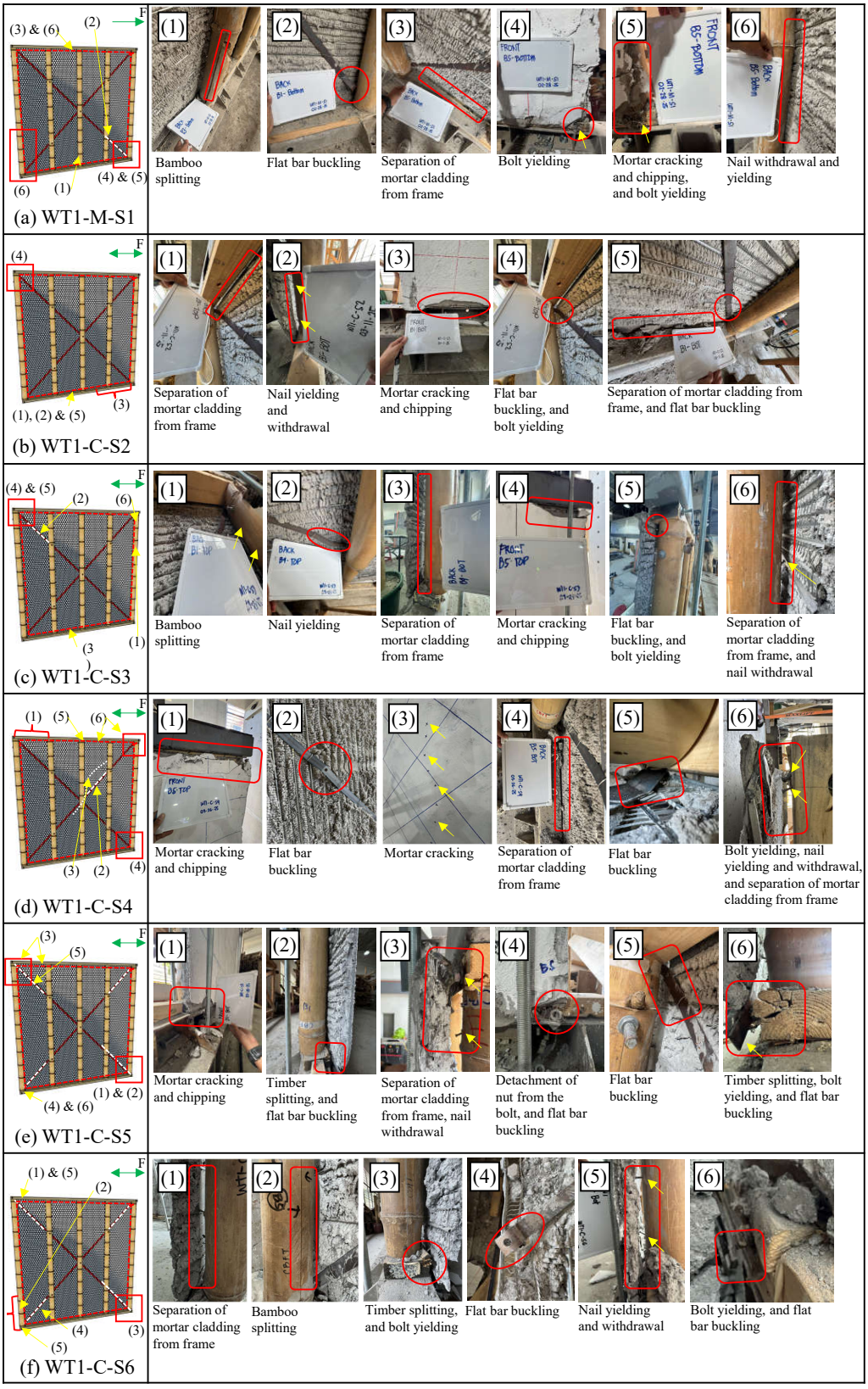

Figure F.3: Damage modes for WT1.

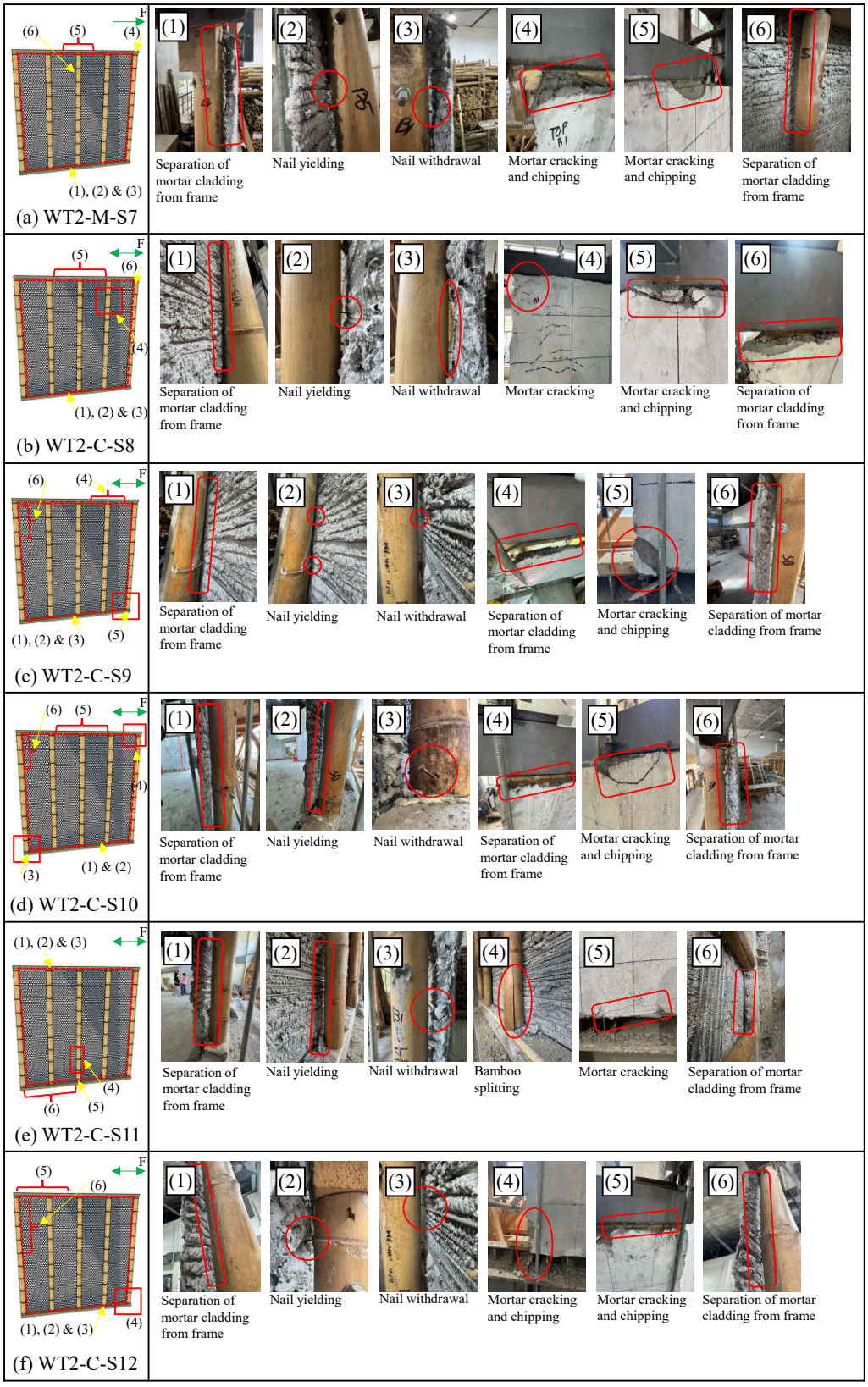

Figure F.4: Damage modes for WT2.

Bibliography

[ASTM International, 2020] ASTM International (2020). ASTM D1761-20 Standard Test Methods for Mechanical Fasteners in Wood and Wood-Based Materials. 28, 81

[Bangoy et al., 2024] Bangoy, C. D., Falcon, J., Lorenzo, H. A., Zeng, S. R., Garciano, L. E., and Cacanando, C. J. (2024). Experimental Study on the Dowel-Bearing Strength of Bambusa blumeana Bamboo Used for Sustainable Housing Construction. *Sustainability 2024*, 16(5530). 8, 26

[BASE, 2024] BASE (2024). Cement bamboo frame technology – building sustainable future today – base. 2

[Benedetti et al., 2022] Benedetti, F., Jara-Cisterna, A., Grandón, J. C., Astroza, N., and Opazo-Vega, A. (2022). Numerical Analysis of the Seismic Performance of Light-Frame Timber Buildings Using a Detailed Model. *Buildings*, 12(7):981. 9

[Bibal, 2024] Bibal, C. B. (2024). *Monotonic and cyclic response of cement-bamboo frame technology walls*. Final Thesis, Mapúa University, Manila. 9, 19

[Cacanando et al., 2025] Cacanando, C. J. D., López, L. F., Atienza, E., and Pradhan, N. P. (2025). Experimental characterization of mechanical properties of Bambusa blumeana bamboo poles and determination of design values. *Construction and Building Materials*, 490:142498. 29, 107

[Casagrande et al., 2016] Casagrande, D., Rossi, S., Sartori, T., and Tomasi, R. (2016). Proposal of an analytical procedure and a simplified numerical model for elastic response of single-storey timber shear-walls. *Construction and Building Materials*, 102:1101–1112. 8

[Dams et al., 2023] Dams, B., Maskell, D., Shea, A., Allen, S., Cascione, V., and Walker, P. (2023). Upscaling bio-based construction: challenges and opportunities. *Building Research & Information*, 51(7):764–782. Publisher: Routledge _eprint: https://doi.org/10.1080/09613218.2023.2204414. 1

[Erasmus, 1984] Erasmus, L. (1984). The mechanical properties of structural steel sections and the relevance of these properties to the capacity design of structures. *Transactions of the Institution of Professional Engineers New Zealand: Civil Engineering*. 7

[European Committee for Standardization, 1994] European Committee for Standardization (1994). EN 1995 Eurocode 5: Design of timber structures. Section: 1 volume (loose-leaf) : illustrations. 9, 24, 69

[Folz and Filiatrault, 2001] Folz, B. and Filiatrault, A. (2001). Cyclic analysis of wood shear walls. *Journal of Structural Engineering*, 127(4):433–441. 8, 20

[FOREC, 2002] FOREC (2002). ASOCIACION COLOMBIANA DE INGENIERIA SISMICA. *FOREC*. 1, 18, 105

[Foschi, 1974] Foschi, R. (1974). Load-slip characteristics of nails. *Wood Science*, 7(1):69–76. 20

[Hadi et al., 2012] Hadi, M., Murakami, S., and Komatsu, K. (2012). Prediction of Nonlinear Cyclic Behaviors of Shear Wall Composed of Acacia mangium Framing and Fiber Cement Board Sheathing. *Open Journal of Civil Engineering*, 2(1):1–9. Number: 1 Publisher: Scientific Research Publishing. 9, 23

[Harries et al., 2022] Harries, K. A., Rogers, C., and Brancaccio, M. (2022). Bamboo joint capacity determined by ISO 22156 'complete joint testing' provisions. *Advances in Bamboo Science*, 1:100003. 28

[Horsting et al., 2024] Horsting, A., Woltjer, P., Van Eckeveld, A., and Sass-Klaassen, U. (2024). Wood it be possible: constructing timber houses in the Netherlands. Technical report, Wageningen Economic Research, Wageningen. 1

[International Organization for Standardization, 1983] International Organization for Standardization (1983). ISO 6891:1983 Timber structures - joints made with mechanical fasteners - general principles for the determination of strength and deformation characteristics. 14

[International Organization for Standardization, 2010] International Organization for Standardization (2010). ISO 21581:2010 Timber structures - Static and cyclic lateral load test methods for shear walls. 14, 19, 28, 81, 82, 106

[International Organization for Standardization, 2017] International Organization for Standardization (2017). ISO 12122-6 Timber structures — determination of characteristic values. 28

[International Organization for Standardization, 2021] International Organization for Standardization (2021). ISO 22156:2021 Bamboo structures — Bamboo culms — Structural design. 17, 28, 29

[International Organization for Standardization, 2022] International Organization for Standardization (2022). ISO/TR 21141:2022 Timber structures — Timber connections and assemblies — Determination of yield and ultimate characteristics and ductility from test data. 14

[Johansen, 1949] Johansen, K. W. (1949). Theory of timber connections. Medium: text/html,application/pdf,text/html Publisher: [object Object]. 25

[Kaminski et al., 2024] Kaminski, S., Grant, D., Harries, K., Trujillo, D., and López, L. (2024). *Seismic performance of whole culm bamboo structures and recommendations for design using ISO 22156*. 17

[Kaminski et al., 2016] Kaminski, S., Lawrence, A., and Trujillo, D. (2016). *Design Guide for Engineered Bahareque Housing*. 18

[Kaminski et al., 2023] Kaminski, S., López, L., Trujillo, D., Zea Escamilla, E., Correa-Giraldo, V., and Correal-Daza, J. (2023). *Composite bamboo shear walls - A shear wall system for affordable and sustainable housing in tropical developing countries*. 19

[Khodabakhshi et al., 2025] Khodabakhshi, N., Chu, S. K. W., Mouka, T., Kum, K. H., and Dimitrakopoulos, E. G. (2025). Stiffness characterization of bolted multi-culm bamboo members. *Journal of Building Engineering*, 103:112080. 26, 28

[Källsner and Girhammar, 2009] Källsner, B. and Girhammar, U. A. (2009). Analysis of fully anchored light-frame timber shear walls—elastic model. *Materials and Structures*, 42(3):301–320. 9, 21, 22, 23, 105

[Li et al., 2015] Li, Z., Xiao, Y., Wang, R., and Monti, G. (2015). Studies of nail connectors used in wood frame shear walls with ply-bamboo sheathing panels. *Journal of Materials in Civil Engineering*, 27(7). Publisher: American Society of Civil Engineers (ASCE). 9

[Liu et al., 2020] Liu, Y., Wang, Y., Zhang, Y., Chen, M., and Nie, X. (2020). Force–displacement relations of bolted timber joints with slotted-in steel plates parallel to the grain. *Journal of Wood Science*, 66(1):83. 24, 28

[Lopez et al., 2004] Lopez, M., Bommer, J., and Mendes, P. (2004). The seismic performance of bahareque dwellings in el salvador. *13th World Conference on Earthquake Engineering*. 1, 17

[Malkowska et al., 2022] Malkowska, D., Norman, J., and Trujillo, D. (2022). Theoretical and experimental study on laterally loaded nailed bamboo connection. *Construction and Building Materials*. 14, 27, 28

[Mouka and Dimitrakopoulos, 2022] Mouka, T. and Dimitrakopoulos, E. G. (2022). Prediction of bamboo culm embedment properties parallel to grain via dimensional analysis. *Construction and Building Materials*, 347:128434. 26

[Rammer and Zelinka, 2015] Rammer, D. R. and Zelinka, S. L. (2015). Withdrawal Strength and Bending Yield Strength of Stainless Steel Nails. *Journal of Structural Engineering*, 141(5):04014134. 69

[Sawata et al., 2006] Sawata, K., Sasaki, T., and Kanetaka, S. (2006). Estimation of shear strength of dowel-type timber connections with multiple slotted-in steel plates by European yield theory. *Journal of Wood Science*, 52(6):496–502. 25

[Trujillo and Malkowska, 2018] Trujillo, D. and Malkowska, D. (2018). Empirically derived connection design properties for Guadua bamboo. *Construction and Building Materials*, 163:9–20. 27

[Wakashima et al., 2003] Wakashima, Y., Sonoda, S., and Nakatani, H. (2003). Evaluation of seismic performance of nailed plywood shear walls by pseudo-dynamic tests I. Examination of a pseudo-dynamic test using substructuring techniques. *Mokuzai Gakkaishi/Journal of the Japan Wood Research Society*, 49(4):267–274. 9, 23

List of Figures

List of Tables